

General Disclaimer

One or more of the Following Statements may affect this Document

- This document has been reproduced from the best copy furnished by the organizational source. It is being released in the interest of making available as much information as possible.
- This document may contain data, which exceeds the sheet parameters. It was furnished in this condition by the organizational source and is the best copy available.
- This document may contain tone-on-tone or color graphs, charts and/or pictures, which have been reproduced in black and white.
- This document is paginated as submitted by the original source.
- Portions of this document are not fully legible due to the historical nature of some of the material. However, it is the best reproduction available from the original submission.

NASA CR-

152501

Final Report

on

**PRECIPITATION-ATTENUATION STUDIES
BASED ON MEASUREMENTS OF ATS-6 20/30-GHz
BEACON SIGNALS AT CLARKSBURG, MARYLAND**

AUGUST 1976

(NASA-CR-152501) PRECIPITATION-ATTENUATION N77-23295
STUDIES BASED ON MEASUREMENTS OF ATS-6
20/30-GHz BEACON SIGNALS AT CLARKSBURG, *HC A05/nf A01*
MARYLAND Final Report, May 1974 - Dec. 1975
(Comsat Labs., Clarksburg, Md.) 97 p G3/32 30798
Unclas

Prepared for

**National Aeronautics and Space Administration
Goddard Space Flight Center
Greenbelt, Maryland**

under

NASA Contract NAS 5-20740

by

D.J. FANG and J.M. HARRIS

**COMSAT Laboratories
Clarksburg, Maryland 20734**



| | | | |
|---|--------------------------------------|--|------------|
| 1. Report No. | 2. Government Accession No. | 3. Recipient's Catalog No. | |
| 4. Title and Subtitle Precipitation-Attenuation Studies Based on Measurements of ATE-6 20/30- GHz Beacon Signals at Clarksburg, Md. | | 5. Report Date July 1, 1976 | |
| | | 6. Performing Organization Code | |
| 7. Author(s) D. J. Fang and J. M. Harris | | 8. Performing Organization Report No. CLP-74-110 | |
| 9. Performing Organization Name and Address Transmission Systems Laboratory COMSAT Labs Clarksburg, Maryland 20734 | | 10. Work Unit No. | |
| | | 11. Contract or Grant No. NAS5-20740 | |
| 12. Sponsoring Agency Name and Address NASA, GSFC Greenbelt, Maryland 20771 E. Hirschmann, Code 951, Technical Officer | | 13. Type of Report and Period Covered Final Report May 1974-Dec 1975 | |
| | | 14. Sponsoring Agency Code 60 | |
| 15. Supplementary Notes Title of NAS5-20740: "Establishment of A 20/30-GHz Receive Terminal" | | | |
| 16. Abstract COMSAT Labs participated in the Millimeter Wave-length Propagation Experiment under NASA contract NAS5-20740, performing measurements of the 20/30-GHz ATS-6 satellite beacon signals and auxiliary measurements such as radiometric sky temperature and minute precipitation at Clarksburg, Maryland. These measurements were intended to broaden the data base required to advance the understanding of the propagation characteristics of the earth-satellite path at frequencies over 10 GHz. Analyses of the data collected from the measurement program have established a detailed correlation between the satellite signal and the signals from auxiliary ground-based measurements. The indirectly derived statistics agreed reasonably well (or can be reconciled) with the earlier published results. The correlations may therefore be used for indirectly estimating long-term cumulative attenuation statistics in the absence of <u>direct satellite signal measurements.</u> | | | |
| 17. Key Words (Selected by Author(s)) ATS-6 Millimeter Wave Experiment, precipitation, attenuation, radiometric sky temperature | | 18. Distribution Statement | |
| 19. Security Classif. (of this report) | 20. Security Classif. (of this page) | 21. No. of Pages | 22. Price* |

Table of Contents

| | | <u>Page No.</u> |
|----|-----------------------------------|-----------------|
| 1. | INTRODUCTION | 1-1 |
| 2. | SYSTEM CONFIGURATION | 2-1 |
| 3. | RADIOMETRIC EXPERIMENT | 3-1 |
| 4. | RAIN GAUGE EXPERIMENT | 4-1 |
| 5. | SATELLITE BEACON EXPERIMENT | 5-1 |
| 6. | CONCLUSIONS | 6-1 |
| 7. | REFERENCES | 7-1 |

APPENDIX A. PRELIMINARY REPORT ON ATMOSPHERIC
ATTENUATION STUDIES ON ATS-6 SAT-
ELLITE 20/30 GHz BEACON SIGNALS

APPENDIX B. A NEW METHOD OF ESTIMATING MICRO-
WAVE ATTENUATION OVER A SLANT
PROPAGATION PATH BASED ON RAIN
GAUGE DATA

List of Illustrations

| <u>Figure No.</u> | <u>Title</u> | <u>Page No.</u> |
|-------------------|--|-----------------|
| 2-1 | Block Diagram of the 3-Meter 20-GHz Receiver/11.6-GHz Radiometer Transportable System | 2-2 |
| 2-2 | Block Diagram of the 5-Meter 20- and 30-GHz Receiver/Radiometer System | 2-3 |
| 2-3a | Typical Sky Temperature-Attenuation Record from the 3-Meter System with Simultaneous Precipitation Records Taken from Ground Rain Gauges Beneath the Boresight Direction 0, 1.08, and 3.23 km Away from the 3-Meter System | 2-6 |
| 2-3b | Typical Records of Simultaneously Measured 20/30-GHz Radiometric Sky Temperatures and ATS-6 Beacon Signals from the 5-Meter System | 2-7 |
| 3-1 | Cumulative Attenuation Statistics at 11.6 GHz at Clarksburg, Maryland, and CML 12-GHz Curves Based on Earlier Radiometric Measurement at 15.3 GHz Pointing at ATS-5 Satellite | 3-3 |
| 3-2a | Simultaneous Record of Radiometric Sky Temperature and Satellite Beacon Signal at 30 GHz for an Event of June 6, 1975 | 3-5 |
| 3-2b | Scattergram of Figure 3-2a | 3-6 |
| 3-2c | Simultaneous Record at 30 GHz for an Event of May 16, 1975 | 3-7 |
| 3-2d | Scattergram of Figure 3-2c | 3-8 |

List of Illustrations (Continued)

| <u>Figure No.</u> | <u>Title</u> | <u>Page No.</u> |
|-------------------|---|-----------------|
| 3-3 | Composite Scattergram of All the Simul- taneous Records of Radiometric Sky Tem- peratures vs Satellite Beacon Signals at 30 GHz | 3-9 |
| 3-4a | Simultaneous Record of Radiometric Sky Temperature and Satellite Beacon Signal at 20 GHz for an Event of June 7, 1975 | 3-10 |
| 3-4b | Scattergram of Figure 3-4a | 3-11 |
| 3-4c | Simultaneous Record at 20 GHz for an Event of May 16, 1975 | 3-12 |
| 3-4d | Scattergram of Figure 3-4c | 3-13 |
| 3-5 | Composite Scattergram of All the Simul- taneous Records of Radiometric Sky Tem- peratures vs Satellite Beacon Signals at 20 GHz | 3-14 |
| 3-6 | Simultaneous Records of Radiometric Sky Temperatures at 11.6 GHz and Satellite Beacon Signals at 20 GHz and Their Cor- responding Scattergrams (10 sheets) | 3-16 |
| 3-7 | Composite Scattergram of Radiometric Sky Temperature at 11.6 GHz vs Satellite Beacon Signal at 20 GHz | 3-26 |
| 3-8 | 20-GHz Cumulative Attenuation Statistics Derived from 11.6-GHz Radiometric Data Based on Empirical Equation (3-2) | 3-28 |
| 4-1 | Cumulative Statistics of Precipitation at Clarksburg, Maryland | 4-3 |
| 5-1a | Scattergram of 30-GHz vs 20-GHz Attenua- tion Recorded May 16, 1975 | 5-2 |

List of Illustrations (Continued)

| <u>Figure No.</u> | <u>Title</u> | <u>Page No.</u> |
|-------------------|---|-----------------|
| 5-1b | Scattergram of 30-GHz vs 20-GHz Attenuation Recorded June 7, 1975 | 5-3 |
| 5-1c | Scattergram of 30-GHz vs 20-GHz Attenuation Recorded June 6, 1975 | 5-4 |
| 5-1d | Composite Scattergram of 30-GHz vs 20-GHz Attenuation from All Available Simultaneous Records | 5-5 |
| 5-2 | Recordings of 20/30-GHz Low-Elevation-Angle Signals | 5-8 |
| 5-3 | 30-GHz Beacon Signals at an Elevation Angle of About 6.5° | 5-9 |
| 5-4 | 20-GHz Recordings | 5-11 |
| 5-5 | Peak-to-Peak Signal Fluctuations at 20/30 GHz at Low Elevation Angles | 5-12 |

List of Tables

| <u>Table No.</u> | <u>Title</u> | <u>Page No.</u> |
|------------------|---|-----------------|
| 2-1 | Important Performance Parameters of the 3-Meter System | 2-4 |
| 2-2 | Important Performance Parameters of the 5-Meter System | 2-4 |
| 2-3 | Performance Parameters of A.I.L. 2392C Radiometer | 2-5 |
| 2-4 | Data Collection Statistics | 2-9 |
| 3-1 | Summary of $T_{11.6} = \alpha A_{20}^{\beta}$ Numerical Fitting | 3-27 |

1. INTRODUCTION

The radio frequency bands below 10 GHz have been used for satellite-earth communications since the beginning of the space communications era. These bands are approaching saturation due to the ever increasing traffic. Consequently, for a number of years satellite communications engineers have been studying higher frequency bands for future satellite communications systems to obtain an in-depth understanding of the propagation characteristics of earth-satellite paths at frequencies higher than 10 GHz, which are significantly different from those at lower frequencies.

Some understanding of the propagation characteristics has already been obtained from theoretical studies of microwave transmissions at centimeter and millimeter wavelengths. A representative list of pertinent publications is given in References 1-6. A more detailed understanding of the subject requires analysis and interpretation of data collected from a variety of experiments using satellites, rain gauges, radars, radiometers, terrestrial links, etc. Of all possible experiments, those using direct measurements of signals from a satellite are the most desirable, since they provide a direct simulation of a communications link along a slant path between a satellite and an earth terminal.

The first satellite experiment for the determination of slant path signal fading statistics for frequencies over 10 GHz was the NASA ATS-5 15.3/31.65-GHz Millimeter Wave Experiment (MWE). Effects of precipitation, primarily rain, were studied extensively by NASA and other research organizations working with NASA,⁷ including COMSAT Labs. The results clearly suggested that propagation impairments at 15.3/31.65 GHz were different from those at lower frequencies, and that the models established for

engineering applications at lower frequencies were no longer applicable.

The ATS-6 20/30-GHz MWE program, developed and implemented by NASA Goddard Space Flight Center, was a follow-up and a refinement of the earlier ATS-5 MWE program. It provided direct measurements on 20- and 30-GHz earth-satellite links from the eastern U.S. to the synchronous satellite located at 94°W longitude. The satellite was launched on May 30, 1974, and became operational for the MWE in July 1974. It provided three modes of operation: continuous wave, multitone, and communications, all selectable at 20 and/or 30 GHz. The MWE system is described in detail in Reference 8. Under NASA contract NAS5-20740, COMSAT Labs participated in the MWE program, performing measurements of the 20/30-GHz satellite beacon signals and other auxiliary measurements such as radiometric sky temperature and precipitation at Clarksburg, Maryland. These measurements were designed to broaden the data base required to advance the understanding of propagation characteristics at frequencies over 10 GHz.

There are several practical problems associated with a propagation experiment using a satellite. Due to the tremendous cost and complexity involved in designing and launching the spacecraft, assessing and assigning the priorities of various experiments operating at locations around the U.S., and scheduling and operating the system in coordination with various ground terminals, such a satellite propagation experiment is at most intermittent in time and spot-beam coverage, and can simultaneously accommodate only a few research institutions. The practical approach for researchers is therefore to study the results generated by a limited number of direct satellite transmission measurements so that these results can be correlated with those generated by various auxiliary ground-based experiments, such as rain gauges, radars, radiometers, and terrestrial links. The

ultimate goal is to establish definitive criteria for using the results of the relatively inexpensive and continuously available ground-based experiments to make valid engineering estimates of the important propagation parameters for space communications applications.

Such an approach is particularly pertinent to the ATS-6 MWE program. The MWE program was not assigned a high priority throughout most of the experimental period, and transmission time was not plentiful. In addition, the regular assigned transmissions, which averaged about one hour per day, were not always useful, since precipitation rarely occurred within the scheduled transmission time. While MWE experimenters were encouraged to send requests for 20/30-GHz transmission to NASA ATS-6 Operation Center when a precipitation event was occurring or anticipated at the site, responses to these requests were seldom positive due to other higher priority work in progress or scheduled. Obviously, the ATS-6 MWE was not intended to provide continuous transmissions for the determination of long-term fading statistics as some of the experimenters might have hoped, but rather to provide adequate transmissions for experimenters to study the propagation characteristics under various meteorological conditions based on a number of individual but significant events.

In view of these factors, the COMSAT Labs MWE program consisted of the following measurements: satellite beacon signals at 20 and 30 GHz; radiometric sky temperatures at 11.6, 20, and 30 GHz; precipitation at six sites aligned beneath the slant path; and rain cloud motion. Understanding the correlations between the beacon signals and the data from the ground-based measurements became a major goal of the program.

The COMSAT experimental signal receiving configurations, including the 3- and 5-meter antenna-receiver systems, are

described in Section 2. Data analyses of radiometric measurements of sky temperature at 11.6, 20, and 30 GHz are discussed in Section 3, which also includes some of the earlier sky temperature results collected by COMSAT under the ATS-5 MWE program for comparison. Section 4 is devoted to modeling of the data from rain gauges. A new method for using the rain gauge records to predict the slant path attenuation is postulated and examined. The satellite beacon experiment, described in Section 5, includes measurements of the 20/30-GHz MWE beacon at 42° elevation angle during the regular experimental period as well as at low elevation angles during the period when the satellite was moving from its 94°W longitude position to the eastern position at 35°E longitude at the end of May 1975. Conclusions are given in Section 6.

An interim contract report, "Preliminary Report on Atmospheric Attenuation Studies on ATS-6 Satellite 20/30 GHz Beacon Signals," which largely documented the hardware configurations and data analysis routines, is attached as Appendix A. Most of the contents of the interim report have not been duplicated in the present report, which focuses on the results of data analysis and engineering implications.

2. SYSTEM CONFIGURATION

Measurements were performed at COMSAT Labs, Clarksburg, Maryland, about 65 km northwest of Washington, D.C. The measurement systems can be summarized as follows:

- a. a 3-meter-diameter transportable antenna-receiver system including a 20-GHz receiver for receiving satellite beacon signals and a radiometric receiving system at 11.6 GHz for observing sky temperature using the same antenna,
- b. a 5-meter-diameter antenna-receiver system including 20- and 30-GHz receivers for the satellite beacon signals and two radiometric receivers at 20 and 30 GHz for observing sky temperature using the same antenna, and
- c. a network of six rain gauges extending 7 km underneath the boresight path toward the satellite at 94°W longitude for examining the precipitation along the propagation path.

In addition, a 5.5° beamwidth RCA AVQ-10 weather radar at 4.5 GHz was employed for large-scale visual observation of the motion pattern of rain clouds and to predict the approach of a precipitation cloud.

Figures 2-1 and 2-2 are block diagrams of the 3- and 5-meter systems, respectively. The antennas are solid-surface aluminum paraboloids equipped with focal-point feeds and polarization rotators. Both antennas have servo-controlled elevation and azimuth positioners and decimal position readouts with a resolution of 0.1° and 0.01° for the 3- and 5-meter antennas, respectively. The nominal pointing direction to ATS-6 is SSW 204° from true north at an elevation angle of 42°.

As indicated in the figures, tunnel diode and uncooled parametric amplifiers were used in the 20-GHz front ends of the

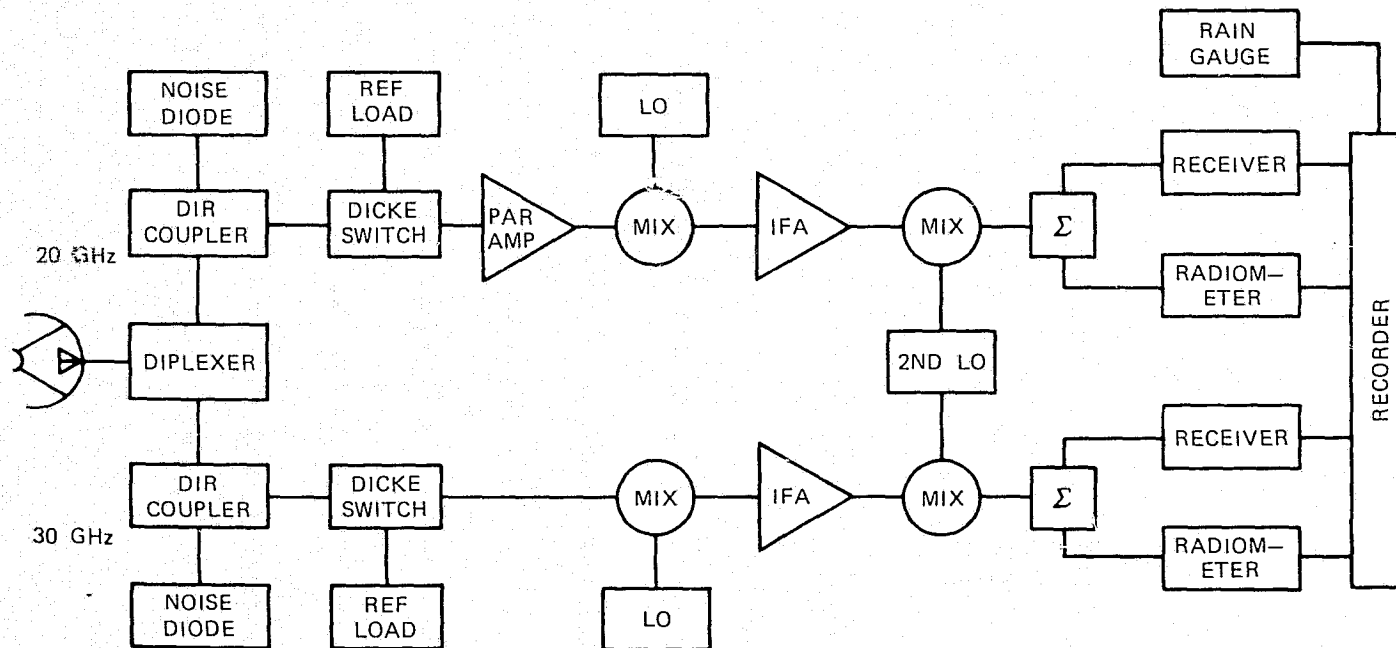


Figure 2-1. Block Diagram of the 3-Meter 20-GHz Receiver/
11.6-GHz Radiometer Transportable System

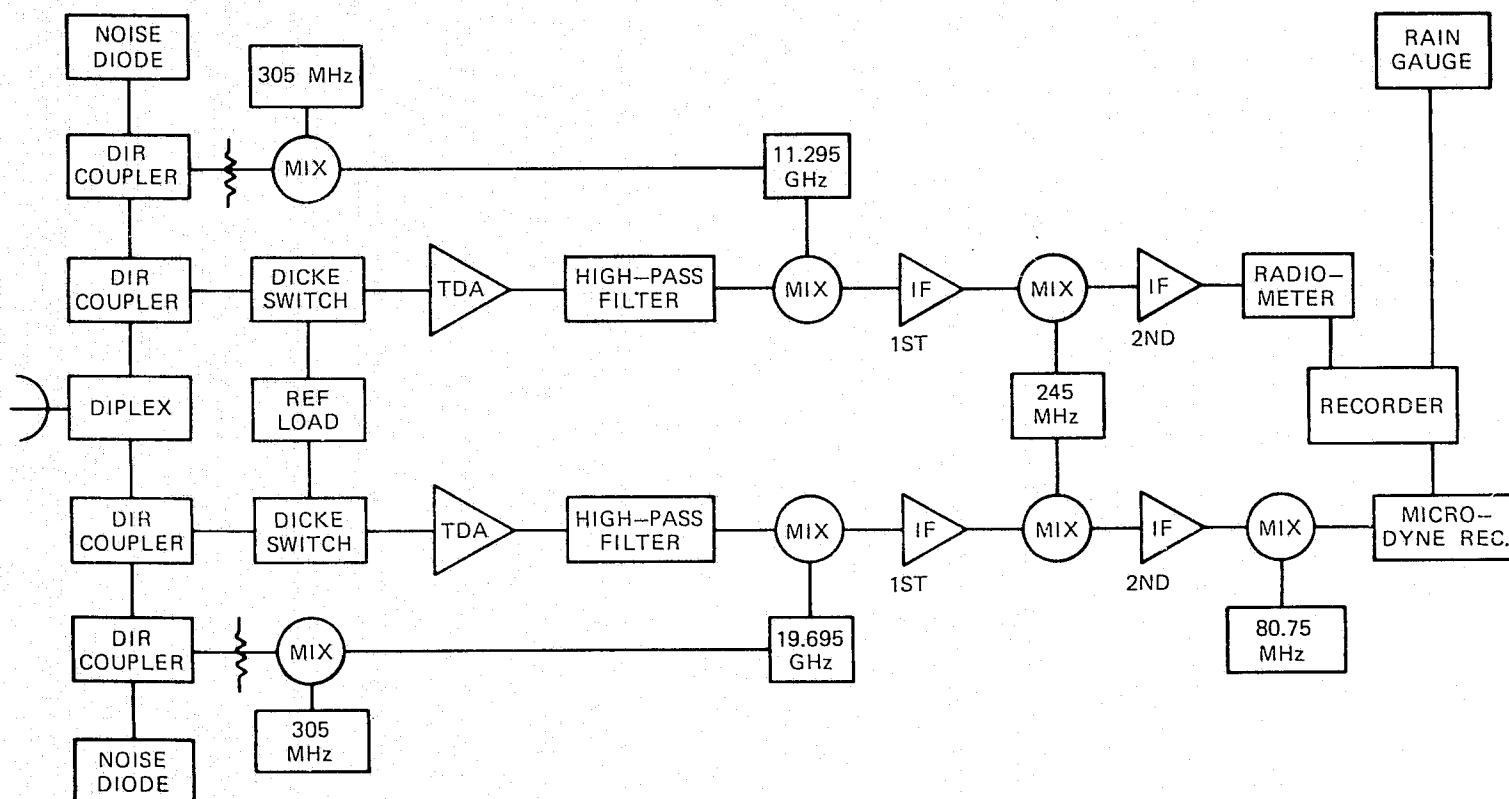


Figure 2-2. Block Diagram of the 5-Meter 20- and 30-GHz Receiver/Radiometer System

3- and 5-meter systems, respectively. The 30-GHz system had a low-noise mixer front end. IF processors which detected the down-converted signals by means of individual narrowband phase-locked receivers produced output amplitudes that were proportional to the satellite beacon signal attenuation levels. These outputs were then fed to stripchart recorders. Important performance parameters of the 3- and 5-meter systems are listed in Tables 2-1 and 2-2, respectively.

Table 2-1. Important Performance Parameters of the 3-Meter System

| Parameter | 11.6 GHz | 20 GHz |
|--------------------------|----------|---------|
| Antenna Gain | 48.7 dB | 53.5 dB |
| Antenna Beamwidth (1 dB) | 0.3° | 0.17° |
| Pointing Accuracy | ±0.1° | ±0.1° |
| Noise Figure | 5 dB | 8 dB |
| Radiometer Sensitivity | 1 K | -- |
| Radiometer Bandwidth | 100 MHz | -- |
| Receiver Bandwidth | -- | 10 kHz |

Table 2-2. Important Performance Parameters of the 5-Meter System

| Parameter | 20 GHz | 30 GHz |
|--------------------------|---------|---------|
| Antenna Gain | 57 dB | 60.5 dB |
| Antenna Beamwidth (1 dB) | 0.12° | <0.10° |
| Pointing Accuracy | ±0.01° | ±0.01° |
| Noise Figure | 4 dB | 8 dB |
| Radiometer Sensitivity | 1 K | 1 K |
| Radiometer Bandwidth | 100 MHz | 100 MHz |
| Receiver Bandwidth | 10 kHz | 10 kHz |

Both antenna systems were equipped with on-line radiometric subsystems. Operating in a Dicke-switched mode, these radiometers also included a noise source at a known temperature for calibration purposes. The A.I.L. (Airborne Instrument Laboratories) model 2392C radiometric receiver produced an output voltage proportional to the sky noise temperature. In the switched mode, the output was the net change of sky noise temperature from that on a clear sky day. Performance parameters of the A.I.L. radiometric receivers are summarized in Table 2-3,

Table 2-3. Performance Parameters of
A.I.L. 2392C Radiometer

| | |
|------------------------|---------------------------------------|
| IF Bandwidth | 100 MHz (5-105 MHz) |
| Noise Figure | 7 dB |
| Input Impedance | 50 Ω |
| Input SWR | Less than 2:1 over the passband |
| IF Gain | 85 dB maximum |
| Switch Rate | 5-500 Hz, with $\pm 0.05\%$ stability |
| Switched System Output | ± 5 V at 2 mA |
| Integration Time | 0.1, 1, 3, 5, 10, and 30 s |

The rain gauges were tipping bucket gauges, for which each tip represented 0.254 mm of rainfall accumulation. The gauges were aligned beneath the satellite boresight path at distances of 0, 0.92, 1.08, 3.23, 5.53, and 7.4 km from the beacon receiver. Each gauge was equipped with a mechanically driven stripchart recorder with a time accuracy of better than 3 minutes per week.

Typical records of sky temperature, attenuation, and precipitation are shown in Figures 2-3a and 2-3b. The records of the 11.6-GHz radiometer and the rain gauge at the site (0 km) were uninterrupted for more than a year beginning in September 1974. Other data were also available continuously once the

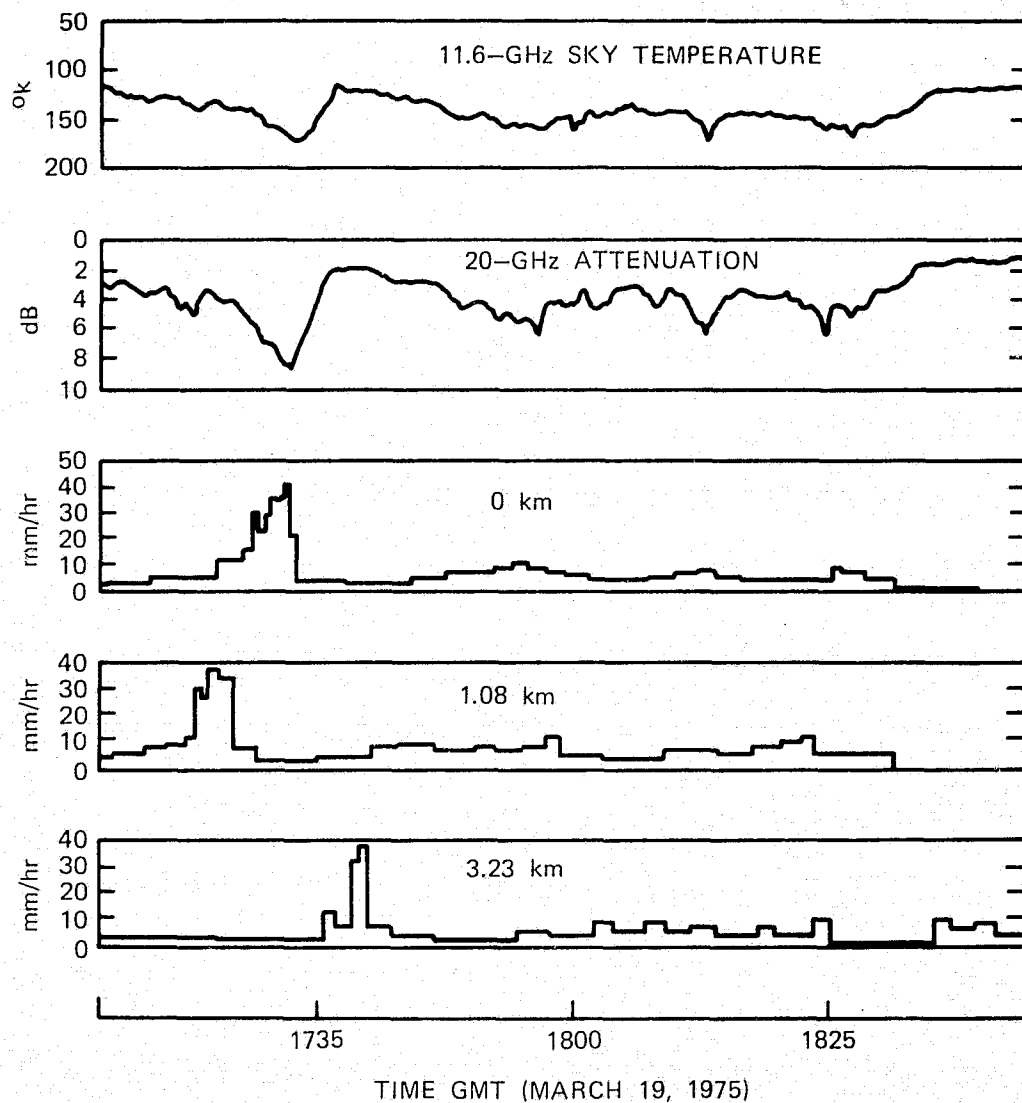


Figure 2-3a. Typical Sky Temperature-Attenuation Record from the 3-Meter System with Simultaneous Precipitation Records Taken from Ground Rain Gauges Beneath the Boresight Direction 0, 1.08, and 3.23 km Away from the 3-Meter System (elevation angle of antenna pointing is 42°)

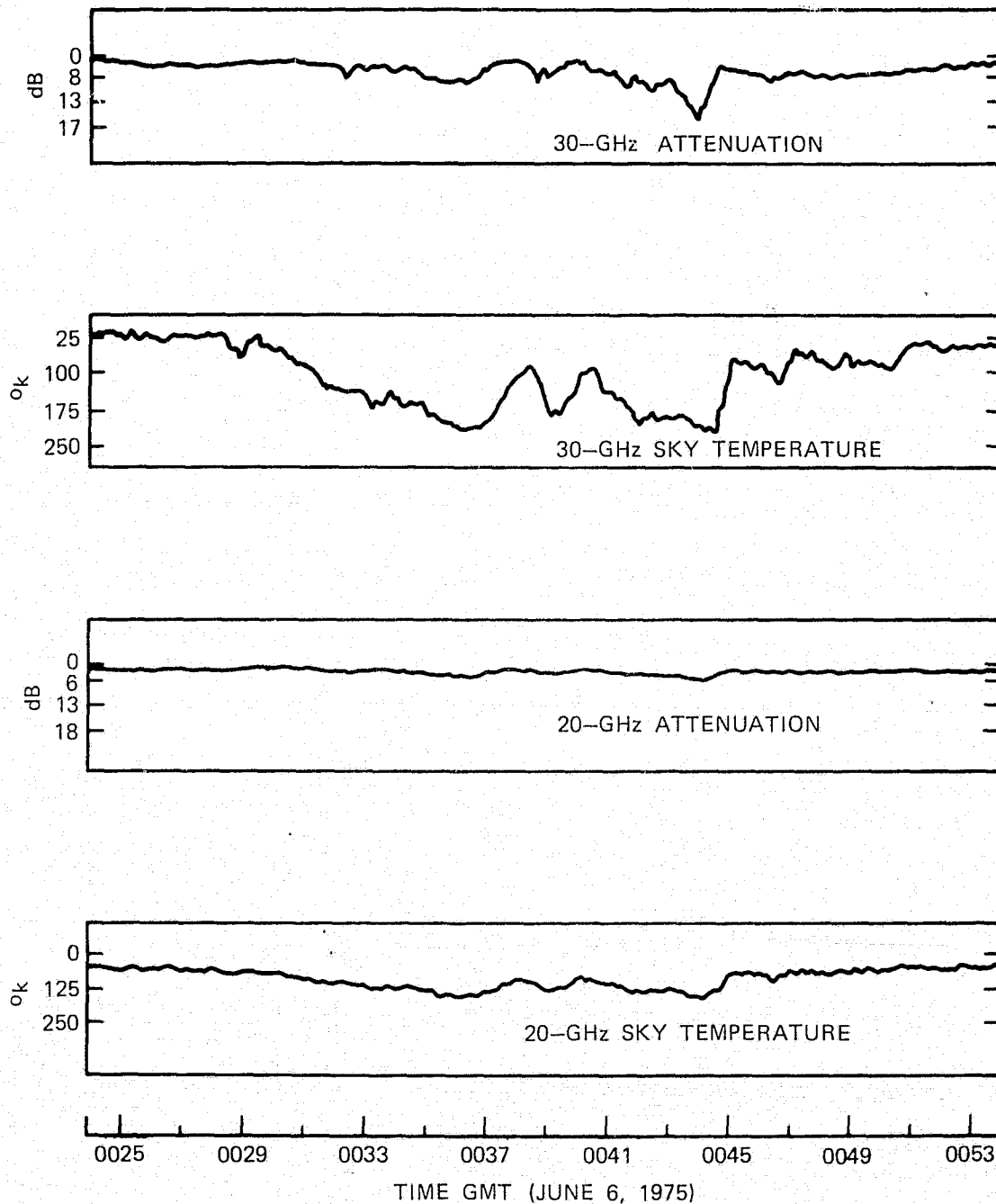


Figure 2-3b. Typical Records of Simultaneously Measured 20/30-GHz Radiometric Sky Temperatures and ATS-6 Beacon Signals from the 5-Meter System (elevation angle of antenna pointing is 15°)

equipment became operational. The only exceptions were the 20/30-GHz satellite beacon signal data, which were rather intermittent due to the limited availability of the ATS-6 MWE transmission. Details are summarized in Table 2-4.

In a preliminary effort, all the stripchart records, such as those shown in Figure 2-3, were scanned. In the subsequent analysis, useless clear sky data and defective data were deleted first. The magnitudes were then properly scaled and the simultaneity in time was calculated. Next, minute-by-minute digitization was applied to the data before they were key punched on IBM cards for analysis.

Table 2-4. Data Collection Statistics (August 1974-August 1975)

| System | Equipment | Date Available | Total Data Collection Time |
|---------|-----------------------|----------------|--------------------------------|
| 3 Meter | 20-GHz CW Receiver | July 1974 | 150 hr |
| | 11.7-GHz Radiometer | July 1974 | Continuous since July 1974 |
| | Rain Gauge | July 1974 | Continuous since July 1974 |
| 5 Meter | 20-GHz CW Receiver | March 1975 | 30 hr |
| | 20-GHz Radiometer | March 1975 | Continuous since March 1975 |
| | 30-GHz CW Receiver | April 1975 | 25 hr |
| | 30-GHz Radiometer | April 1975 | Continuous since April 1975 |
| Others | 5.4-GHz Weather Radar | September 1974 | No data collection |
| | Rain Gauge Network | February 1975 | Continuous since February 1975 |

3. RADIOMETRIC EXPERIMENT

A radiometer measures the radiative thermal emission collected by its antenna reflector. For engineering purposes the emission measured by a radiometer can be separated into three separate terms:

- a. the transmission term (the emission from an active radiator, such as the sun),
- b. the absorption term (the reradiation from an atmospheric medium when it is illuminated by an active radiator), and
- c. the scattering term (the scattering of incident electromagnetic waves of radiation from scatterers in the medium).

A more detailed discussion of these terms and their precise mathematical representations can be found in References 3 and 9.

All three terms are frequency dependent. For frequencies less than 10 GHz, the scattering term is negligible since the single scattering albedo is less than 10 percent.³ The absorption term, which is absent on clear sky days, is critically sensitive to meteorological conditions such as clouds, rain, and snow. The radiation attenuation, A , which is the quantity researchers attempt to evaluate on the basis of the radiometric experiments, is included in both the transmission term and the absorption term. The Dicke-switched radiometer system calibrates an internal noise load on a clear sky day so that on any non-clear days the system output, compared by switching to the pre-calibrated internal noise load, represents the temperature increase from clear sky conditions contributed solely by the absorption term. With some simplifications of the radiative heat transfer model, such as the assumption that the absorption is

uniform along a well-defined ray path through the medium, the following engineering equation can be derived:

$$A = -10 \log_{10} \left(1 - \frac{T_{\text{meas}}}{T_{\text{amb}}} \right) \quad (3-1)$$

where

A = attenuation, dB
T_{meas} = measured radiometric temperature, K
T_{amb} = ambient temperature of the medium, K
 ≅ 1.12 [ground temperature] - 50

Equation (3-1) is used to reduce the 11.6-GHz radiometer data for determining the long-term fading statistics. The result is shown in Figure 3-1, where T_{amb} is assumed to be 290 K. Also shown in Figure 3-1 are curves known as CML curves, which were obtained a few years ago by COMSAT¹⁰ at Clarksburg using a radiometer at 15.3 GHz pointing at a slightly different direction (antenna centered at 220° azimuth from true north at 35° elevation toward ATS-5).

The difference between the two sets of curves is evident. The CML curve was derived in two steps. The attenuation, A, was calculated at 15.3 GHz using equation (3-1) and then linearly scaled from 15.3 GHz down to 12 GHz. Since equation (3-1) becomes less dependable as the frequency increases and since the validity of such frequency scaling is uncertain, the validity of the CML curves is questionable. The 11.6-GHz curve, which utilizes equation (3-1) at a relatively low frequency and involves no scaling, is believed to be an improved version of the earlier CML curves.

The inadequacies of equation (3-1) at frequencies significantly higher than 10 GHz can be investigated by studying records of simultaneous radiometric sky temperature and satellite

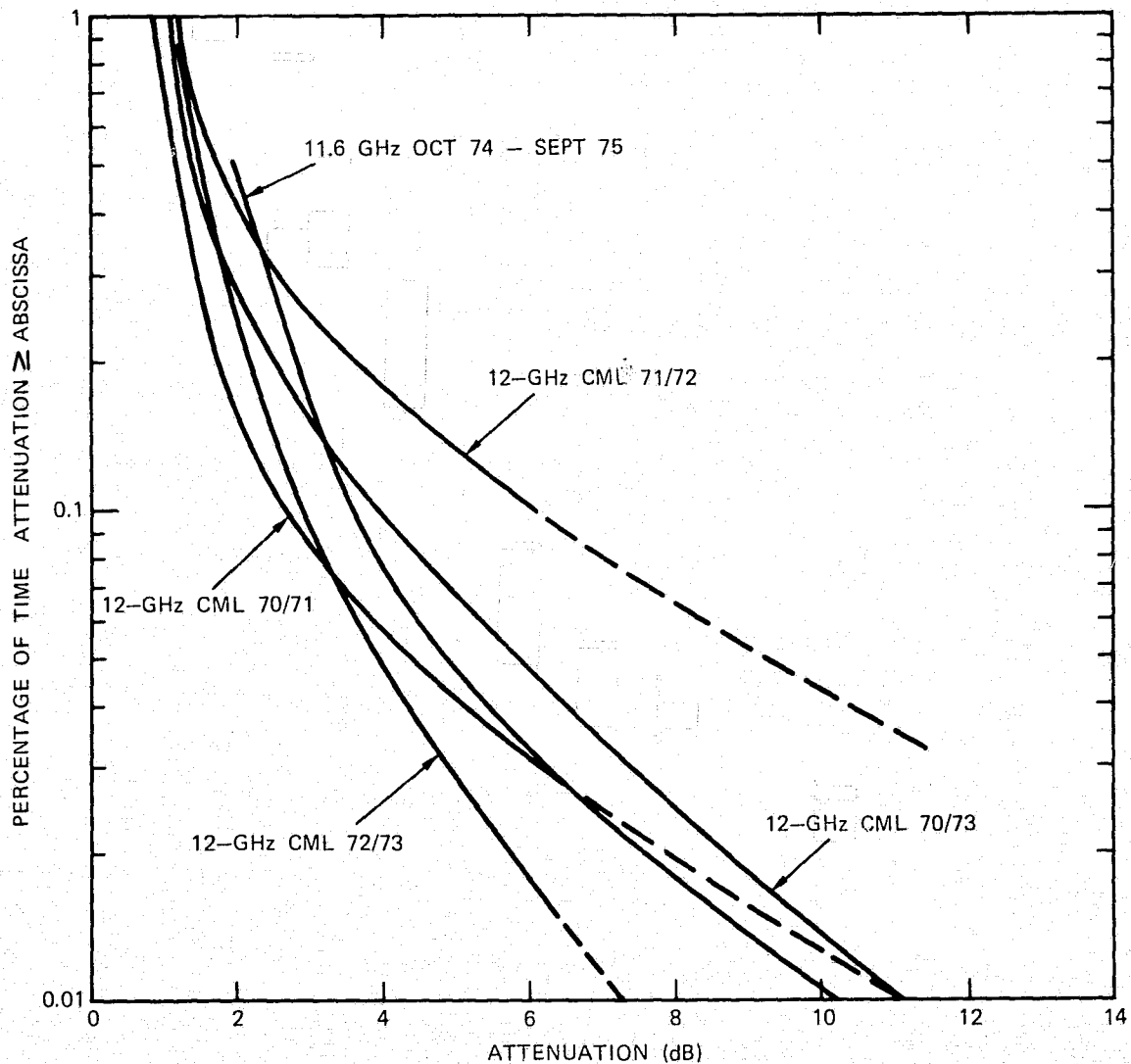


Figure 3-1. Cumulative Attenuation Statistics at 11.6 GHz at Clarksburg, Maryland, and CML 12-GHz Curves Based on Earlier Radiometric Measurement at 15.3 GHz Pointing at ATS-5 Satellite

beacon signal level measurements at 20/30 GHz. Figure 3-2 consists of the 30-GHz records and their corresponding scattergrams for two prominent precipitation events. Figure 3-3 is a composite scattergram based on data collected from several events in which the peak precipitation was greater than or equal to 20 mm/hr. Figures 3-4 and 3-5 are similar records for 20 GHz. Data points corresponding to signal levels less than 1 dB are omitted in the figures.

As can be seen from the scattergrams, unless an extremely low value of ambient temperature, T_{amb} , is assumed (which is rather unreasonable, since T_{amb} is essentially frequency independent), the curves based on equation (3-1) will significantly underestimate the attenuation at 20/30 GHz. As the frequency increases, the scattering term becomes so significant that it effectively saturates the sky temperature measurable by a radiometer, while the satellite beacon signal attenuation level increases with frequency without such saturation. It follows that there is no longer any physical basis for using equation (3-1) to model the relationship between A and T_{meas} . To demonstrate the correlations between the two quantities, simple numerical fit curves are provided, as shown in the figures. These curves, which are for empirical applications, are useful only for low to medium values of T_{amb} and A . A practical engineering relationship consistent with the physics of radiative transfer at higher frequencies has yet to be derived.

For space communications engineers interested primarily in long-term statistics of the signal fading levels, the empirical method of generating the long-term fading statistics from radiometric data is to first establish the correlation between the radiometric sky temperature and signal fading level by analyzing several reliable records obtained during prominent precipitation events, such as the one shown in Figure 2-3a. This

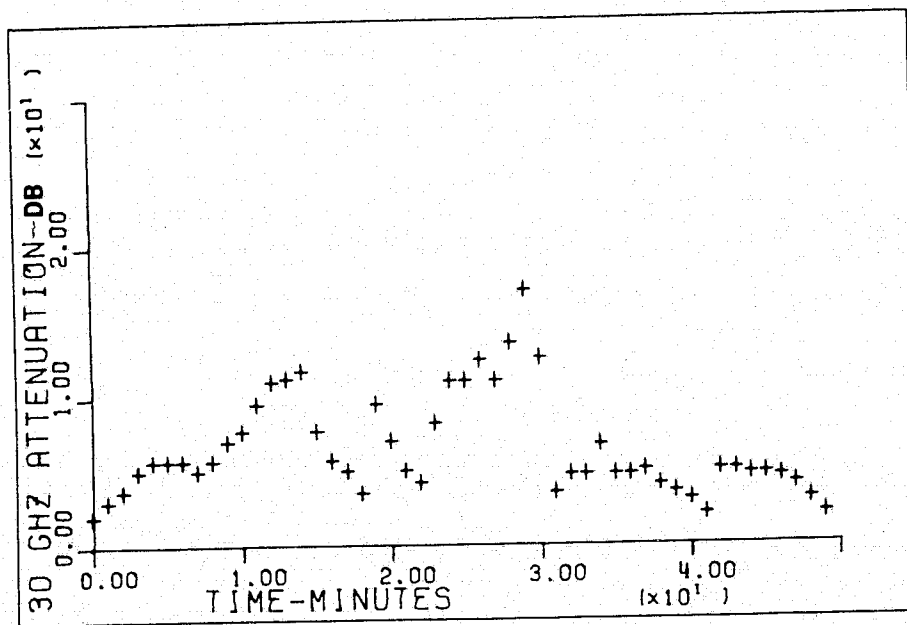
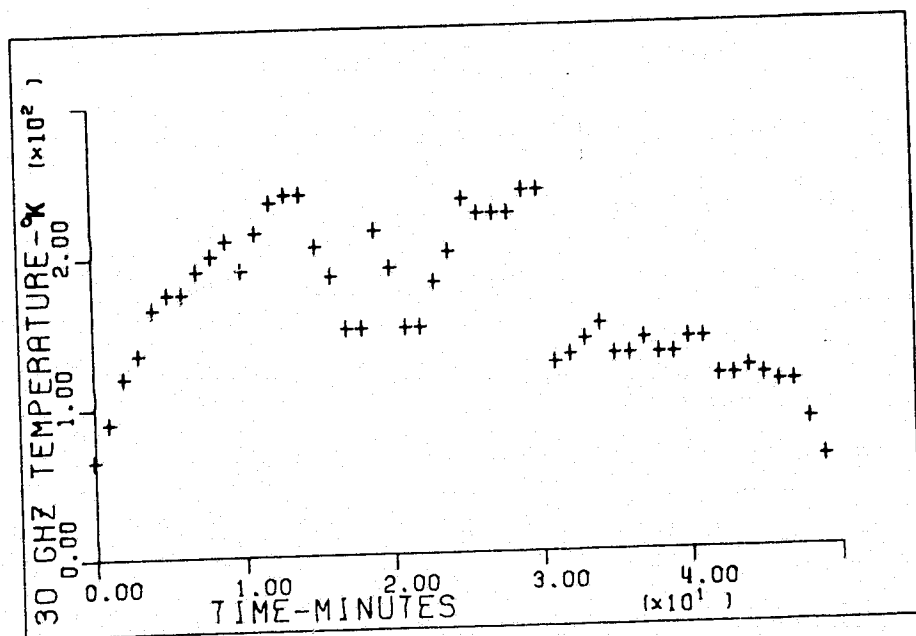


Figure 3-2a. Simultaneous Record of Radiometric Sky Temperature and Satellite Beacon Signal at 30 GHz for an Event of June 6, 1975

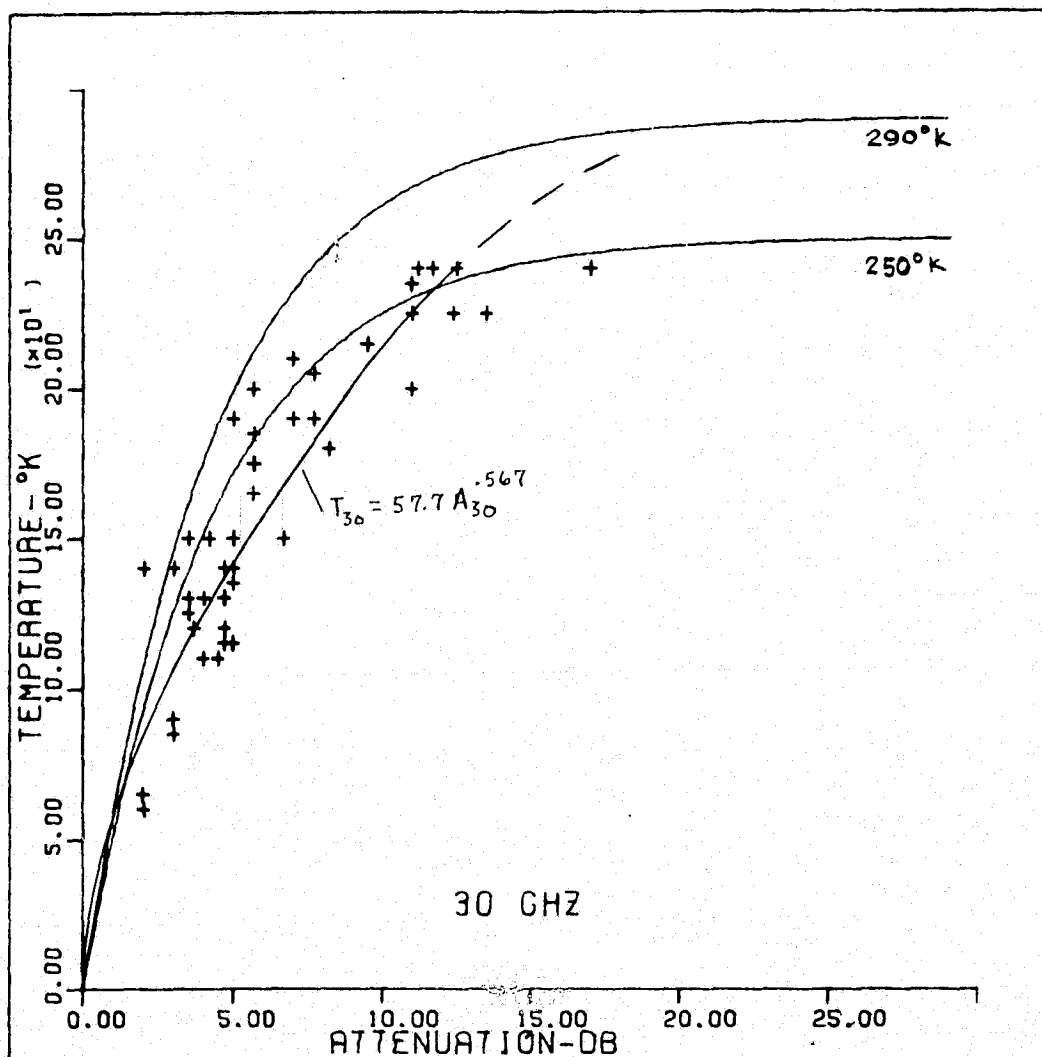


Figure 3-2b. Scattergram of Figure 3-2a [top two curves are based on equation (3-1) with $T_{amb} = 250 \text{ K}$ and 290 K , respectively]

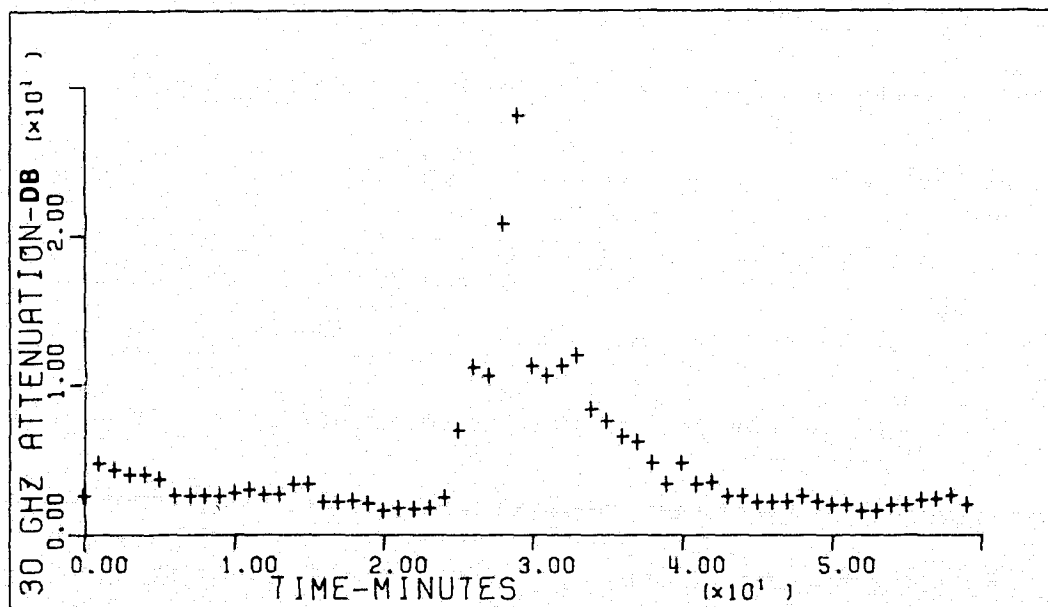
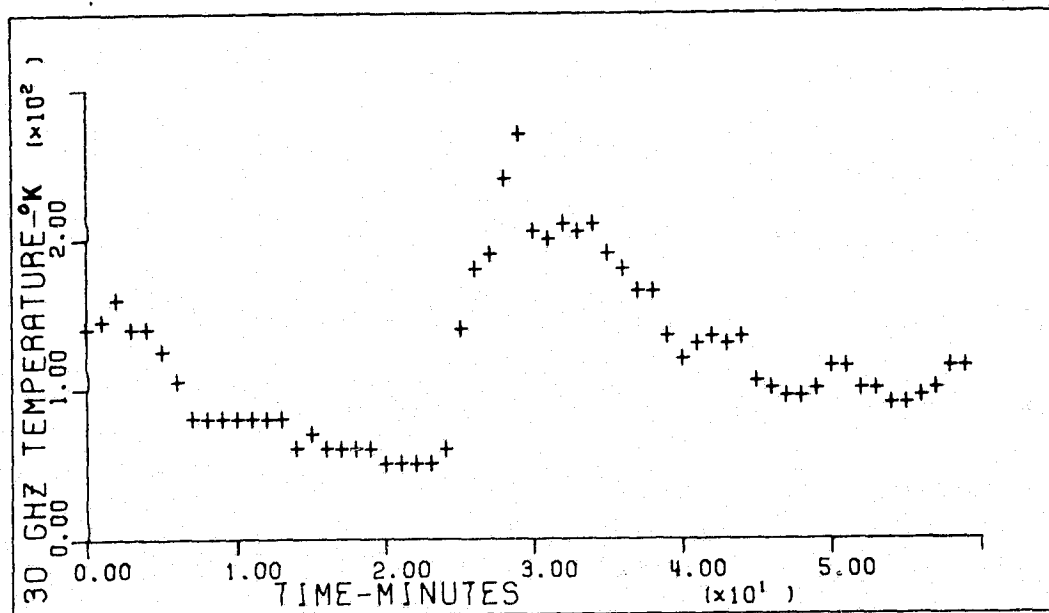


Figure 3-2c. Simultaneous Record at 30 GHz for
an Event of May 16, 1975

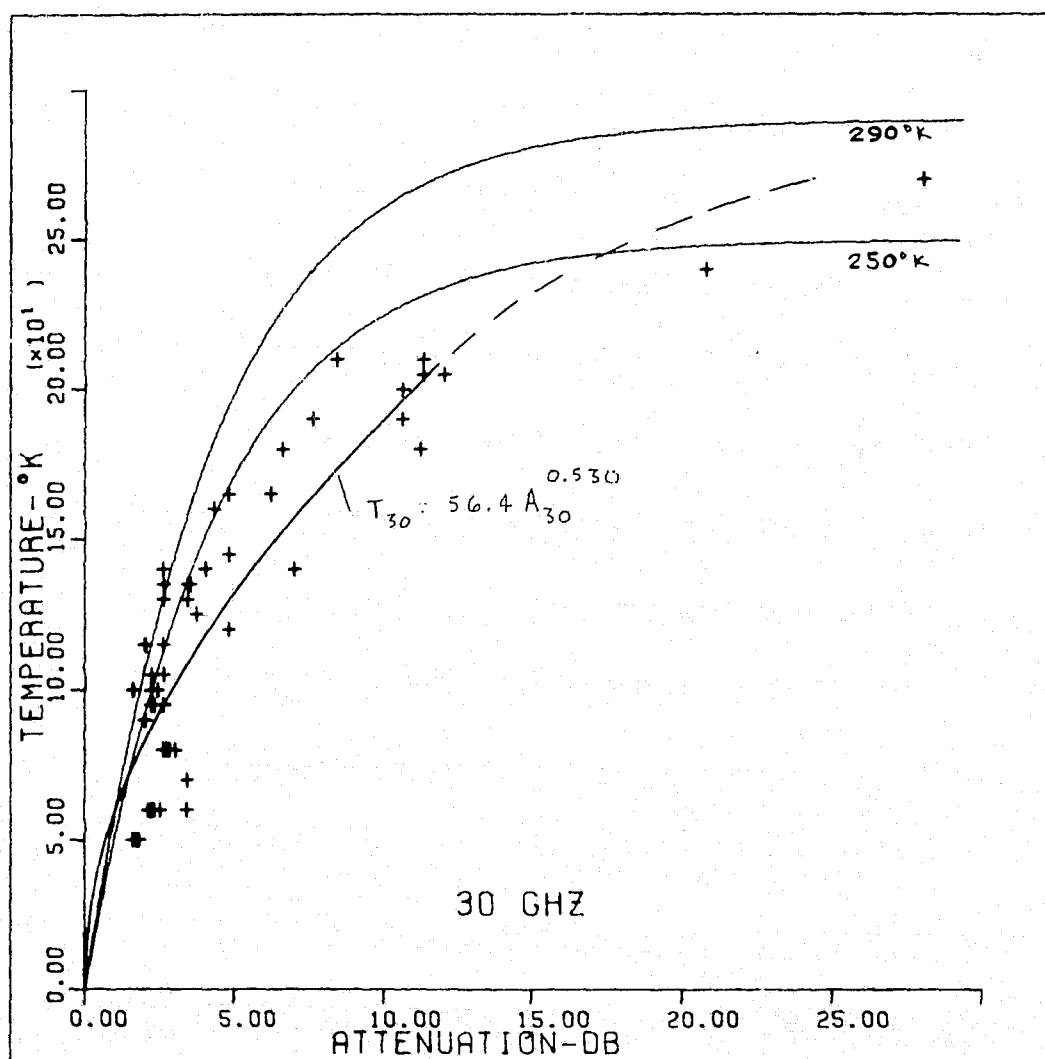


Figure 3-2d. Scattergram of Figure 3-2c

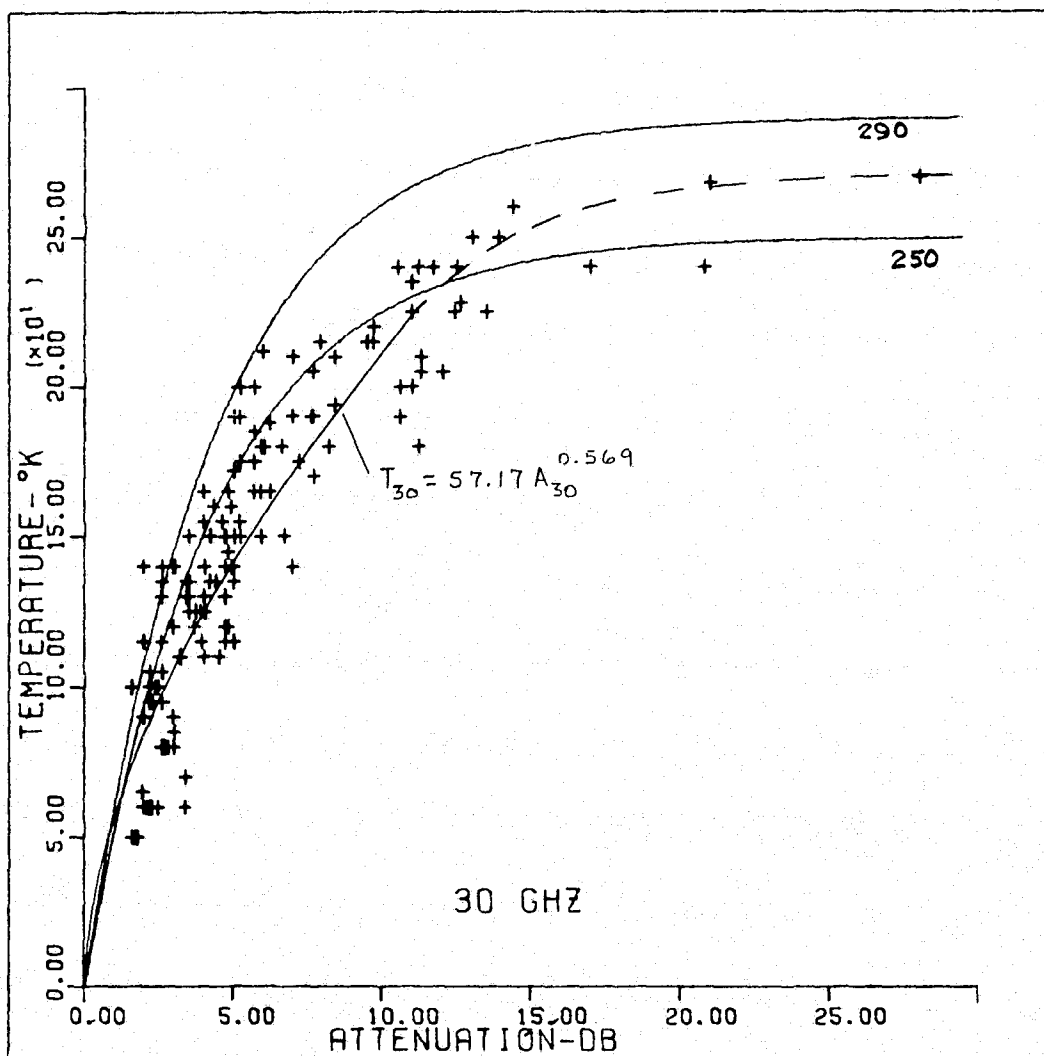


Figure 3-3. Composite Scattergram of All the Simultaneous Records of Radiometric Sky Temperatures vs Satellite Beacon Signals at 30 GHz (the best numerical fit curve is $T_{30} = 57.17 A_{30}^{0.569}$)

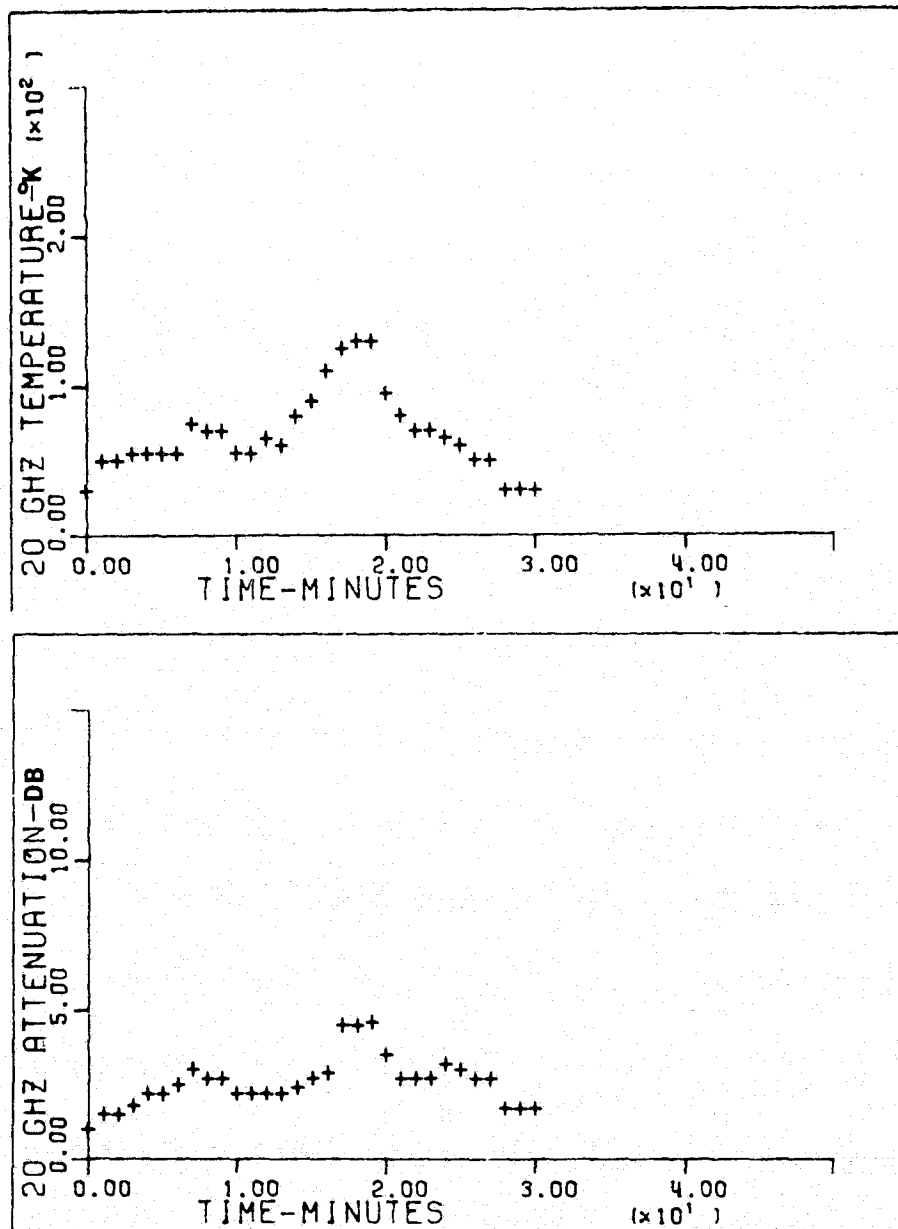


Figure 3-4a. Simultaneous Record of Radiometric Sky Temperature and Satellite Beacon Signal at 20 GHz for an Event of June 7, 1975

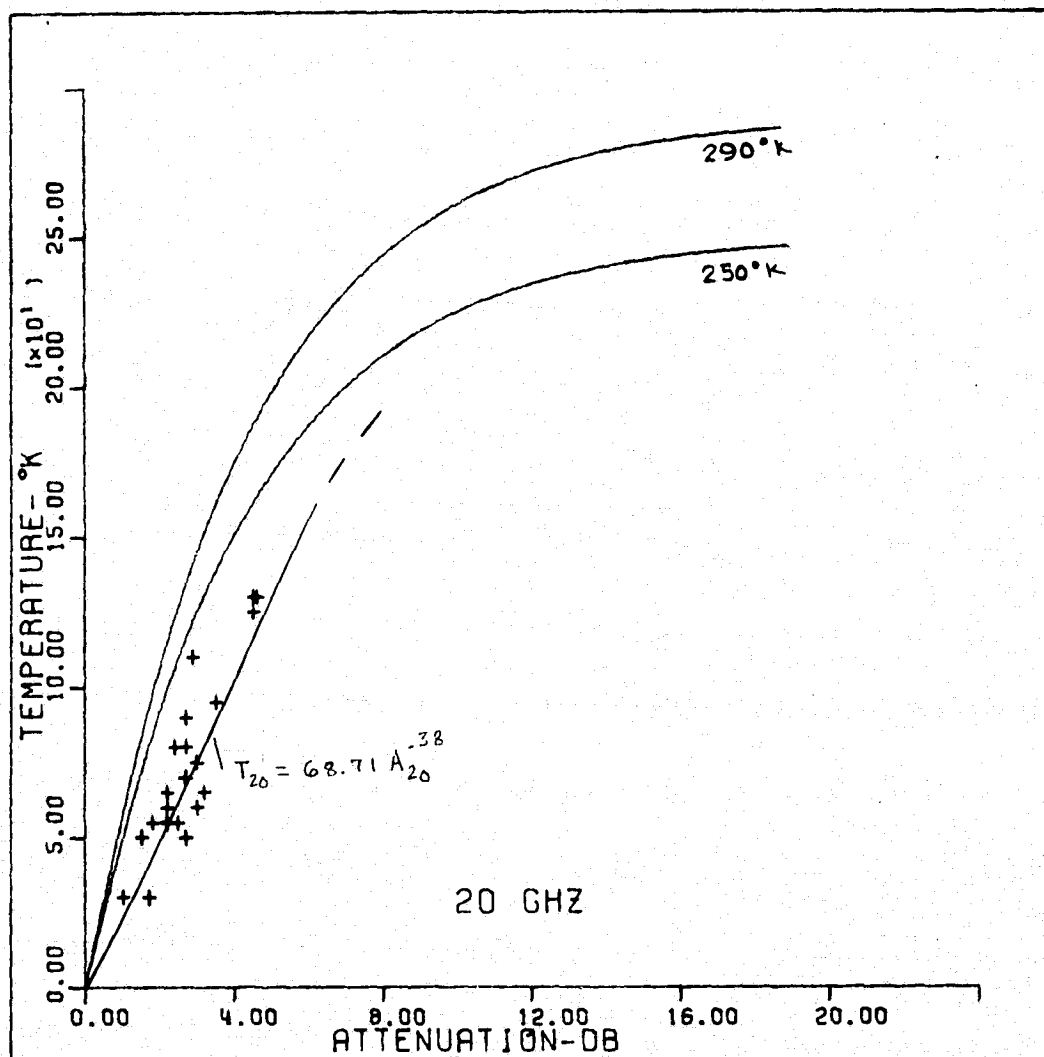


Figure 3-4b. Scattergram of Figure 3-4a [top two curves are based on equation (3-1) with $T_{amb} = 250$ K and 290 K, respectively]

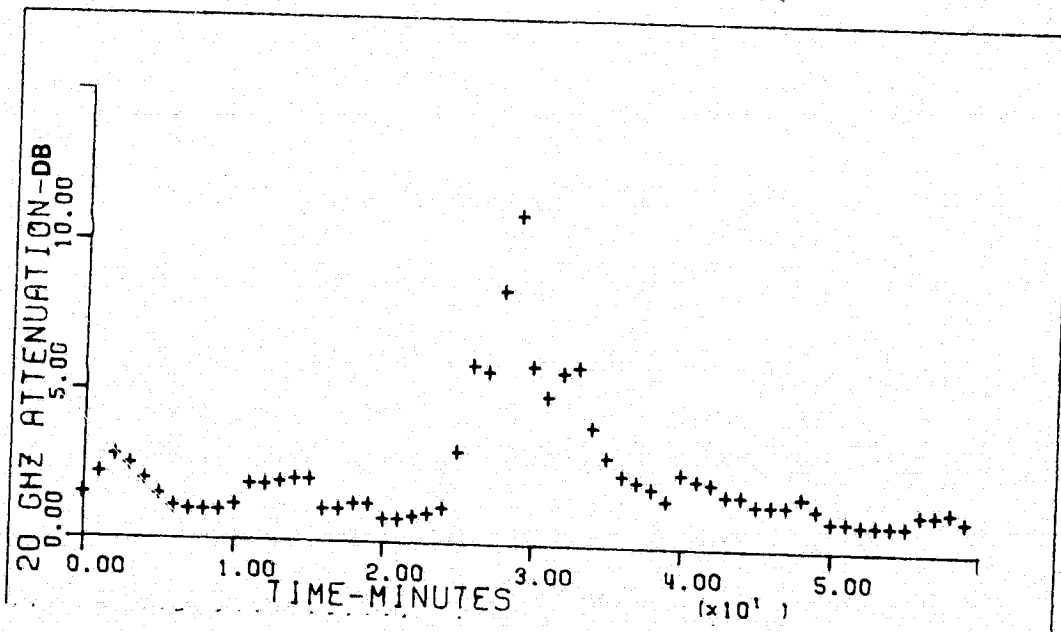
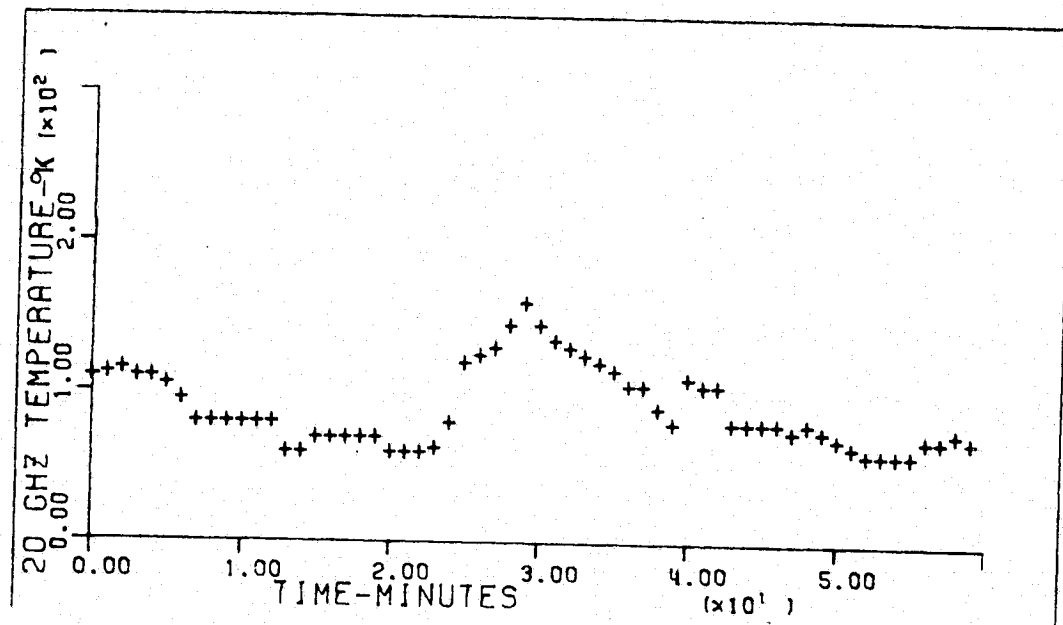


Figure 3-4c. Simultaneous Record at 20 GHz for
an Event of May 16, 1975

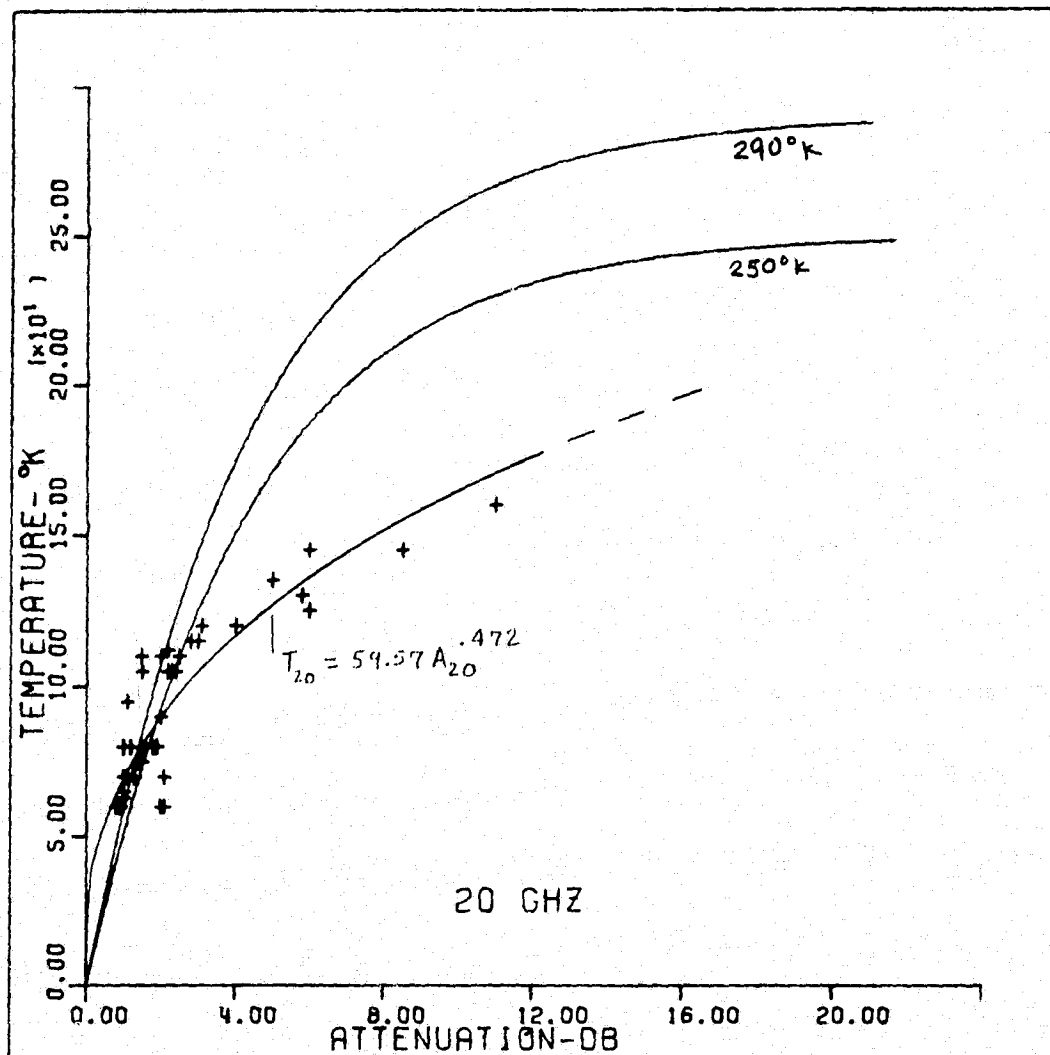


Figure 3-4d. Scattergram of Figure 3-4c

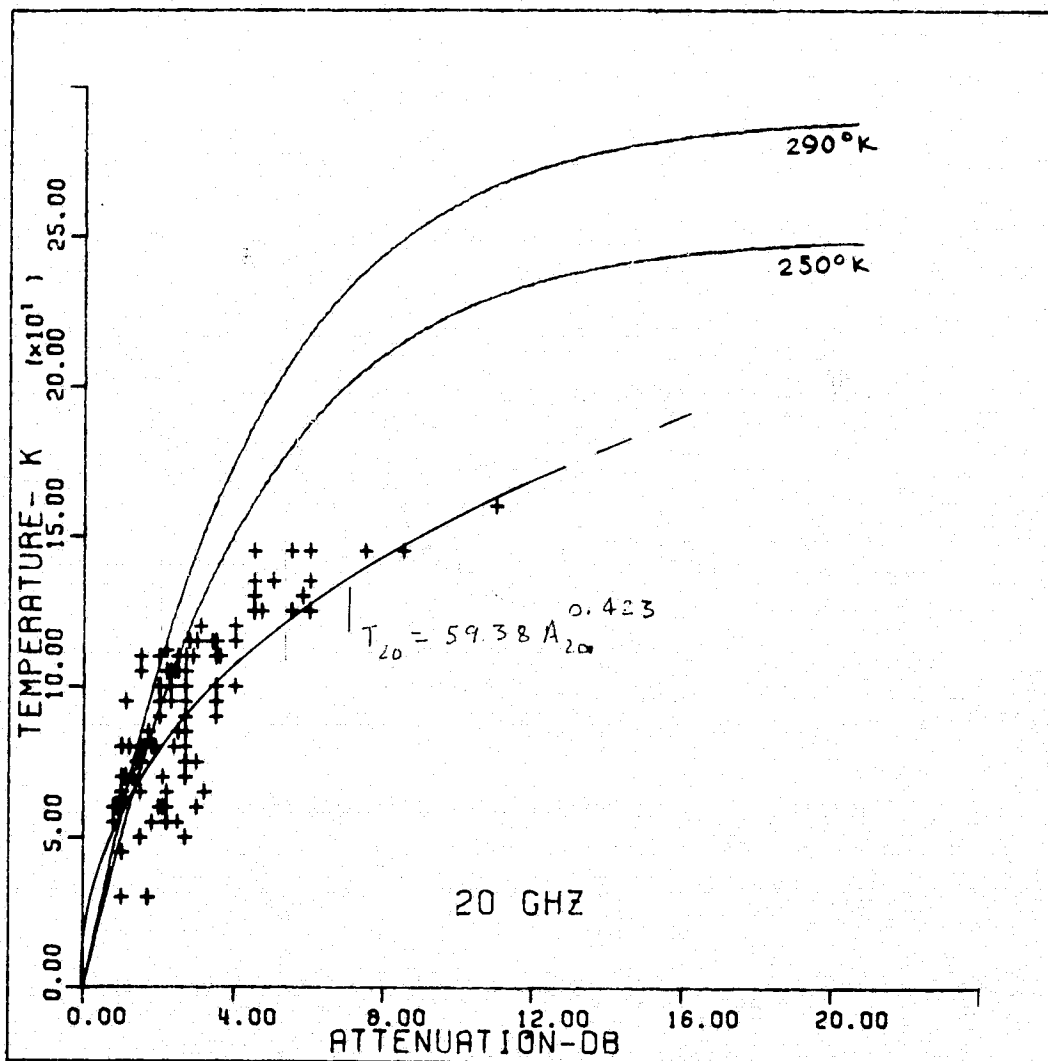


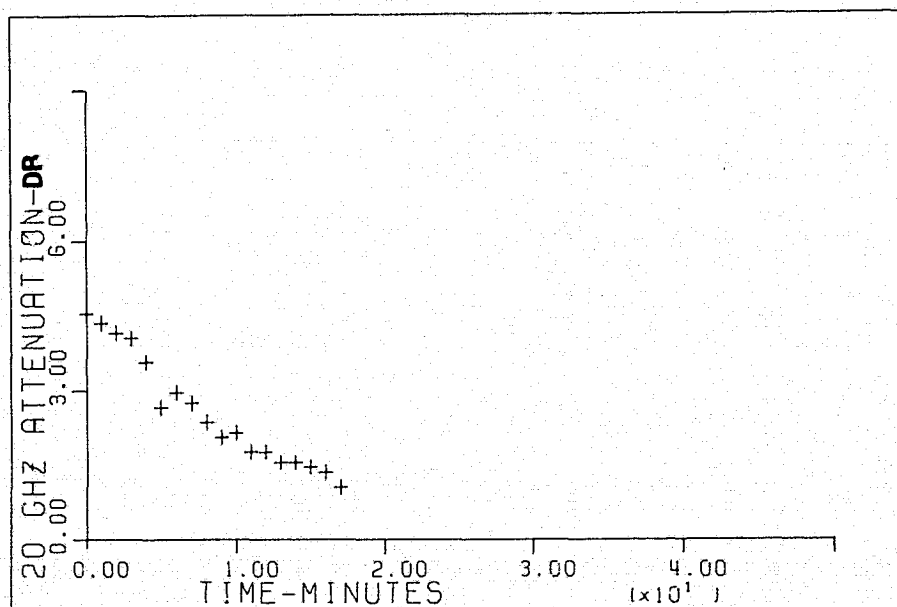
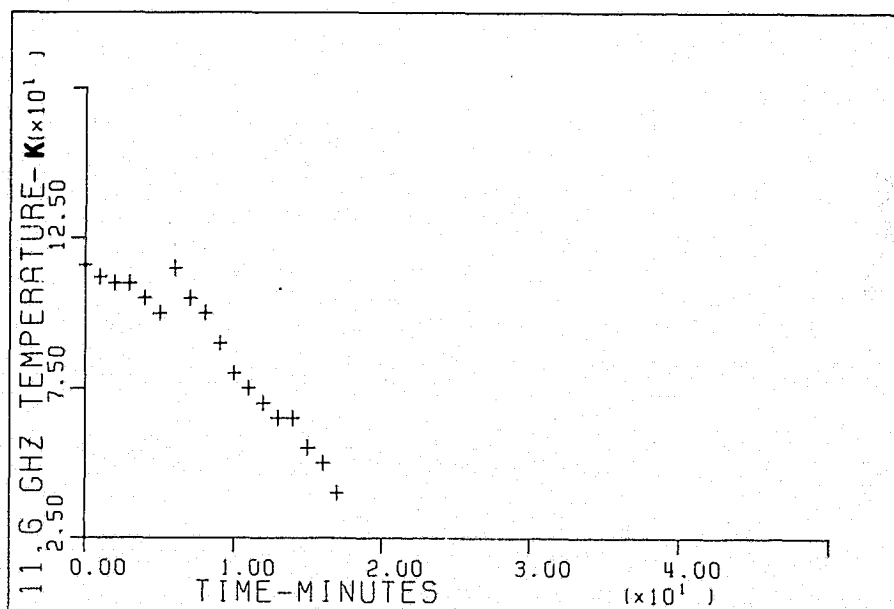
Figure 3-5. Composite Scattergram of All the Simultaneous Records of Radiometric Sky Temperatures vs Satellite Beacon Signals at 20 GHz (the best numerical fit curve is $T_{20} = 59.38 A_{20}^{0.423}$)

correlation is then used as a general guideline for scaling the large amount of radiometric data. This method is also consistent with the general approach of the ATS-6 20/30-GHz MWE, as stated in Section 1.

The correlations between the 11.6-GHz sky temperature and the 20-GHz beacon signal level for prominent individual events are plotted in Figure 3-6; Figure 3-7 is a composite plot for all the events. Again, data points corresponding to a beacon signal level less than 1 dB are omitted from the figures. Empirical curves obtained by numerical fitting of the data are summarized in Table 3-1. Based on the composite data, the following relationship is derived:

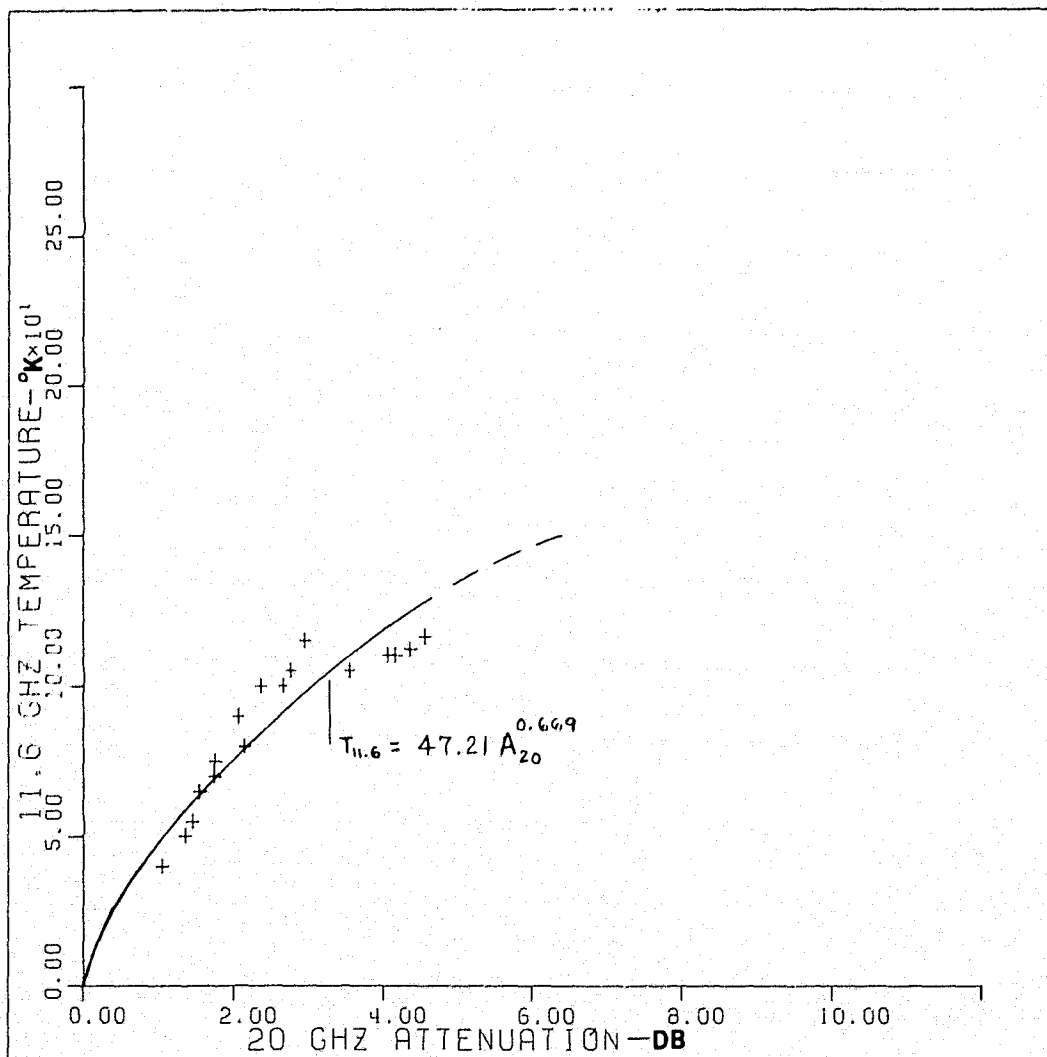
$$A_{20} \text{ (dB)} = 7.418 \times 10^{-4} T_{11.6}^{1.8215} \quad (3-2)$$

where A_{20} is the beacon signal attenuation at 20 GHz and $T_{11.6}$ is the sky temperature measured by the 11.6-GHz radiometer. The 1-year $T_{11.6}$ data obtained at Clarksburg have been analyzed, and the final results are presented in Figure 3-8. Since the $T_{11.6}$ reading could not be precise at high temperatures, the cumulative statistics for A_{20} greater than 10 dB are shown as a dashed line.



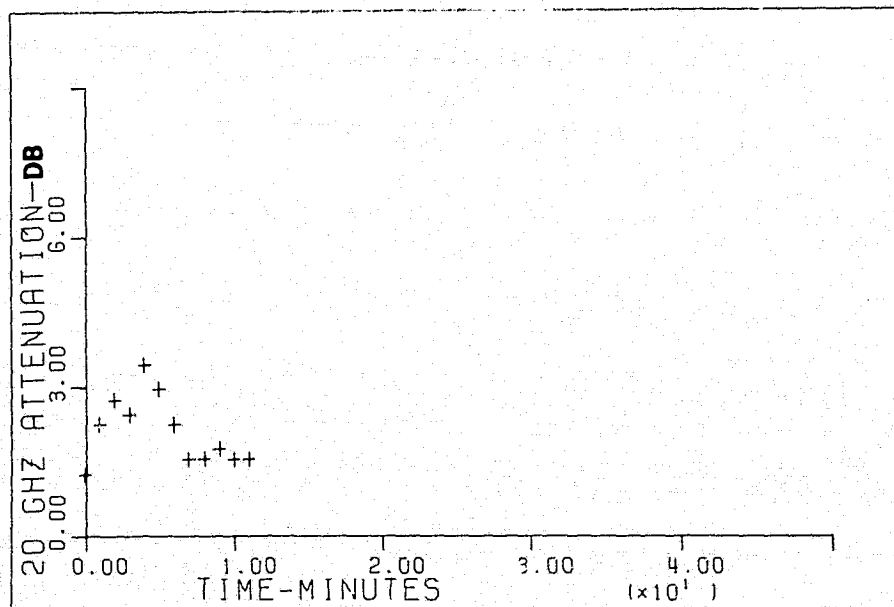
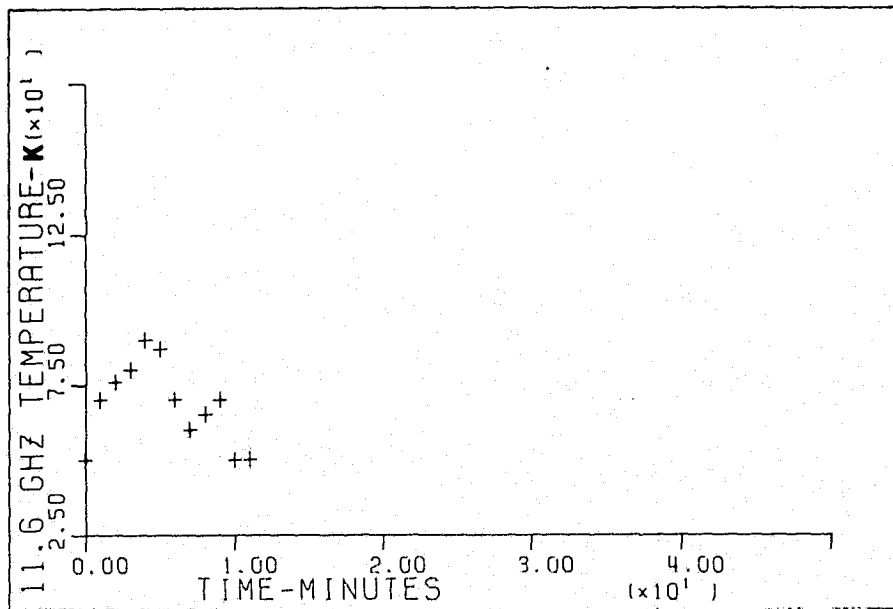
a. Temperature and Attenuation vs Time for
Event of October 16, 1974

Figure 3-6. Simultaneous Records of Radiometric Sky
Temperatures at 11.6 GHz and Satellite Beacon
Signals at 20 GHz and Their Corresponding
Scattergrams (sheet 1 of 10)



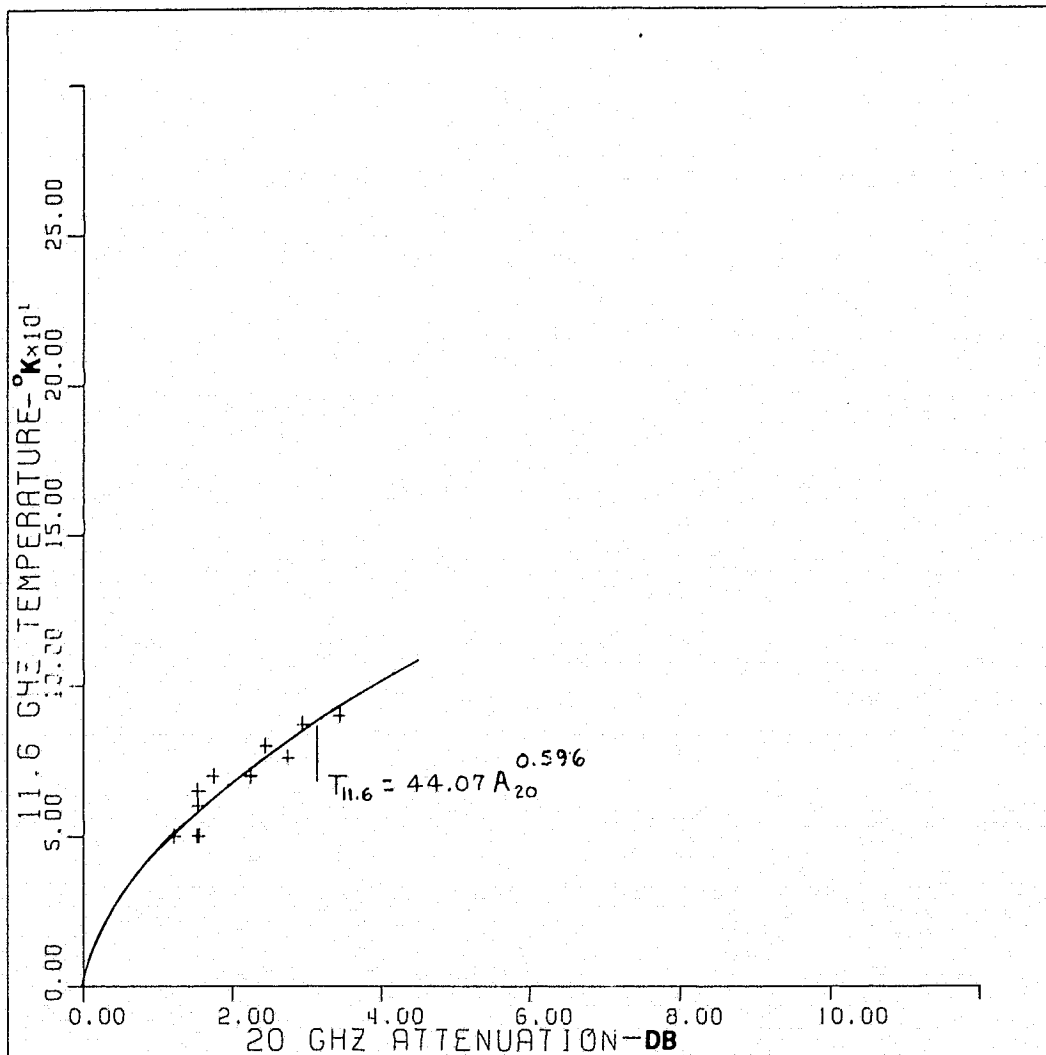
b. Temperature vs Attenuation for Event
of October 16 1974

Figure 3-6. Simultaneous Records of Radiometric Sky
Temperatures at 11.6 GHz and Satellite Beacon
Signals at 20 GHz and Their Corresponding
Scattergrams (sheet 2 of 10)



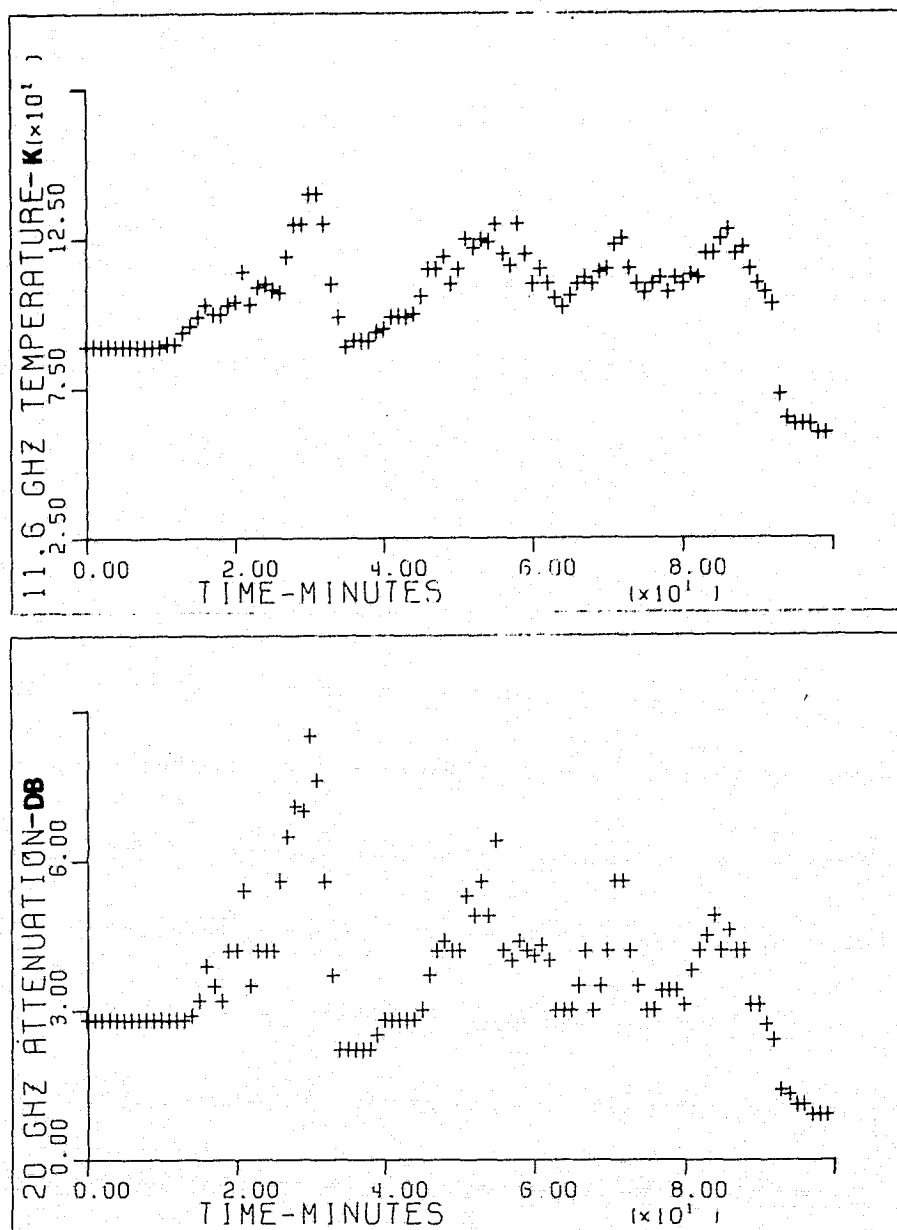
c. Temperature and Attenuation vs Time for
Event of November 25, 1974

Figure 3-6. Simultaneous Records of Radiometric Sky
Temperatures at 11.6 GHz and Satellite Beacon
Signals at 20 GHz and Their Corresponding
Scattergrams (sheet 3 of 10)



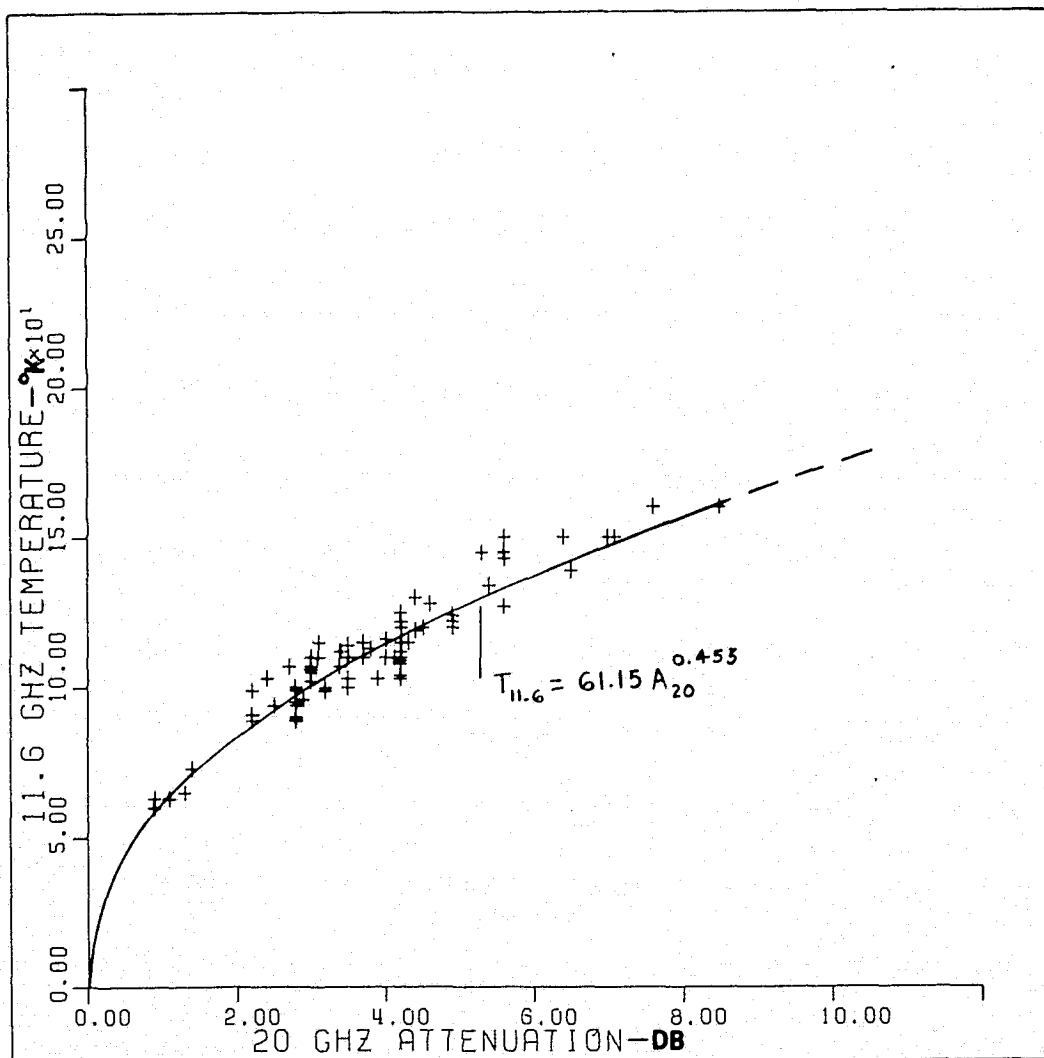
d. Temperature vs Attenuation for Event
of November 25, 1974

Figure 3-6. Simultaneous Records of Radiometric Sky
Temperatures at 11.6 GHz and Satellite Beacon
Signals at 20 GHz and Their Corresponding
Scattergrams (sheet 4 of 10)



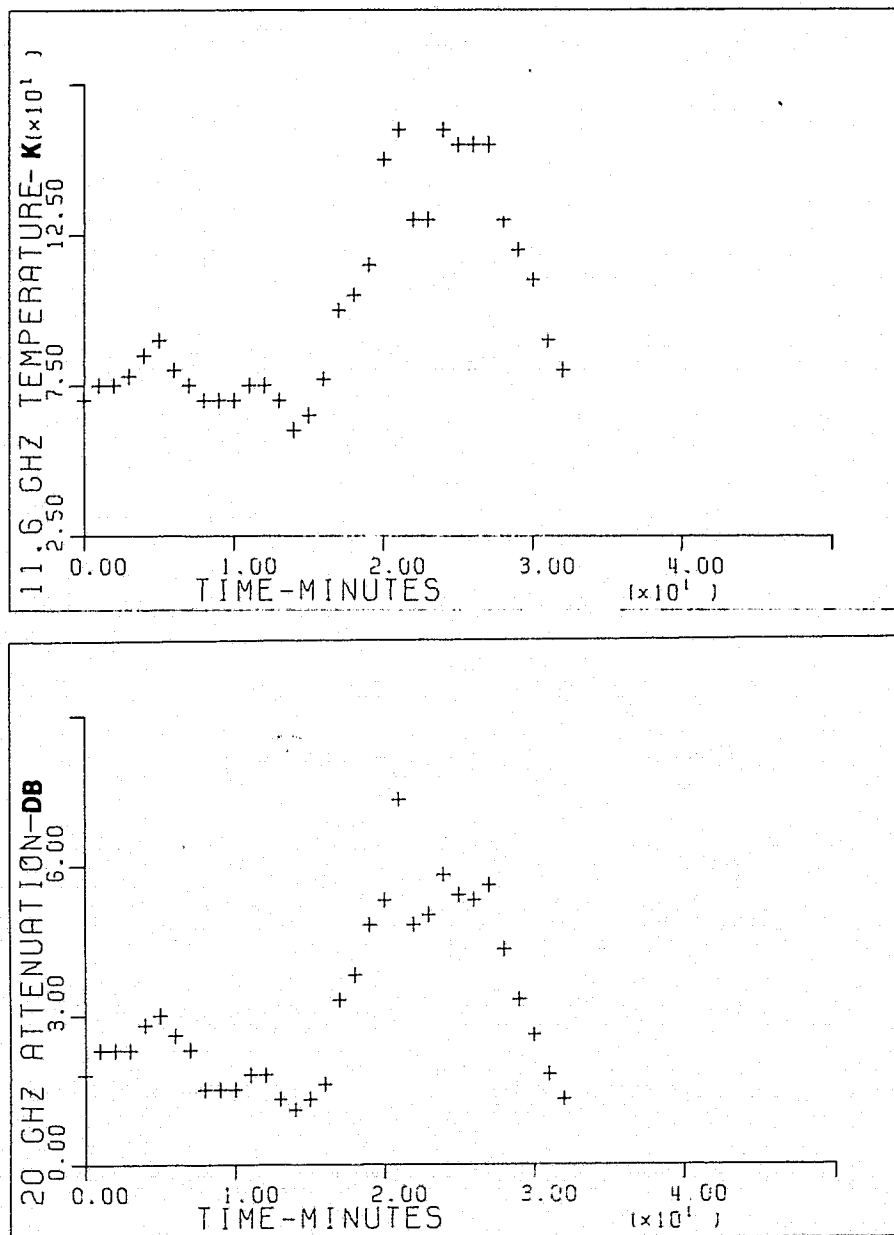
e. Temperature and Attenuation vs Time for
Event of March 19, 1975

Figure 3-6. Simultaneous Records of Radiometric Sky
Temperatures at 11.6 GHz and Satellite Beacon
Signals at 20 GHz and Their Corresponding
Scattergrams (sheet 5 of 10)



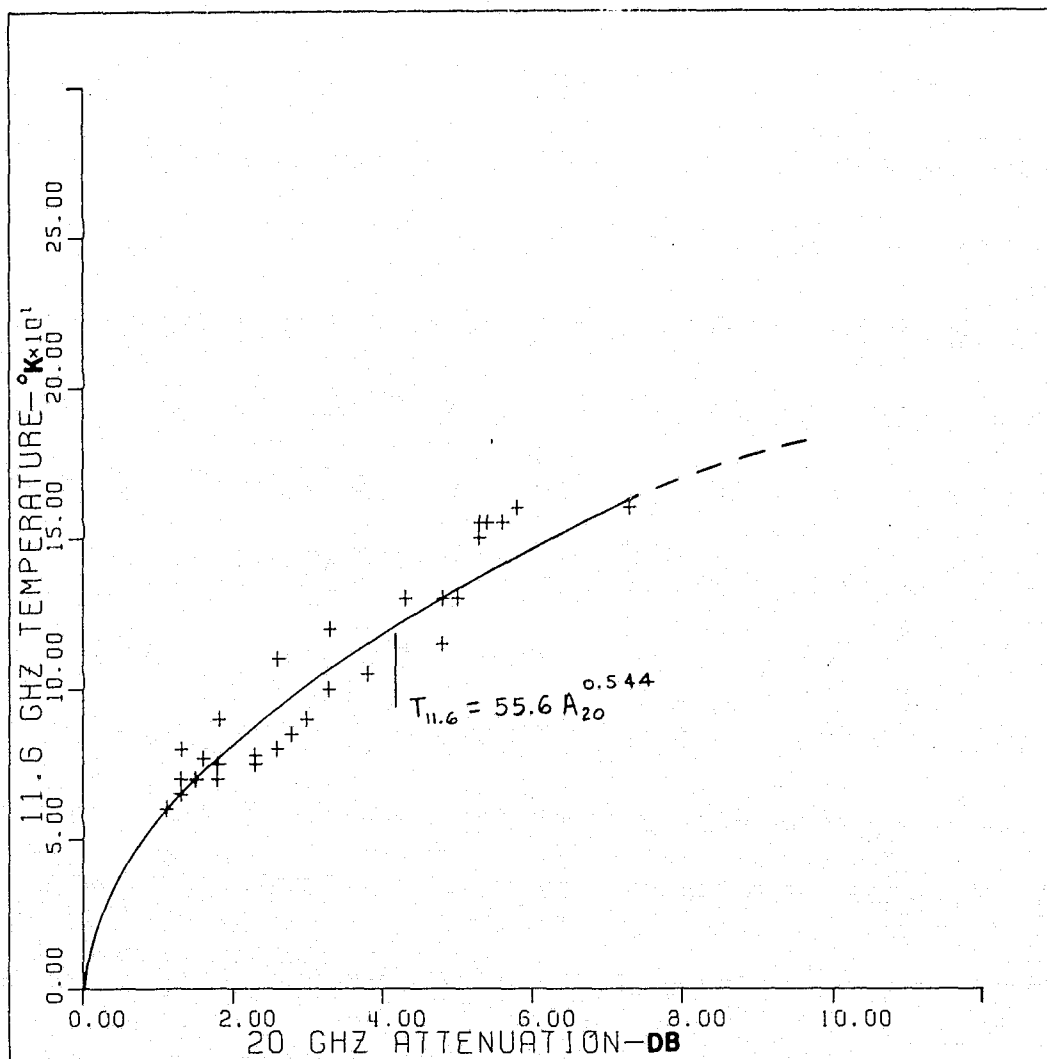
f. Temperature vs Attenuation for Event
of March 19, 1975

Figure 3-6. Simultaneous Records of Radiometric Sky
Temperatures at 11.6 GHz and Satellite Beacon
Signals at 20 GHz and Their Corresponding
Scattergrams (sheet 6 of 10)



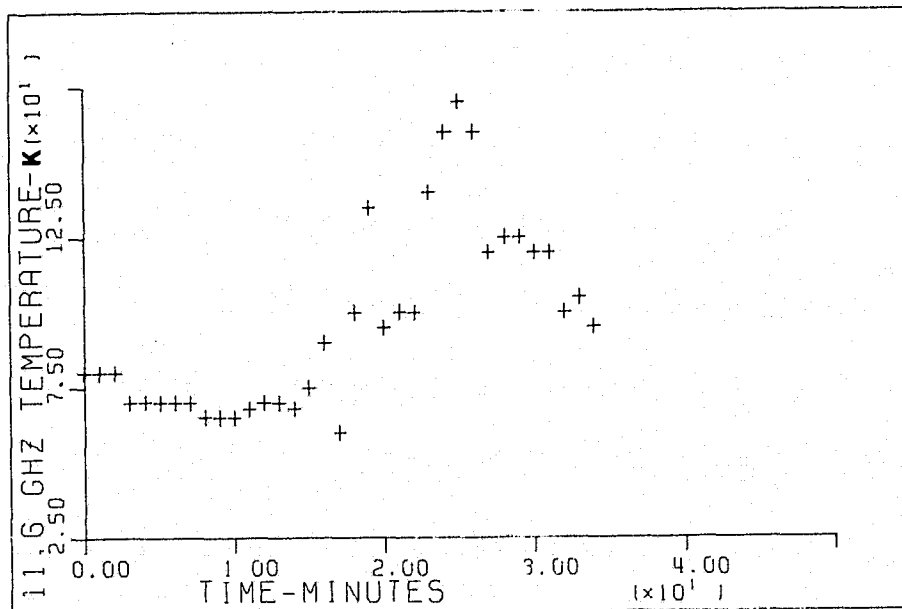
g. Temperature and Attenuation vs Time for Event of April 29, 1975

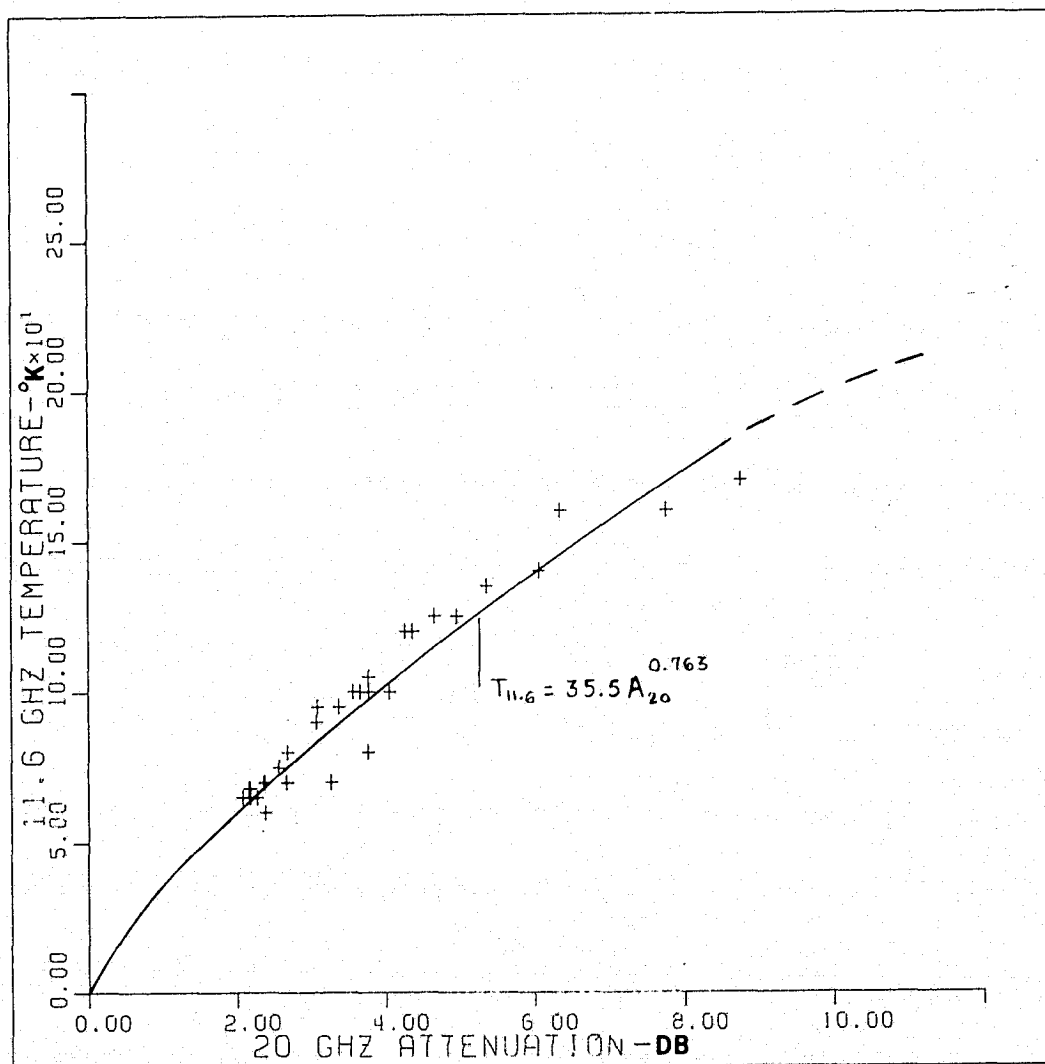
Figure 3-6. Simultaneous Records of Radiometric Sky Temperatures at 11.6 GHz and Satellite Beacon Signals at 20 GHz and Their Corresponding Scattergrams (sheet 7 of 10)



h. Temperature vs Attenuation for Event
of April 29, 1975

Figure 3-6. Simultaneous Records of Radiometric Sky
Temperatures at 11.6 GHz and Satellite Beacon
Signals at 20 GHz and Their Corresponding
Scattergrams (sheet 8 of 10)





j. Temperature vs Attenuation for Event
of May 22, 1975

Figure 3-6. Simultaneous Records of Radiometric Sky
Temperatures at 11.6 GHz and Satellite Beacon
Signals at 20 GHz and Their Corresponding
Scattergrams (sheet 10 of 10)

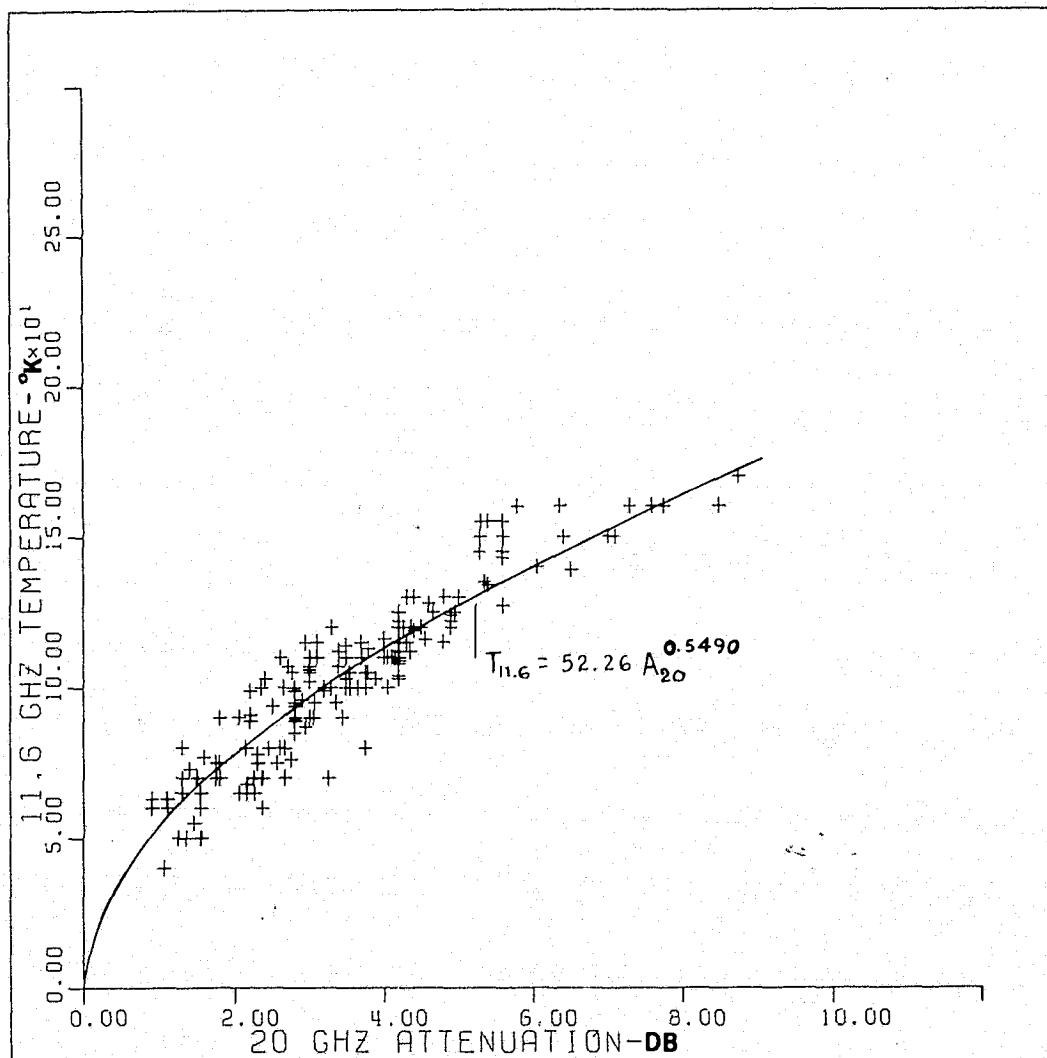


Figure 3-7. Composite Scattergram of Radiometric Sky Temperature at 11.6 GHz vs Satellite Beacon Signal at 20 GHz (the numerical fit curve is $T_{11.6} = 52.26 A_{20}^{0.5490}$)

Table 3-1. Summary of $T_{11.6} = \alpha A_{20}^{\beta}$ Numerical Fitting

| Event Date | Figure No. | Total Minutes of Data | α | β | Normalized Correlation Coefficient |
|-------------------|------------|-----------------------------|----------|---------|--|
| October 16, 1974 | 3-6a, 3-6b | 18 | 47.2104 | 0.6685 | 0.9298 |
| November 25, 1974 | 3-6c, 3-6d | 12 | 44.0706 | 0.5962 | 0.9106 |
| March 19, 1975 | 3-6e, 3-6f | 100 | 61.1552 | 0.4525 | 0.9540 |
| April 29, 1975 | 3-6g, 3-6h | 33 | 55.6229 | 0.5435 | 0.9406 |
| May 22, 1975 | 3-6i, 3-6j | 35 | 35.5146 | 0.7630 | 0.9457 |
| Composite | 3-7 | 198 | 52.2651 | 0.5490 | 0.9029 |

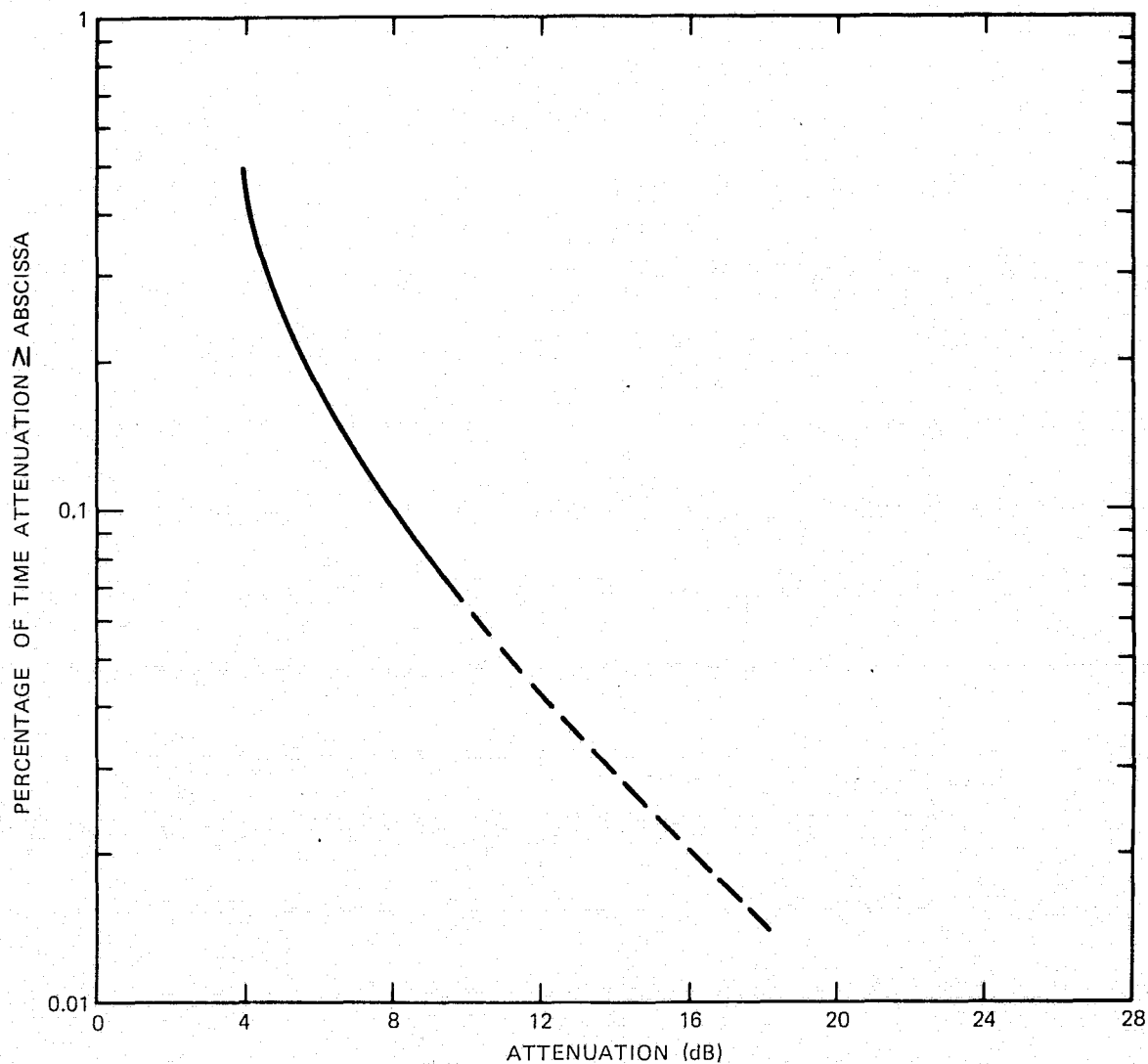


Figure 3-8. 20-GHz Cumulative Attenuation Statistics
Derived from 11.6-GHz Radiometric Data Based on
Empirical Equation (3-2)

4. RAIN GAUGE EXPERIMENT

A basic problem in estimating the microwave attenuation over a satellite-earth propagation path based on rain gauge data is that, for a given storm event, the attenuation and the rainfall records very often do not have a consistent detailed correlation. As shown in Figure 2-3a, while the correlation between the radiometer curve and the satellite signal level is good, the rain gauge data do not have a consistent correlation with the 20-GHz curve. A particularly puzzling point is the peak registered on the rain gauge 3.23 km away from the receiver.

The lack of consistency in correlation is not uncommon. For example, in an earlier ATS-5 15.3/31.65-GHz NASA experiment at Rosman, North Carolina,⁷ it was found that neither the ground-averaged nor the height-averaged rainfall data of 10 rain gauges beneath the boresight path exhibited a sufficiently detailed correlation with the satellite signals. Hence, the correlation could be made meaningful only by literally shifting the time scale of the rain gauge data so that the peaks of the rainfall matched the peaks of the signal attenuation. This shifting scheme has been widely employed for determining the fading depth versus precipitation rate in both satellite beam signal and radiometric experiments. The theoretical basis for such a scheme has yet to be established.

In the present COMSAT experiment, data with such apparent discrepancies in time and magnitude have been collected and analyzed. A new model has been established for adjusting the rain gauge data by taking into consideration the different falling times of raindrops of different sizes. This model can effectively account for the fact that the rain rate registered at one instant on a ground rain gauge away from the receiver is actually responsible for wave attenuation at an earlier instant when the

rainfall intercepts the slant propagation path. For instance, correlations of the March 19 event shown in Figure 2-3a can be improved markedly after the falling time adjustment is made. Details of the model have been published in Reference 11, which is included as Appendix B.

Further improvement of the model is obviously desired. Most importantly, the wind motion, which certainly affects the falling processes of raindrops, has been completely omitted. Evaporation, condensation, sublimation, accretion, and coalescence are all involved to different degrees. In addition, it is necessary to consider the positions of the rain gauges with reference to the height of the rain cloud and the characteristic size of the rain cells; both are dependent upon the rain type and other meteorological conditions. As a general rule, to avoid the discrepancy between the precipitation rate determined by attenuation and the precipitation rate derived from the rain gauge fields, the rain gauges should be placed so that the evaluation of the rain rate is interpolated to an elevation lower than the boundary of the rain cloud and so that the distance between rain gauges is smaller than the characteristic size of the rain cells. The model may also be significantly refined by using other drop size distributions such as the Joss distribution, which is more appropriate for thunderstorms in certain climatological regions than the Laws and Parsons distribution.

Another aspect of the rain gauge data analysis is the cumulative precipitation statistics, $T(R)$. These statistics have been compiled and plotted as a solid line in Figure 4-1 based on records of the rain gauge for the 3-meter system from October 1, 1974, to September 30, 1975. The annual accumulated rainfall depth for the period is 1100 mm. It is of interest to compare this curve with that derived from the Rice and Holmberg model,¹² which has been widely used by systems engineers to scale

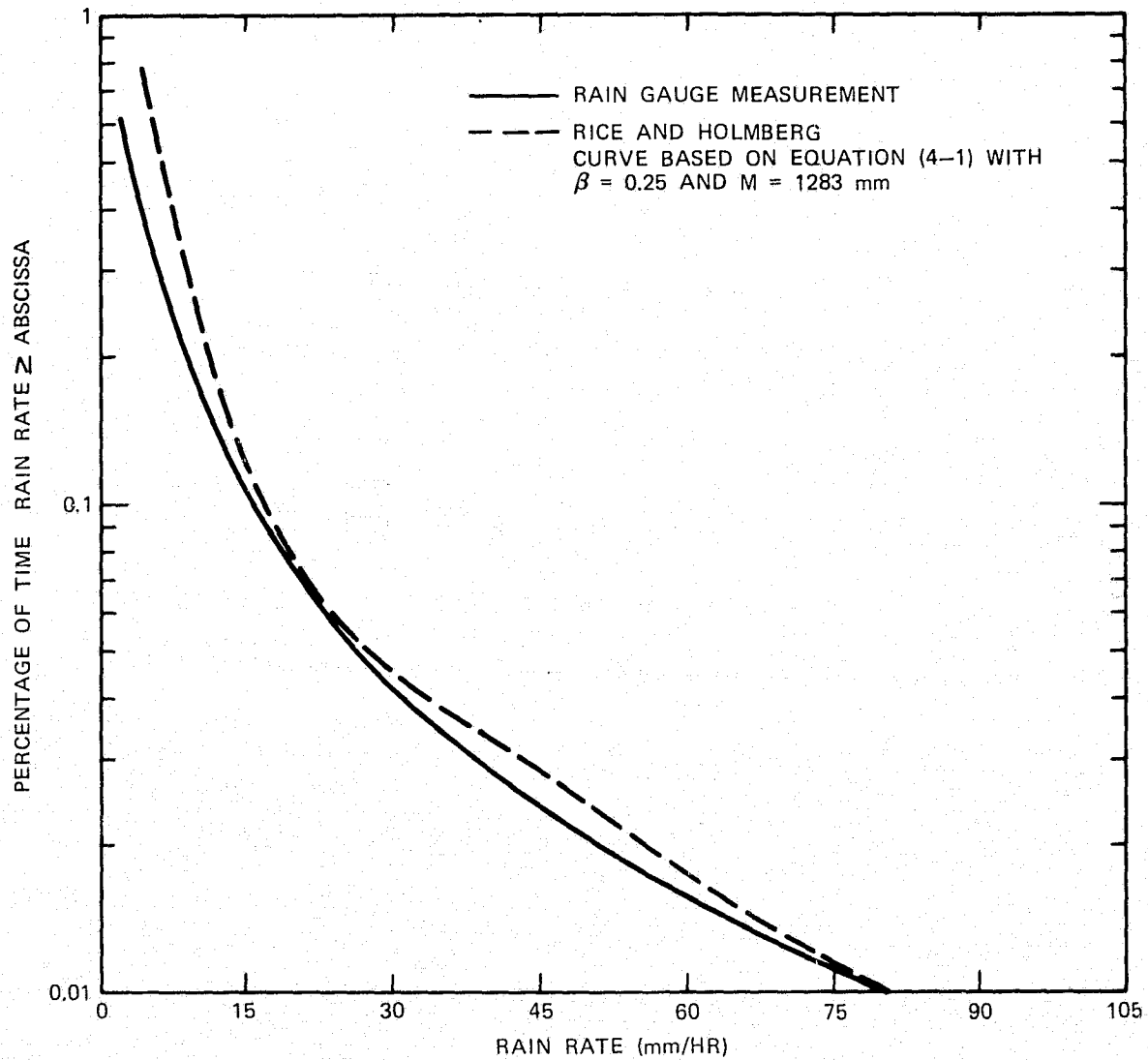


Figure 4-1. Cumulative Statistics of Precipitation
at Clarksburg, Maryland

empirically cumulative statistics, with simple precipitation data from local weather bureau records as the only input.

Based on past knowledge,¹⁰ the model for the Clarksburg area yields

$$T(R) = \frac{100}{24 \times 365} M \left\{ 0.03\beta e^{-0.03R} + 0.2(1 - \beta) \cdot \left[e^{-0.258R} + 1.86 e^{-1.63R} \right] \right\} \quad (4-1)$$

where β , the ratio of annual thunderstorm rainfall depth to M , the total annual rainfall depth, has been designated as 0.25. The value of M estimated from tabulations of the local weather stations for the 1-year period beginning October 1, 1974, is 1283 mm. (As a result of the saturation of the tipping bucket mechanism, the rain gauges used in the experiment would register a relatively lower volume of rain rate in heavy storm events. Hence, the higher value of M [1283 mm as opposed to 1100 mm] was not unexpected.) The Rice and Holmberg curve of $T(R)$ for $M = 1283$, shown as a dashed line in Figure 4-1, is reasonably close to the solid curve for cumulative statistics less than 0.1 percent. Incidentally, if $M = 1100$ in equation (4-1), the curve will be almost a direct overlay of the solid curve. For all practical purposes, the Rice and Holmberg model is sufficient for scaling the cumulative statistics.

It should be noted that the model's annual rainfall depth factor, M , can have a year-to-year variation of over 20 percent. For example, the total rainfall depth of September 1975, a wet month, was about 250 mm more than that of September 1974, a dry month. If the annual period is shifted one month forward, i.e., from September 1, 1974, to August 31, 1975, the total rainfall depth will not be 1283 mm, but will be only about 1040 mm. It therefore appears that the Rice and Holmberg model may not be as consistent as desired from one year to another.

5. SATELLITE BEACON EXPERIMENT

As stated in Section 1, an important limitation of the satellite beacon experiment was the infrequency of beacon transmissions during precipitation events. Although regular weekly transmission times averaging about one hour per day were assigned to COMSAT for data collection and equipment calibration, precipitation rarely occurred on-site at these times. Requests to NASA ATS Operations Control Center for 20/30-GHz beacon transmission when precipitation was occurring or anticipated seldom resulted in positive responses. There were also occasions when beacon transmissions were abruptly terminated while valuable experimental data in thunderstorm conditions were being collected.

Figure 5-1 consists of scattergrams for prominent events of beacon signal fading at 20 and 30 GHz. Least-mean-square regression fittings of the form

$$A_{30} = \alpha A_{20}^{\beta} \quad (5-1)$$

were performed. The values of α and β range from 1.9 to 2.18 and from 0.997 to 1.06, respectively, with the values of fitting over all the samples given as

$$\alpha = 1.989, \quad \beta = 1.06 \quad (5-2)$$

as shown in Figure 5-1d. All of these values are remarkably consistent with those generated by NASA based on its measurement of ATS-6 MWE 20/30-GHz signals at Rosman, North Carolina, and Greenbelt, Maryland.⁸

The equations given by Medhurst,¹³ which are improved versions of the equations based on Rayleigh assumptions,¹ can be

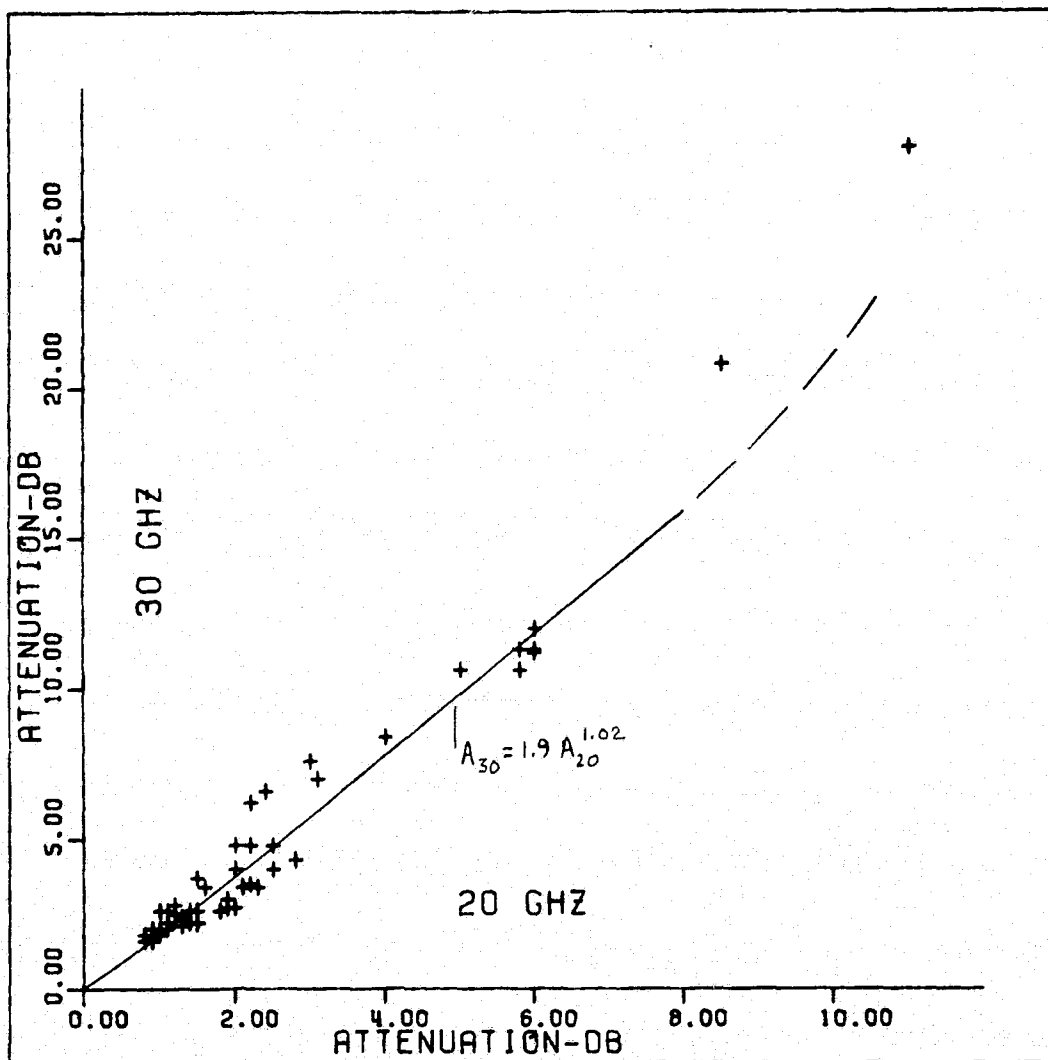


Figure 5-1a. Scattergram of 30-GHz vs 20-GHz
Attenuation Recorded May 16, 1975

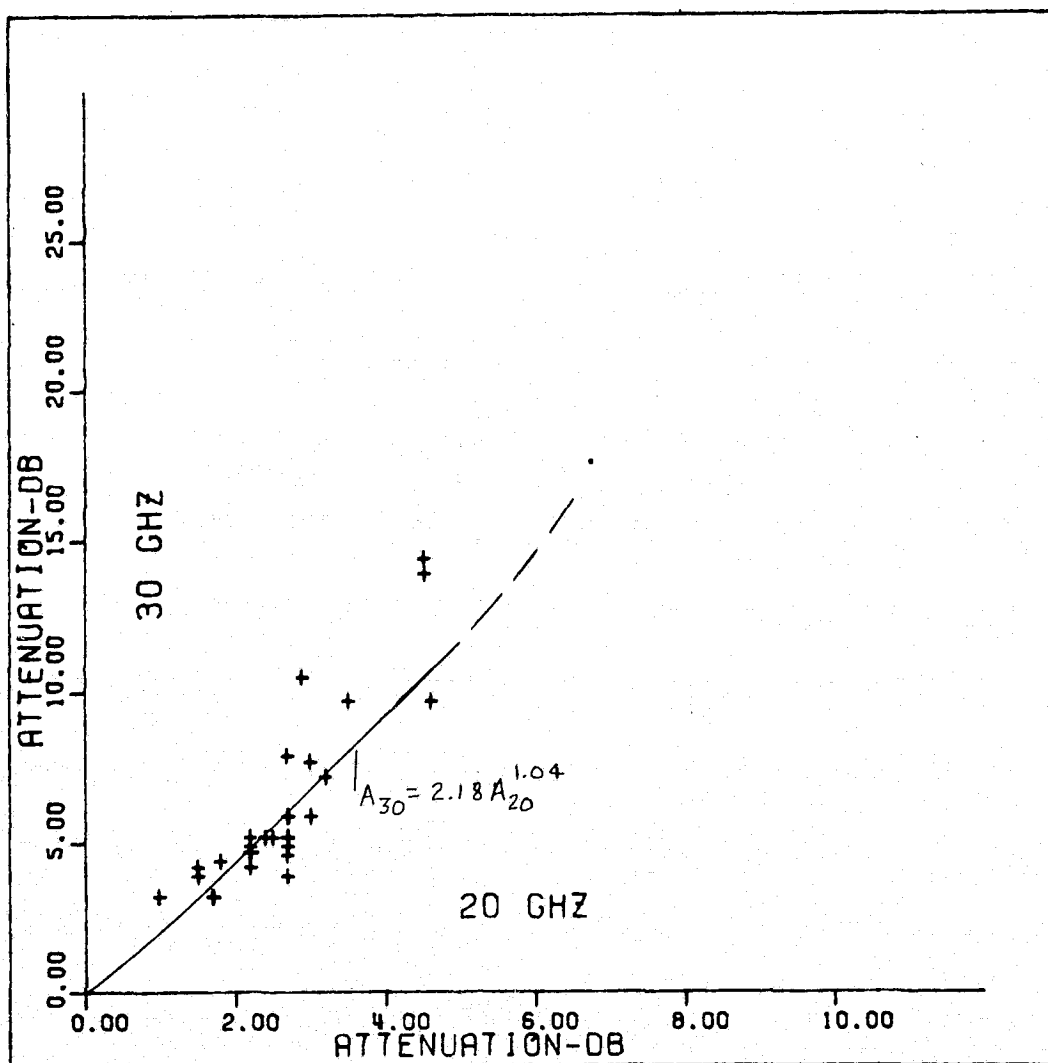


Figure 5-1b. Scattergram of 30-GHz vs 20-GHz
Attenuation Recorded June 7, 1975

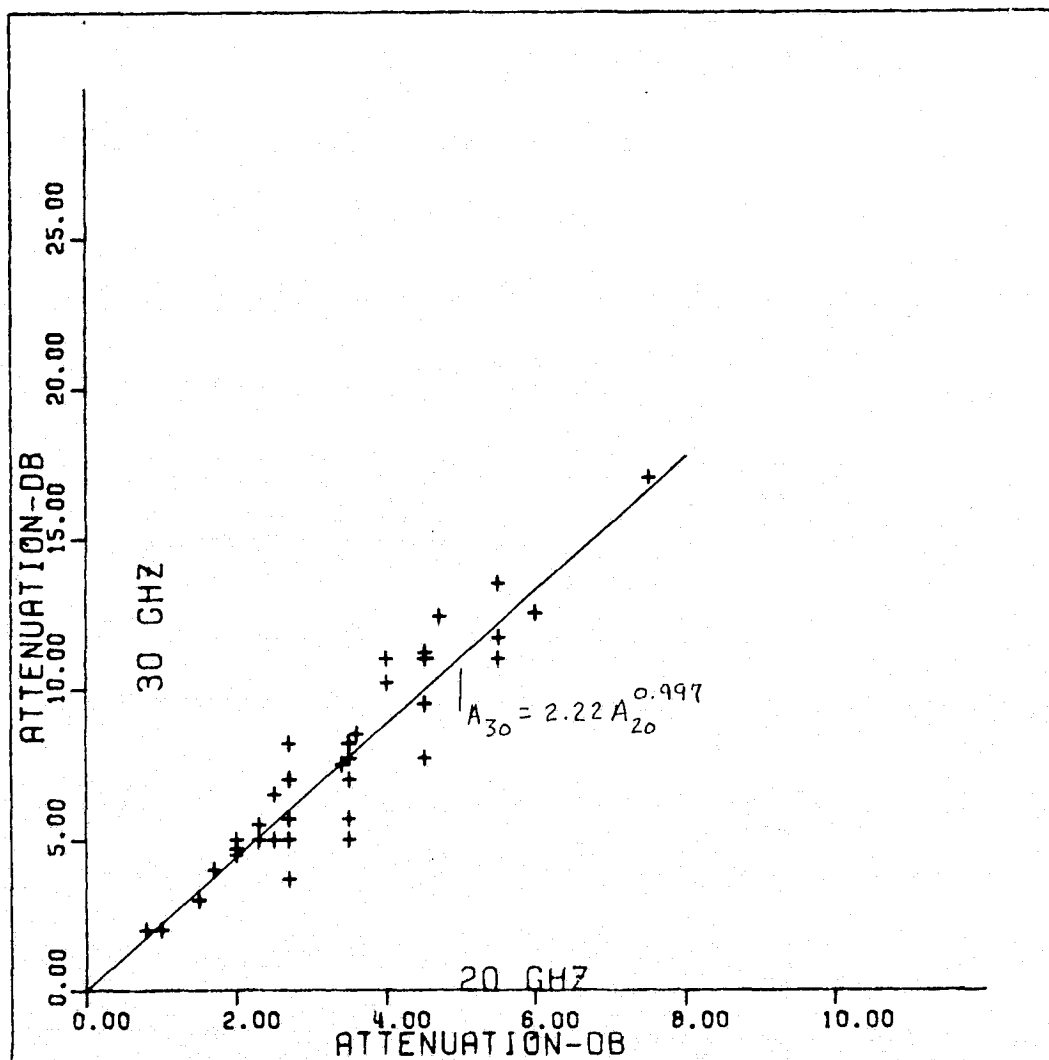


Figure 5-1c. Scattergram of 30-GHz vs 20-GHz
Attenuation Recorded June 6, 1975

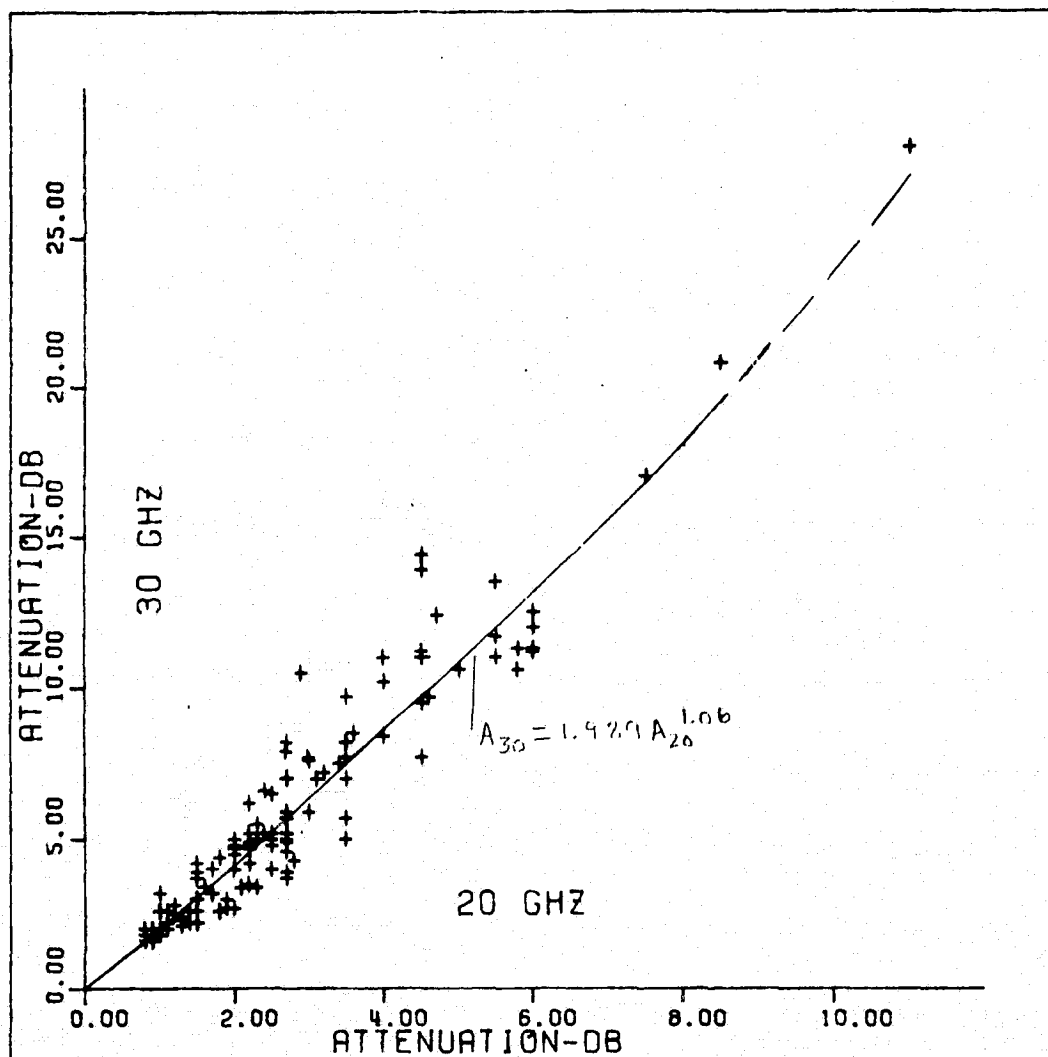


Figure 5-1d. Composite Scattergram of 30-GHz vs 20-GHz Attenuation from All Available Simultaneous Records

used to postulate⁸ the theoretical attenuation relationships at 20 and 30 GHz as

$$A_{20} = 0.0687R^{1.1004} L \quad (5-3a)$$

$$A_{30} = 0.1649R^{1.0353} L \quad (5-3b)$$

where L is the equivalent path length of the precipitation medium. Combining equations (5-3) and (5-1) makes it possible to establish the empirical relationship between L and R:

$$L = \left[\frac{\alpha \times 0.0687^\beta}{0.1649} R^{1.1004 \times \beta - 1.0353} \right]^{1/(1-\beta)} \quad (5-4)$$

for first-order estimations in engineering applications. However, it should be noted that the concept of the effective path length is at most a vague one. Even in a statistical sense, the dependence of L on frequency, elevation angle, and other meteorological factors such as cell size has yet to be understood. Furthermore, the validity of the Rayleigh assumptions at 20 and 30 GHz is not well justified.

In late May 1975 ATS-6 began to move slowly from its original location toward its new position over the Indian Ocean. The path vector elevation angle at the COMSAT Labs' receiver station decreased steadily to zero over a 3-week period. While the 20- and 30-GHz beacon signals were not continuously available, many hours of data were collected at decreasing elevation angles. As ATS-6 approached the horizon (local horizon was at an elevation angle of 1.2°), strong scintillations occurred and in addition there was an increase in the average level of the received signals.

To the first order, the scintillations are believed to be caused by the multipath effect of the signals which rapidly

drift in and out of the receiving antenna beam. Since the beamwidth of an antenna at 30 GHz is much smaller than that at 20 GHz, the scintillations at 30 GHz are more pronounced both in magnitude and frequency than those at 20 GHz. This can be seen from Figure 5-2, which is a typical record of the simultaneous 20- and 30-GHz scintillation measurements.

Although antenna tracking problems and calibration errors, for example, might also have contributed to the signal variations, a continuous effort was made to minimize this effect. The magnitude of the scintillations showed a strong dependence on path elevation angle and local climatological conditions. The peak-to-peak magnitude of the variations increased to more than 10 dB during the final hours of data acquisition near 3.5° elevation angle. In addition, sharp nulls in the signal level, believed to be caused by angle of arrival or low-elevation-angle multipath, were frequently observed. These scintillations had a periodicity ranging from 15 seconds to more than 1 minute and showed a large dependence on the local weather. All of these factors are evident from the records shown in Figures 5-2 and 5-3.

Based on the dynamic range of the receiver and the beamwidth of the antenna, peak-to-peak scintillations of 20 dB or more would be anticipated at low elevation angles. However, scintillations of this magnitude were not observed. The lowest angle at which the satellite made transmissions received at Clarksburg was 3.5°. The path was essentially a treetop path over a flat terrain. During the 2-day period beginning on June 12, 1975, when the satellite descended rapidly from an elevation of 10° to 3.5°, there was persistent precipitation at Clarksburg except during the final two hours. Thus, low-elevation-angle effects under clear sky conditions could not be measured. In fact, the precipitation had contaminated the signal so that the

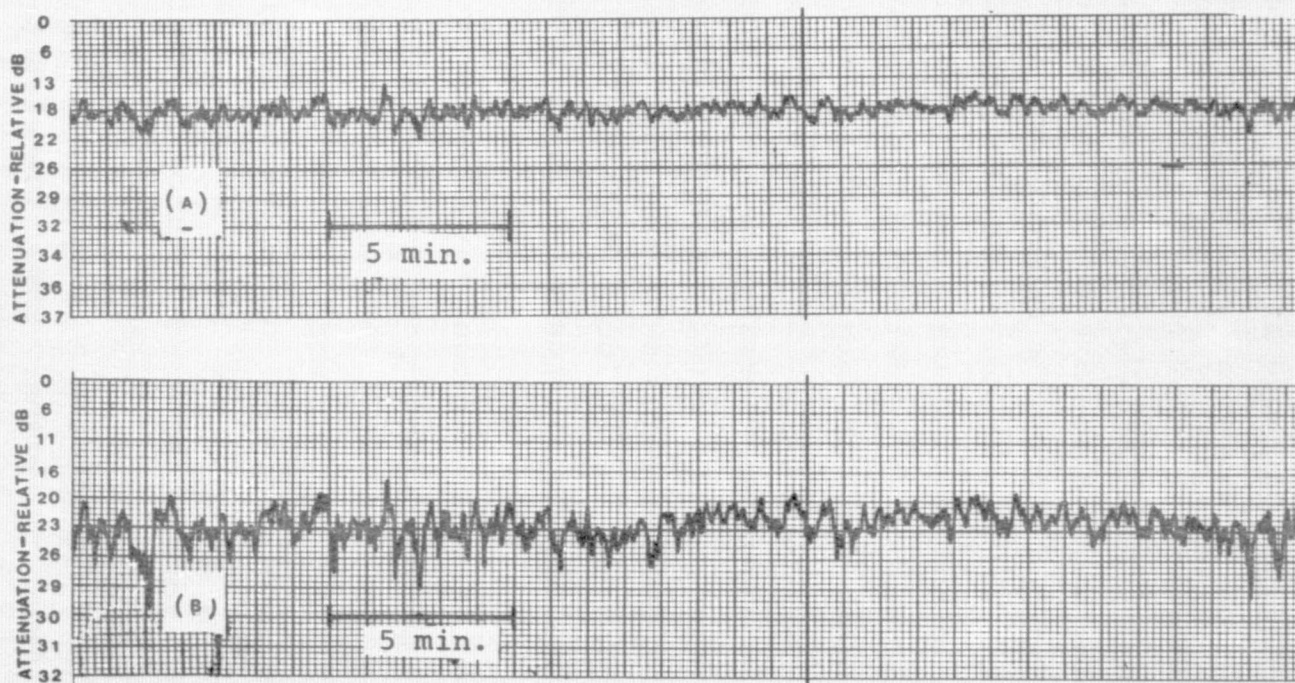


Figure 5-2. Recordings of 20/30-GHz Low-Elevation-Angle Signals
(A and B show steady variations at 20 and 30 GHz, respectively)

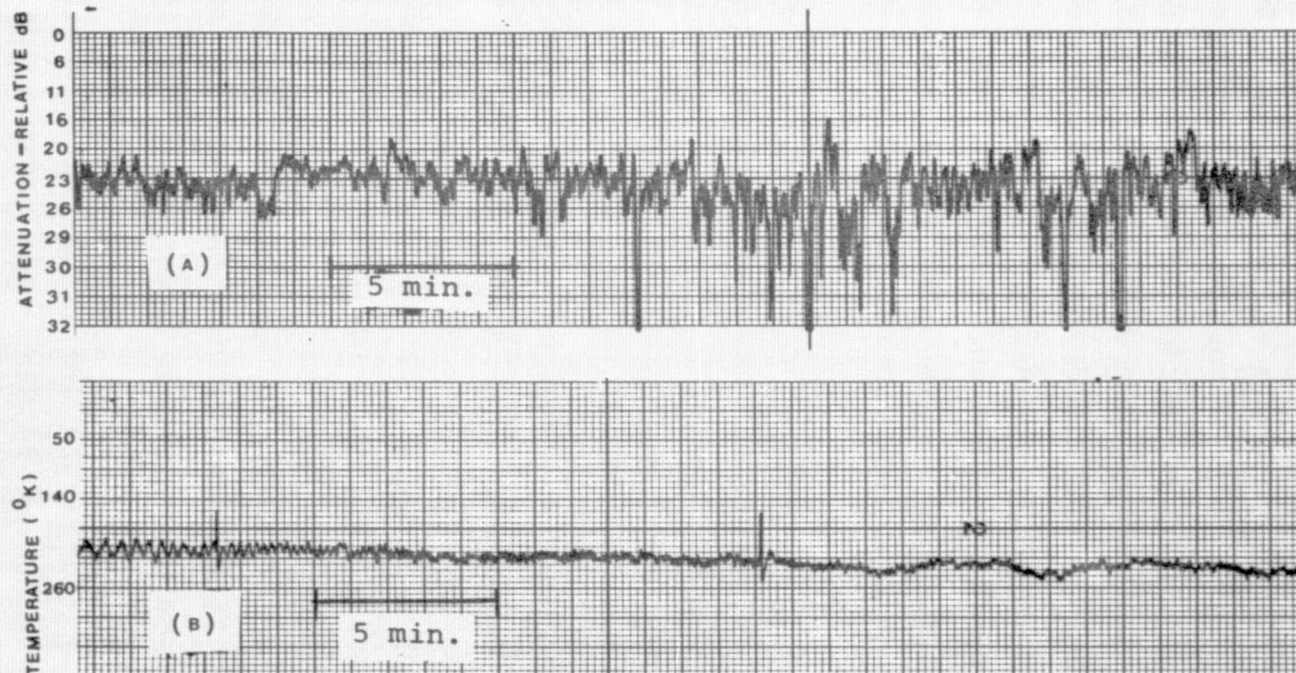


Figure 5-3. 30-GHz Beacon Signals at an Elevation Angle of About 6.5°
 (A and B show simultaneous recordings of 20-GHz ATS-6 signal
 and 30-GHz radiometer as light rain began)

peak-to-peak magnitudes of the fluctuations at 3.5° when the sky was heavily clouded but without precipitation were less than those at higher elevation angles (see Figure 5-4).

The low-elevation-angle scintillations observed at Clarksburg are believed to be a result of the combined effects of angle of arrival changes, refraction and scattering by tropospheric turbulent structures, and precipitation conditions. It is possible to identify the effect of water-laden rain clouds and rain. An interesting example is provided by the 30-GHz recordings of Figure 5-3, which indicate that steady 5-dB peak-to-peak variations of signal level were continuously recorded for more than an hour before the scintillations gradually began to grow in magnitude. While the scintillation magnitude increased, significant absorption was also occurring, as indicated by the mean beacon signal strength and the radiometric output. In addition, Figures 5-3 and 5-4 show the extreme contrast in the nature of scintillations recorded during rain and during early morning clear skies.

Since the scintillation magnitude is expected to be proportional to the path length through the lower atmosphere, the magnitude would be expected to be proportional to the cosecant of the antenna elevation angle. Because of the extreme variability of the local weather during the time when scintillations were recorded, the relationship between elevation angle and scintillation magnitude cannot be easily established. Peak-to-peak scintillation magnitude versus elevation angles is shown in Figure 5-5 with the data sample taken under clear to light drizzle weather conditions.

Also shown in Figure 5-5 is the ratio of the scintillation magnitudes at 20 and 30 GHz. The ratio appears to be relatively constant in most cases. Detailed spectrum analysis of

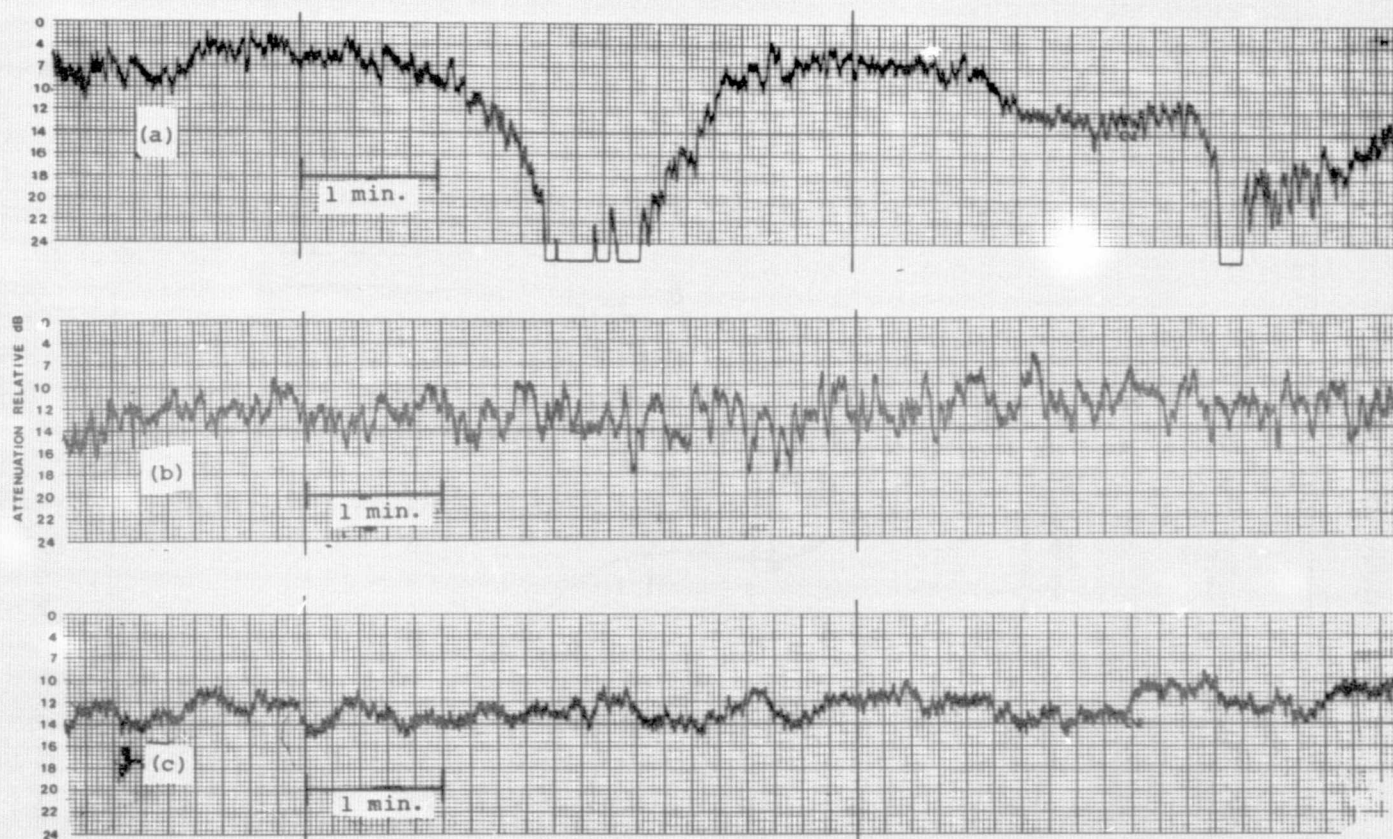


Figure 5-4. 20-GHz Recordings (a: rapid scintillations during rainfall at $\sim 6^\circ$ elevation angle, b: strong scintillations during heavy local cloud cover at $\sim 6^\circ$ elevation angle, c: slow scintillations during overcast skies at $\sim 3.5^\circ$ elevation angle)

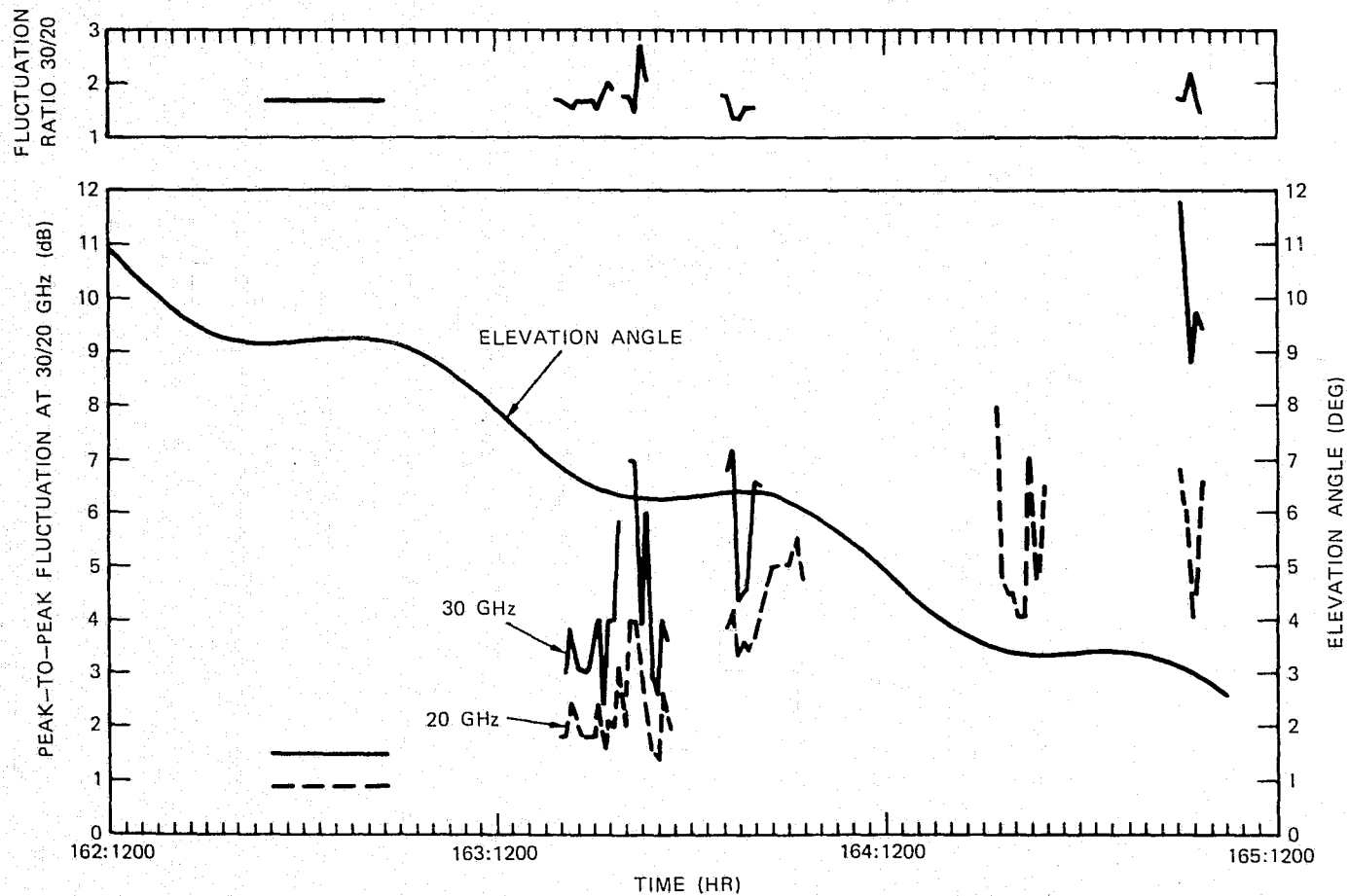


Figure 5-5. Peak-to-Peak Signal Fluctuations at 20/30 GHz
at Low Elevation Angles

the scintillations has not been performed due to the difficulties involved in making such an analysis from the stripchart data. Simple visual observation reveals that the power spectrum is concentrated in the 1- to 2-Hz band. Furthermore, the correlations between the 20- and 30-GHz scintillations are high. The normalized correlation coefficient based on evaluations of some short-piece data samples is about 0.8.

6. CONCLUSIONS

Unlike the earlier ATS-5 15.3/31.65-GHz MWE program in which satellite beacon transmissions were sufficient to permit experimenters to readily establish the various cumulative attenuation-precipitation statistics, the ATS-6 20/30-GHz MWE program provided transmissions which were inadequate for directly deriving any long-term statistics.

To indirectly establish the long-term cumulative attenuation-precipitation statistics, a detailed correlation must be obtained between the satellite signal data and the data generated from auxiliary ground-based measurements on an event-by-event basis. The techniques for obtaining this correlation have been presented and employed satisfactorily in the present study. Furthermore, many of the indirectly derived statistics agree reasonably well (or can be reconciled) with earlier published results generated independently.

In particular, the COMSAT experimenters feel that the following improvements of the MWE program would have been extremely beneficial:

- a. More beacon transmissions from the satellite should have been provided.
- b. Since digitization of the stripchart records was awkward and slow, the data processing should have been performed by minicomputer or microcomputer.
- c. The radar data should have been recorded for analysis.
- d. For the physics, a simple but adequate engineering equation similar to equation (3-1) should be derived for deducing satellite beacon attenuation from radiometric measurements at 20/30 GHz.

e. The use of an additional receiving system with wider beamwidth in the low-elevation-angle measurement might have indicated whether a wide-beam antenna receiver system would improve satellite-earth communications on low-elevation-angle paths.

The MWE program at COMSAT has certainly broadened the necessary data base and advanced the understanding of propagation characteristics at frequencies over 10 GHz. Additional data obtained from more refined satellite experiments such as the CTS and the COMSTAR programs for use in future propagation studies may eliminate propagation anomalies as the major uncertainty in the design of communications systems at frequencies over 10 GHz.

7. REFERENCES

1. J. W. Ryde and D. Ryde, "Attenuation of Centimeter and Millimeter Wave by Rain, Hail, Fogs, and Clouds," Report 8670, General Electric Co. Research Labs, Wembley, England, May 1945.
2. T. Oguchi, "Attenuation and Phase Rotation of Radio Waves Due to Rain: Calculations at 19.3 and 34.8 GHz," Radio Science, Vol. 8, No. 1, 1973, pp. 31-38.
3. R. K. Crane, "Propagation Phenomena Affecting Satellite Communication Systems Operating in the Centimeter and Millimeter Wavelength Bands," Proc. IEEE, Vol. 59, No. 2, 1971, pp. 173-188.
4. T. S. Chu, "Rain-Induced Cross-Polarization at Centimeter and Millimeter Wavelengths," Bell System Technical Journal, Vol. 53, No. 8, 1974, pp. 1557-1579.
5. D. T. Thomas, "Cross-Polarization Distortion in Microwave Radio Transmission Due to Rain," Radio Science, Vol. 6, No. 10, 1971, pp. 833-839.
6. D. J. Fang, "Attenuation and Phase Shift of Microwaves Due to Canted Raindrops," COMSAT Technical Review, Vol. 5, No. 1, Spring 1975, pp. 135-156.
7. L. J. Ippolito, "Effects of Precipitation on 15.3 and 31.65 GHz Earth-Space Transmissions with ATS-V Satellite," Proc. IEEE, Vol. 59, No. 2, 1971, pp. 189-205.

APPENDIX A. PRELIMINARY REPORT ON ATMOSPHERIC
ATTENUATION STUDIES ON ATS-6 SATELLITE
20/30 GHz BEACON SIGNALS

Preliminary Report On

ATMOSPHERIC ATTENUATION STUDIES ON ATS-6
SATELLITE 20/30 GHz BEACON SIGNALS

D. J. Fang and J. M. Harris
COMSAT Laboratories
Clarksburg, Maryland 20734

ABSTRACT

The study is a part of a program of COMSAT participation in the NASA ATS-6 millimeter wave experiment. In the initial data collection phase, the measurement equipment included: (1) A 3 meter diameter antenna-receiver system for accepting 20 GHz satellite CW signals and a radiometer system at 11.6 GHz for monitoring sky noise temperature. (2) A 4.6 meter diameter antenna-receiver system capable of receiving 20 and 30 GHz main CW signals plus radiometers at 20 and 30 GHz. (3) Six rain gauges along the bore sight path toward the satellite for recording instantaneous rainfall rates. (4) A weather radar at 5.4 GHz for detecting the motion pattern of the rain cloud in large scale.

Data analysis is done on an event-by event basis by using received satellite signals as basic reference for correlation with other information derived from the radiometers, the rain gauges and the radar. Important physical characteristics for prominent individual events of heavy rain storms are identified.

I. INTRODUCTION

There are "windows" in the frequency spectrum above 10 GHz where water vapor and oxygen absorption are relatively low. Two such windows are the frequencies below 20 GHz and a band from about 27 to 38 GHz. It follows that potential for future earth-satellite communications is greater in these bands. However, the essential propagation data base needed by system designers for predicting microwave communication system margin is not yet available.

COMSAT Labs' participation in the NASA ATS-6 Millimeter Wave Experiment (MWE) was aimed at collecting propagation data at Clarksburg, Maryland using the ATS-6 20/30 GHz beacons as the transmitting source and obtaining data for the long base-line diversity experiment jointly with NASA/GSFC, NRL and Westinghouse (Friendship). The data should be applicable to the general Washington, D.C. area and to other locations of similar climatological patterns.

The measurement equipment included three beacon signal receivers (two for 20 GHz and one for 30 GHz), three radiometers (11.6, 20 and 30 GHz), six rain gauges beneath the boresight path toward the satellite, and one weather radar (5.4 GHz). The hardware aspects of these systems are discussed in Section II. Analysis of beacon signal data is oriented toward event-by-event analysis of each measured occurrence of precipitation-induced attenuation, as long term statistics of signal attenuation were not available because of the rarity of the satellite beacon transmission during precipitation events (due to the low priority accorded the MWE during most of the stay of ATS-6 at its western station). Details of the data analysis are given in Section III.

An important facet of the work which was not anticipated in the initial study program was the low-elevation-angle measurement of the satellite transmission. This measurement was made during the period when ATS-6 moved gradually from its original location at 94°W Long. to its present location at 35°E Long. It was found that strong scintillations occurred at low elevation angles, and that there was a large increase of signal level as the satellite descended towards the horizon into the diffraction region. Preliminary analysis of the data is shown in Section IV. Conclusions are presented in the last section of the paper.

II. SYSTEM CONFIGURATION

Measurements were performed at COMSAT Labs, Clarksburg, Maryland, some 40 miles northwest of Washington, D.C. Figure 5-1 shows the location of the Clarksburg site relative to the other diversity sites at NRL, GSFC, and Westinghouse. The measurement system can be summarized as follows:

- (1) A 3 meter diameter transportable antenna-receiver system that included a 20 GHz receiver for receiving satellite beacon signals and a radiometric receiving system at 11.6 GHz for observing sky temperature using the same antenna.
- (2) A 4.6 meter diameter antenna-receiver system that included 20 and 30 GHz receivers for the satellite beacon signals and two radiometric receivers at 20 and 30 GHz for observing sky temperature using the same 4.6 meter antenna.
- (3) A network of 6 rain gauges extending for 7 kilometers underneath the boresight path toward the satellite for examining the precipitation under the propagation path.
- (4) A weather radar at 5.4 GHz for detecting the motion pattern of the rain cloud in large scale.

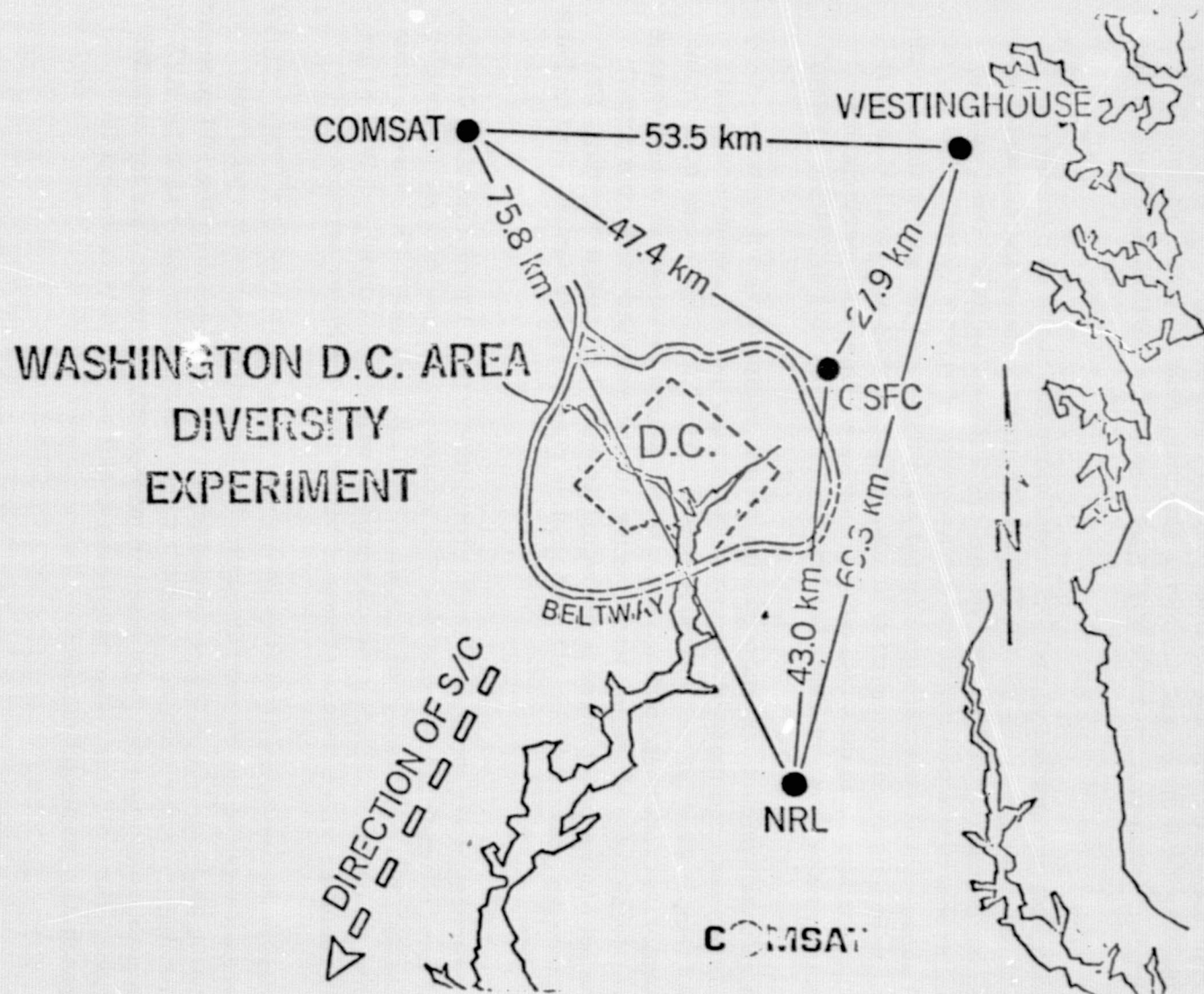


Figure 5-1. Location of COMSAT, Clarksburg Measurement

Figure 5-2 and 5-3 are the block diagrams of the 3 meter and 4.6 meter systems. The antennas are solid-surface aluminum paraboloids equipped with focal-point feeds and polarization rotators. Both antennas have servo-controlled elevation and azimuth positioners and decimal position readouts with a resolution of 0.1° and $.01^\circ$ for the 3 meter and 4.6 meter antennas, respectively. The nominal pointing direction to ATS-6 was 204° SSW from true north at an elevation angle of 42° .

As indicated in Figures 5-2 and 5-3 tunnel diode and uncooled parametric amplifiers are used in the 20 GHz front-ends of the 3 meter and 4.6 meter systems, respectively. The 30 GHz system has a low noise mixer front end. IF-signal processors which detect the down-converted signals by individual narrow-band phase-locked receivers give output amplitudes that are proportional to the satellite beacon signal attenuation levels. These outputs are then fed to strip-chart recorders or to data acquisition computers. Important performance parameters are shown in Table 5-1 (3m system) and Table 5-2 (4.6m system).

Both antenna systems are equipped with on-line radiometric subsystems. Operating in a Dicke-switched mode, these radiometers also include a noise source at known temperature for calibration purposes. The A.I.L. (Airborne Instrument Laboratories) radiometric receivers, (Model 2392C) produces an output voltage proportional to the sky noise temperature. In the switched mode, the output is the net change of sky noise temperature from that of a clear sky day. Performance parameters of the AIL radiometric receivers are summarized in Table 5-3.

The rain gauges are the tipping bucket type, where each tip represents 0.01 inch (0.25 mm) of rainfall accumulation. The gauges are aligned beneath the satellite bore-sight path at distances of 0, 0.92, 1.08, 3.23, 5.53 and 7.4 kilometers from the beacon receiver. Each gauge is equipped with a mechanically driven strip-chart recorder with a time accuracy of better than 3 minutes per week.

The radar system is an RCA AVQ-10 weather radar operating at 5.4 GHz. Three different ranges of 20, 50 and 150 nautical miles can be selected. Maximum elevation angle is 35° . A super-8mm camera can be attached to the PPI scope for filming the radar echoes. Since the radar slant path is lower than the ATS-6 slant path, no attempt has been made to incorporate the radar data for detailed analysis. However, the radar has proved useful as a device to predict the approach of a precipitating cloud.

5-5

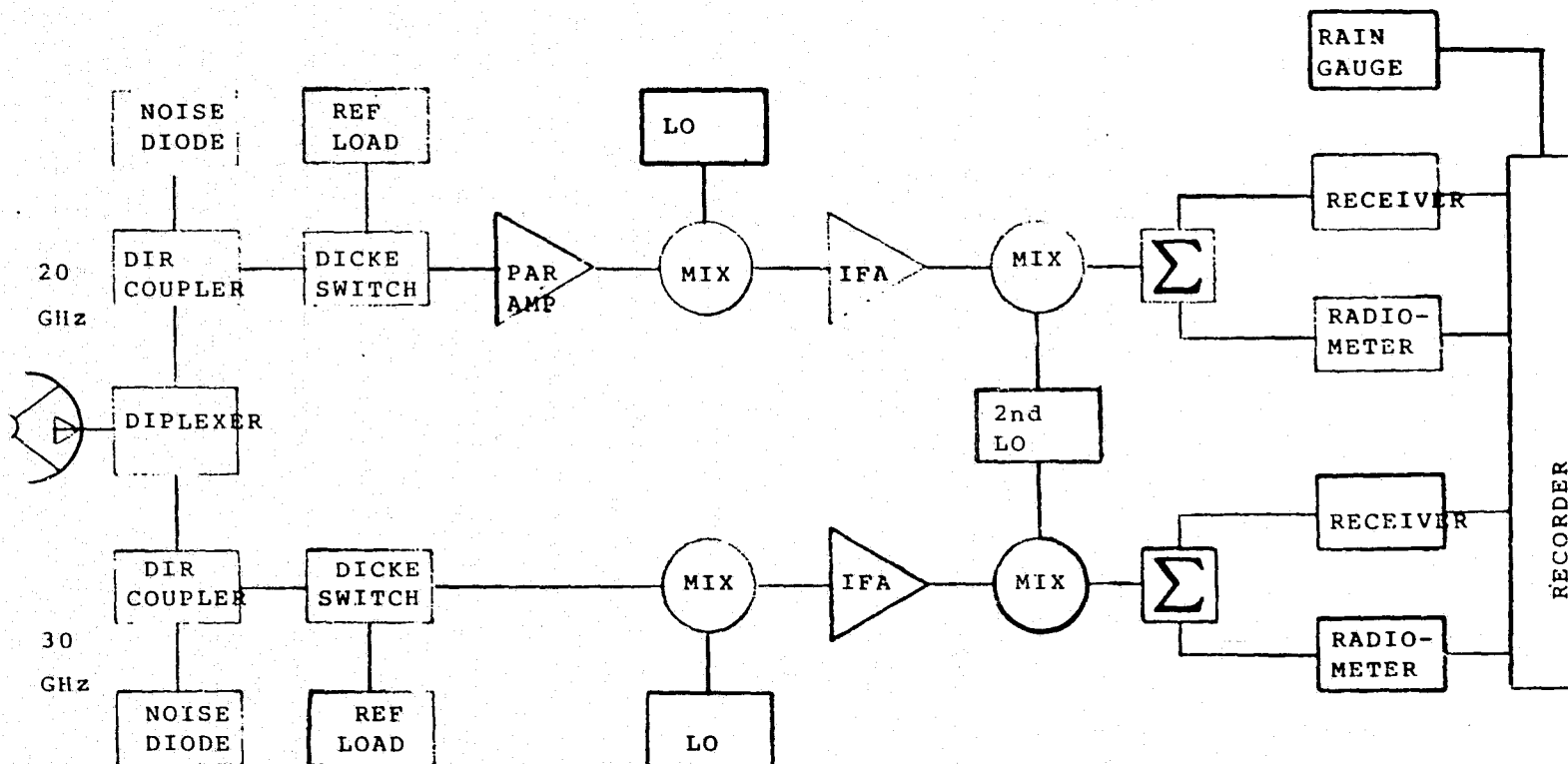


Figure 5-2. Block Diagram: 20/30 GHz Receive/Radiometer System

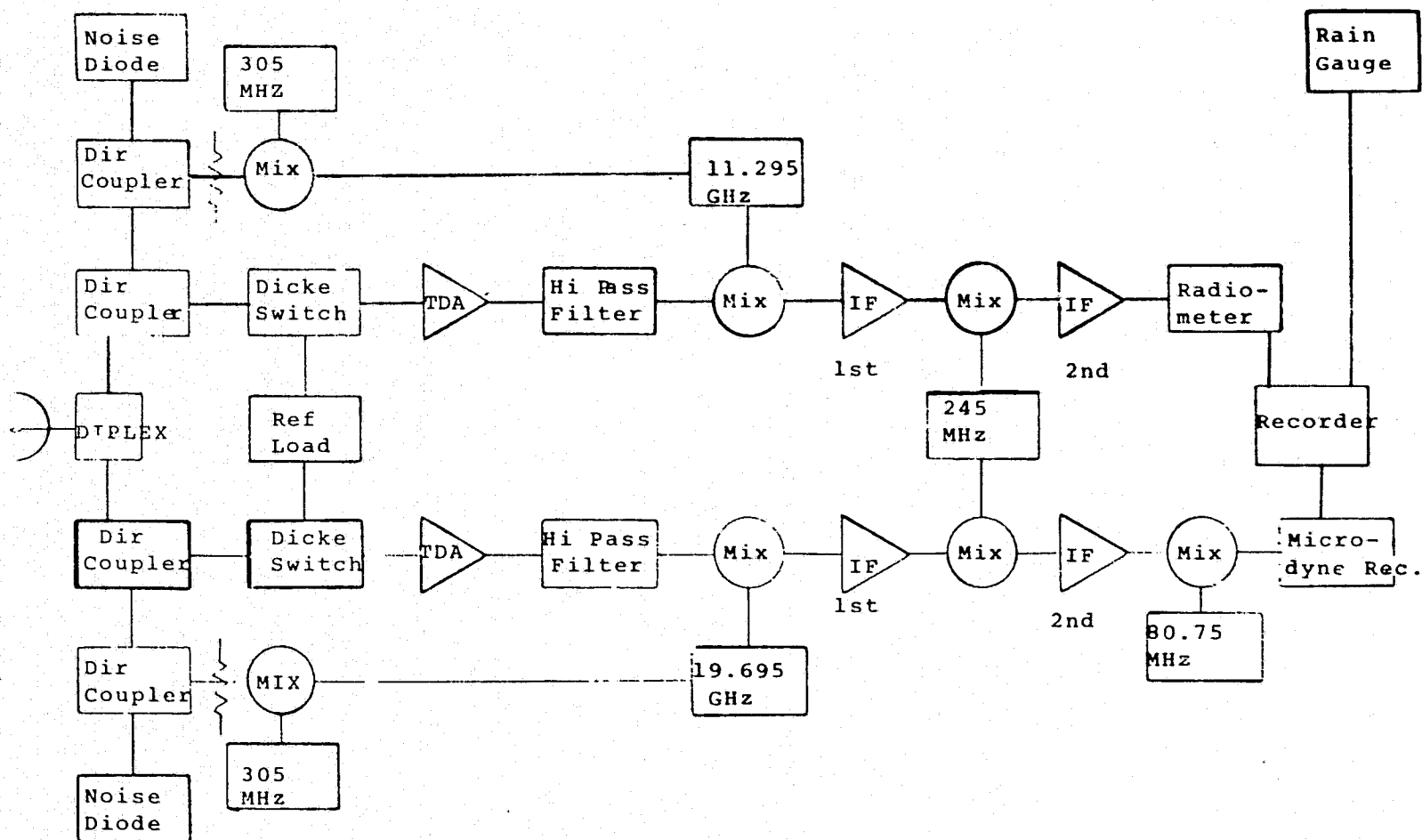


Figure 5-3. Block Diagram: 11.6 and 20 GHz Receiver/Radiometer Transportable System

Table 5-1
Important Performance Parameters of 3m Antenna System

| | 11.6 GHz | 20 GHz |
|------------------------|---------------|---------------|
| Antenna Gain | 48.7 dB | 53.5 dB |
| Pointing Accuracy | $\pm 1^\circ$ | $\pm 1^\circ$ |
| Noise Figure | 5 dB | 8 dB |
| Radiometer Sensitivity | 1°K | — |
| Radiometer Bandwidth | 100 MHz | — |
| Receiver Bandwidth | — | 10 KHz |

Table 5-2
Important Performance Parameters of 4.6m Antenna System

| | 20 GHz | 30 GHz |
|------------------------|------------------|------------------|
| Antenna Gain | 57 dB | 60.5 dB |
| Pointing Accuracy | $\pm 0.01^\circ$ | $\pm 0.01^\circ$ |
| Noise Figure | 4 dB | 8 dB |
| Radiometer Sensitivity | 1°K | 1°K |
| Radiometer Bandwidth | 100 MHz | 100 MHz |
| Receiver Bandwidth | 10 KHz | 10 KHz |

Not all of the above systems were ready for measurement at the same time, as shown in Table 5-4. Delays in preparation of the 4.6m system were caused by the continuous slippage of the shipping schedule of the parametric amplifier. On the other hand, the systems have performed well once operational.

III. DATA ANALYSIS

An important constraint on the entire experiment was the lack of availability of millimeter wave 20/30 GHz beacon transmissions from the satellite during precipitation events. The priority of the millimeter wave experiment was not high. There were regular weekly transmission times assigned at an average of about one hour per day. These transmission times, although used by COMSAT for data collection and equipment calibration, were not really useful due to the fact that precipitation rarely occurred on site at these times. Requests were

Table 5-3
Performance Parameters of AIL Radiometric Receivers

| | |
|-----------------------------|---|
| IF bandwidth | 100 MHz (5 to 105 MHz) |
| Noise figure | 7 dB |
| Input impedance | 50 ohms |
| Input SWR | <2 to 1 over entire passband |
| Gain modulation | -3 to +3 dB, in 0.06-dB steps and continuous control of 0.1 dB |
| IF gain | 85 dB (maximum) |
| IF gain control | 0 to -41 dB, in 1-dB steps |
| Switch rate | 5 to 500 Hz, stability ± 0.05 percent |
| Switching waveform | Square wave |
| RF switch drive | 0 to -14 volt square wave into 10,000 ohms |
| Switched system output | ± 5 volts maximum at 2 ma |
| Total power output | -5 volts maximum at 2 ma |
| Integration time constants: | |
| Switched system | 0.1, 1, 3, 5, 10 and 30 seconds |
| Total power system | 1, 5, and 10 seconds |
| Monitor points | Second detector current; synchronous detector balance |
| DC reference | Up to 3.0 volts (for use with total power output) |
| Input power | 47 watt nominal (capable of operation at 105 to 125 and 220 volt AC, 50 to 440 Hz). |

Table 5-4
System Availability Chart

| System | Equipment | Available Since | Comment |
|----------------------|---------------------|-----------------|--|
| Transportable System | 20 GHz CW-Receiver | July 1974 | Varian 620 computer was equipped for automatic tracking and data collection. But it overflowed frequently. Most time only manual operation was used. |
| | 11.6 GHz Radiometer | July 1974 | |
| | Rain Gauge | July 1975 | |
| 15-Foot System | 20 GHz CW-Receiver | March 1975 | Due to interference problem the 20 GHz radiometer was turned off when CW-Receiver was taking data. |
| | 20 GHz Radiometer | March 1975 | |
| | 30 GHz CW-Receiver | April 1974 | |
| Others | 5.4 GHz Radar | September 1974 | For visual observation only |
| | Rain Gauges | February 1975 | Total of 6, counting the one on site |

made consistently to NASA ATS Operations Control Center for 20/30 GHz beacon transmission whenever precipitation was occurring or anticipated. Positive responses to the requests were infrequent. There were several occasions when beacon transmissions were abruptly terminated while valuable experimental data in a thunderstorm condition was being collected.

With the above constraint in mind, data analysis was performed largely on an event-by-event basis. This includes:

- (i) Correlation of the satellite 20 GHz beacon data and the radiometric sky temperature data.
- (ii) Correlation of the 20 GHz and 30 GHz signal attenuation level.
- (iii) Correlation of the satellite 20 GHz beacon signals and data from the rain-gauge network.

Another phase of data collection, not included with the original plan, involved observation of the satellite descending toward the horizon in late May and early June of 1975. The low-elevation angle data will be presented in a separate section.

- (i) Correlation of the satellite 20 GHz beacon data and the radiometric sky temperature data.

A typical data sample is shown in Figure 5-4, (the event of March 19, 1975, lasting 150 minutes). The scattergram of the data is shown in Figure 5-5. Empirical fit curves are shown as dashed lines. Theoretically derived attenuation curves using linear scaling for ambient sky temperature of 278°K and 300°K are also shown.

- (ii) Correlation of the 20 GHz and 30 GHz signal attenuation level.

A typical data sample is shown in Figure 5-6, the event of June 6, 1975. A scattergram of the data is shown in Figure 5-7.

- (iii) Correlation of the satellite 20 GHz beacon signals and data from the rain-gauge network.

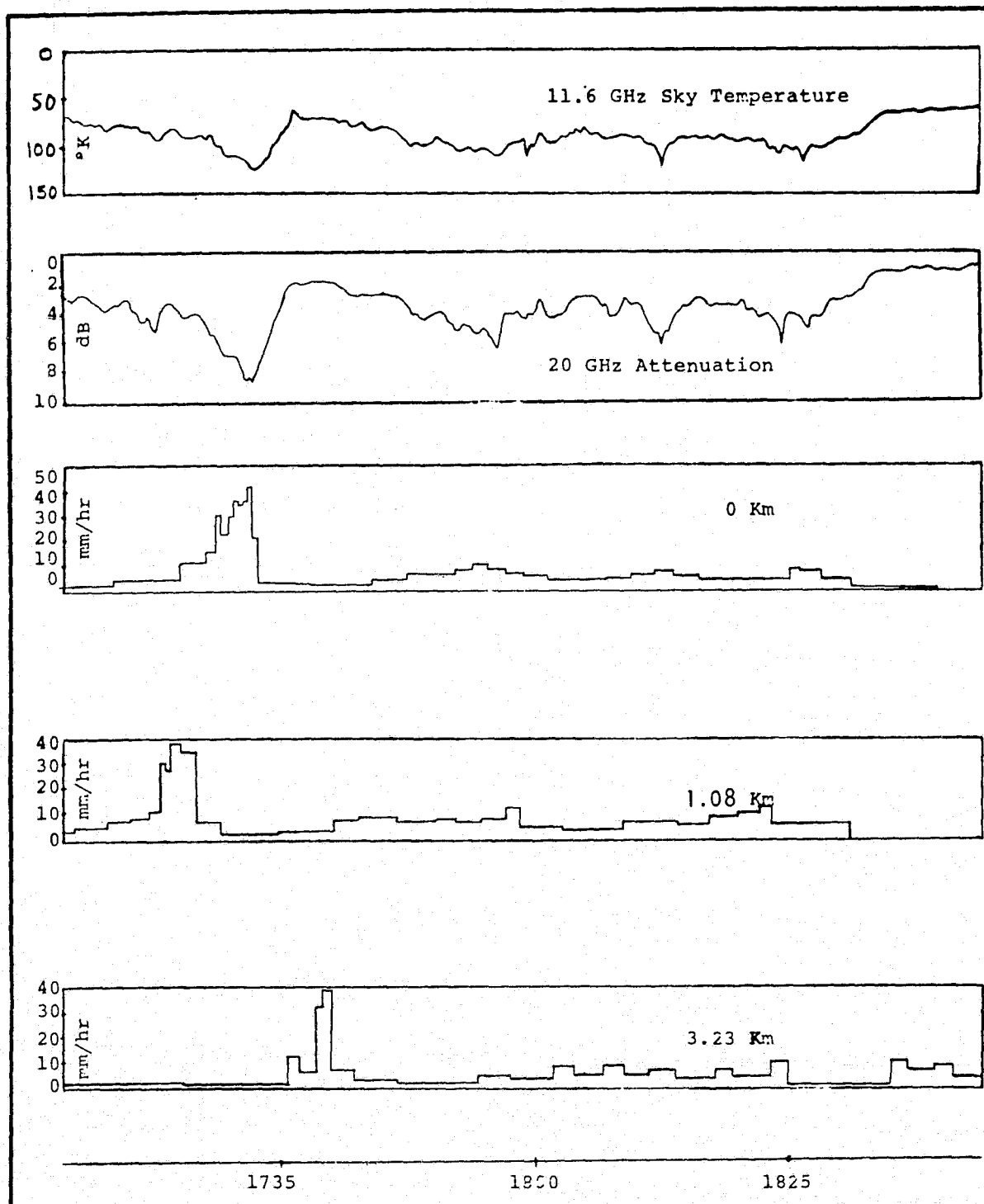


Figure 5-4. Typical Precipitation - attenuation record measured at Clarksburg, Maryland. Ground rain gauges were 0 km, 1.1 km and 3.23 km from 20 GHz receiver and 11.6 GHz radiometer.

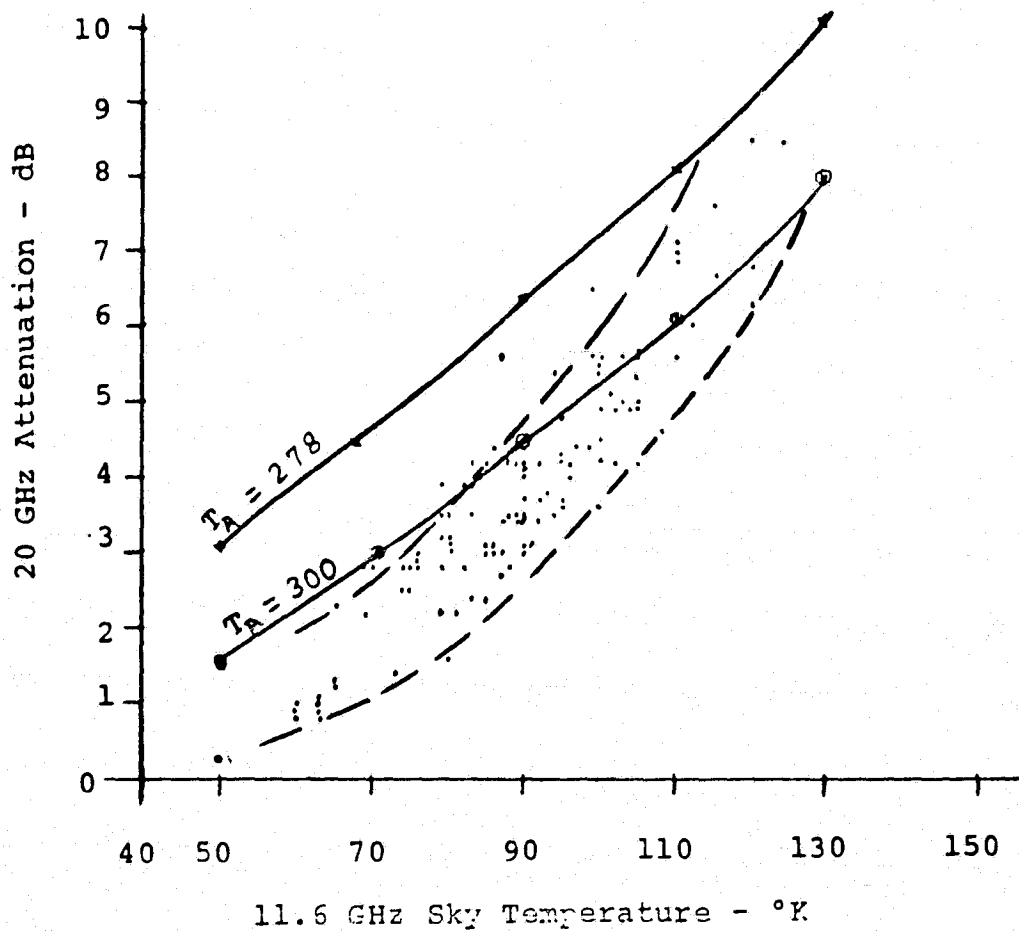


Figure 5-5. Scattergram of 20 GHz attenuation vs. 11.6 GHz sky temperature from data given in Figure 4. Solid lines theoretically derived for ambient temperature T .

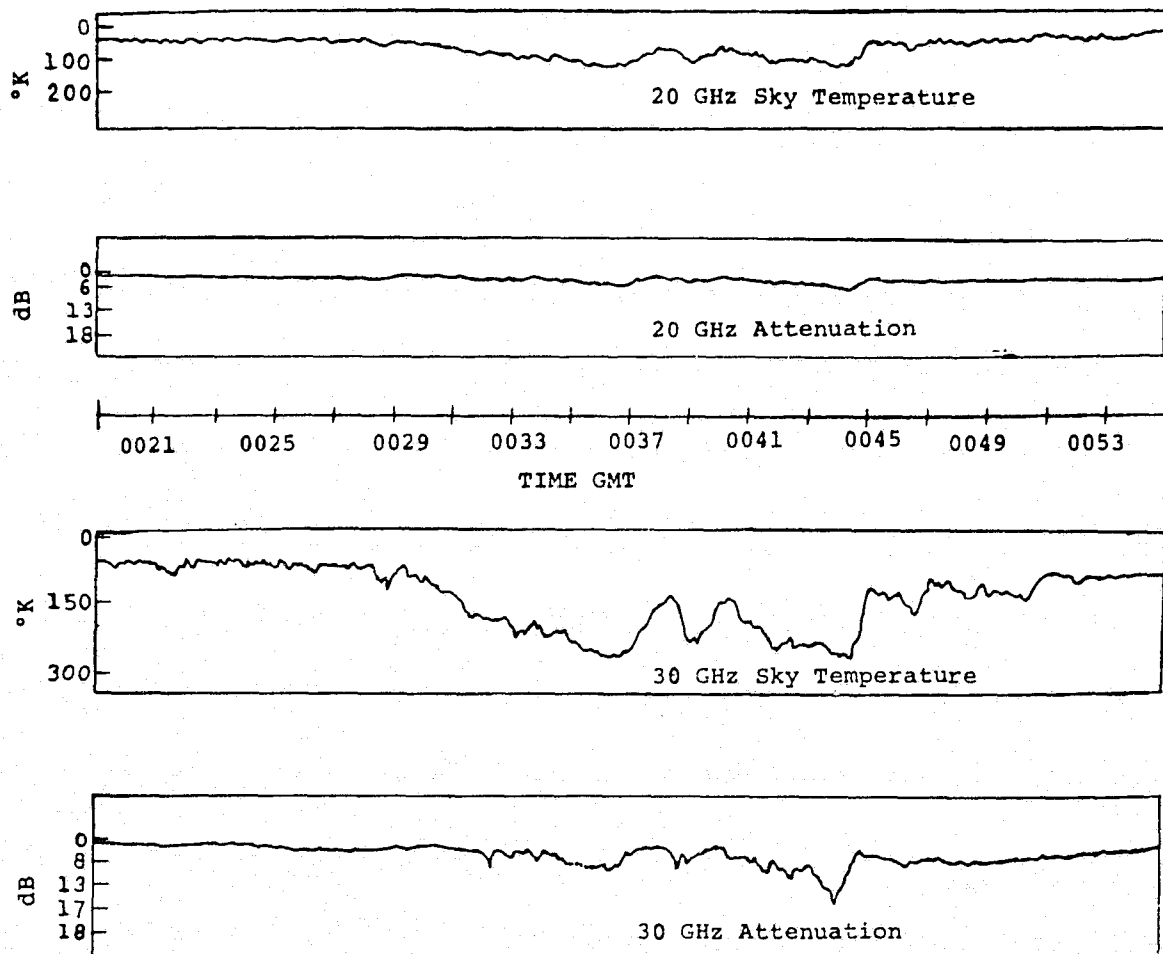


Figure 5-6. Typical records of simultaneously measured 20/30 GHz radiometric sky temperatures and 20/30 GHz ATS-6 signals.

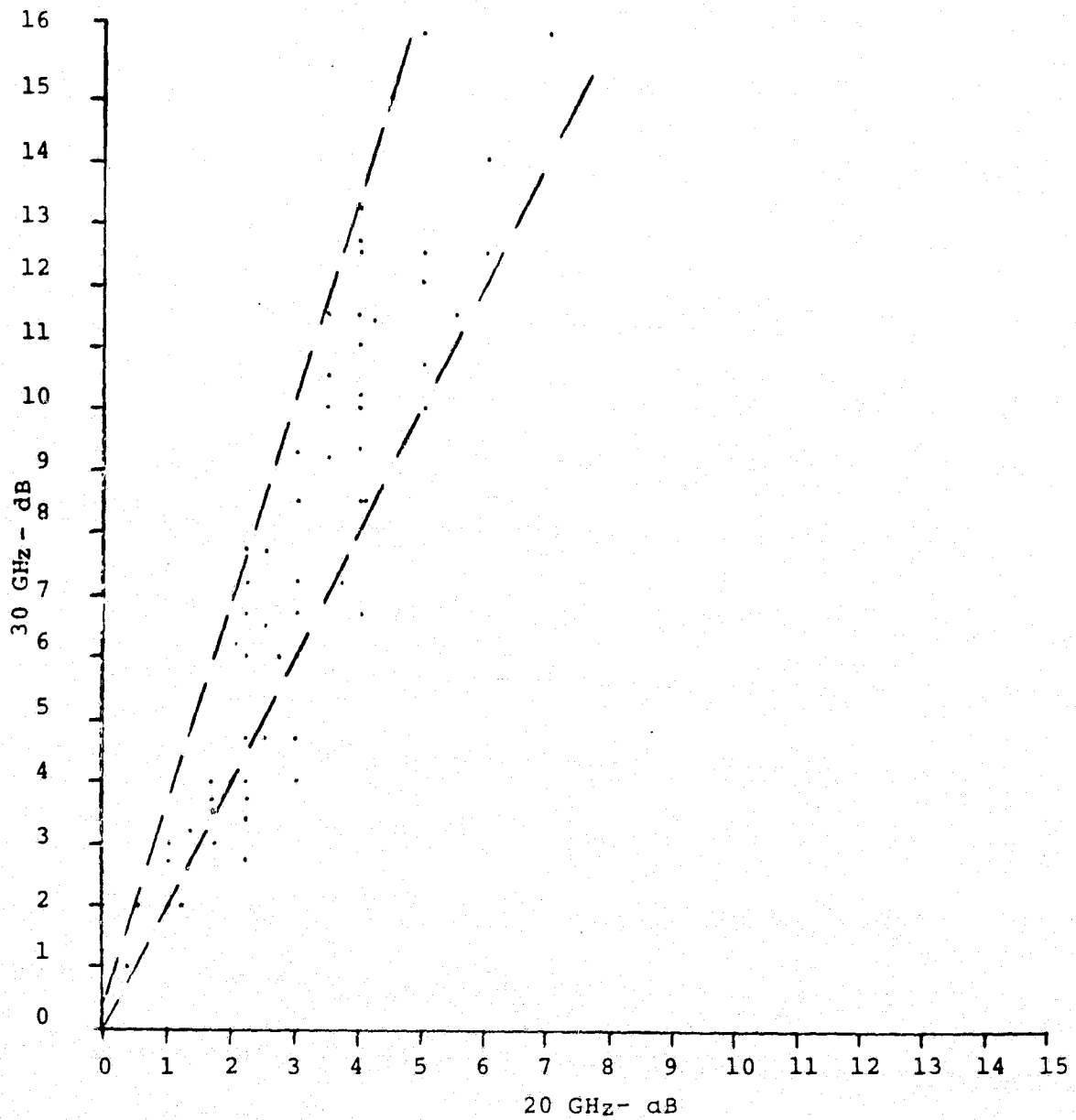


Figure 5-7. Scattergram plot of 30 GHz Attenuation vs.
20 GHz attenuation measured June 6, 1975.

A basic problem in estimating the microwave attenuations over a satellite - earth propagation path based on rain-gauge data is that for a given storm event, the attenuation and the rain-fall records very often do not have a consistent detailed correlation. As shown in Figure 5-4, it is seen that while the radiometer curve correlates well with the satellite signal level, the data from rain gauges do not have a consistent correlation with the 20 GHz curve. A particularly puzzling point is the peak registered on the rain gauge 3.23 km away from the receiver.

We have collected and analyzed the data containing the apparent discrepancies in time and magnitude as those shown in Figure 5-4. A model for adjusting the rain gauge data is provided as follows:

Let the rain-rate measured at an instant t by a ground rain gauge by $R(t)$ which consists of raindrops of sizes from 0.05 to 0.7 centimeter with falling velocity V ranging from 2 to 9 meters/sec. It follows that

$$R_G(t) = \sum_v R_v(t) \quad (1)$$

where $R_v(t)$ is the portion of rain-rate falling at terminal velocity v . If the rain gauge is located h meters vertically below the slant propagation path, then $R_v(t)$ penetrates across the path at an advanced time h/v , when there is no wind. Therefore, the actual rain fall $R_h(t)$ at height h and instant t' is

$$R_h(t') = \sum_{t,v} R_v(t) \quad t - \frac{h}{v} = t' \quad (2)$$

The summation is over all the components of $R_v(t)$ in $R_G(t)$ for an all t and v such that $t - h/v = t'$. The decomposition of R_G into R_v for a different advanced time with $h = 1000$ meters is shown in Table 4-5.

Table 4-5

Actual Rain Rate at 1000-Meter Height Estimated from a Ground Rain Gauge Rainfall Reading
(The estimate is based on Laws and Parsons drop size distribution and Davies' terminal velocity profile [Medhurst, 1965 IEEE paper])

| Actual Rain Rate at 1000-m Height | | | | | | | | | | Ground Measured Rain Rate (mm/hr) |
|-----------------------------------|------|------|-------|-------|-------|-------|-------|-------|-------|--------------------------------------|
| Advanced Time (minutes) | | | | | | | | | | |
| 8.09 | 4.14 | 3.09 | 2.57 | 2.25 | 2.07 | 1.95 | 1.89 | 1.85 | 1.83 | |
| 0.07 | 0.13 | 0.05 | 0 | 0 | 0 | 0 | 0 | 0 | 0 | 0.25 |
| 0.14 | 0.46 | 0.39 | 0.17 | 0.16 | 0.02 | 0.01 | 0 | 0 | 0 | 1.25 |
| 0.18 | 0.07 | 0.82 | 0.48 | 0.20 | 0.08 | 0.04 | 0 | 0 | 0 | 2.5 |
| 0.24 | 1.02 | 1.55 | 1.11 | 0.59 | 0.29 | 0.13 | 0.05 | 0.02 | 0 | 5 |
| 0.33 | 1.44 | 3.06 | 3.18 | 2.16 | 1.26 | 0.54 | 0.29 | 0.15 | 0.09 | 12.5 |
| 0.43 | 1.9 | 4.6 | 5.98 | 4.98 | 3.20 | 2.05 | 0.88 | 0.53 | 0.48 | 25 |
| 0.6 | 2.7 | 6.25 | 9.95 | 10.45 | 7.8 | 5.45 | 3.35 | 1.65 | 1.8 | 50 |
| 1.0 | 4.6 | 8.8 | 13.9 | 17.1 | 18.4 | 15.0 | 9.0 | 5.8 | 6.4 | 100 |
| 1.5 | 6.15 | 11.4 | 17.55 | 20.85 | 26.55 | 24.15 | 17.85 | 11.55 | 12.45 | 150 |

The model has been applied to the rain-rate records collected from the 6 rain gauge networks in correlating rain data with the ATS-6 20 GHz beacon signals. In most cases, the method has the merit of relocating and dispersing the peaks of precipitation curves of field rain gauges in the direction of better alignment with the pattern of attenuation curves. Figure 5-8 is the outcome of the adjusted rain-rate distribution of the same event shown in Figure 6-4. Assuming that the same rain rate of a rain gauge applies over the distance between the middle points of the two adjacent rain gauges, attenuation can then be estimated from theoretical considerations. The estimated value and the actual 20 GHz attenuation value are compared in Figure 5-9. The scattergram, Figure 5-9(b) derived from the adjusted rain data of Figure 5-8 exhibits a significant improvement in comparison with the scattergram, Figure 5-9(a), derived directly from Figure 5-4.

IV. LOW ELEVATION ANGLE MEASUREMENT

In late May, 1975 ATS-6 began to move slowly from its original location toward its new position over the Indian Ocean. The path vector elevation angle at the COMSAT Labs' receivers station decreased steadily to zero over a three week period of time. While the 20 GHz and 30 GHz beacon signals were not continuously available, several hours of data were collected at varying elevation angles. As ATS-6 approached the horizon, (local horizon was at an elevation angle of 1.2°), strong scintillations occurred as well as an increase in the average level of the received signals.

The scintillations appear to be caused by irregular refraction and scattering in the earth's lower atmosphere. Although antenna tracking difficulties and calibration errors, among other things, may also have contributed to the signal variations, a continuous effort was made to minimize this effect. The magnitude of the scintillations showed a strong dependence on path elevation angle and local climatological conditions. Peak-to-peak magnitude of the variations grew to greater than 10 dB during the final hours of data acquisition near 3° elevation angle. In addition, sharp nulls in the signal level were frequently observed and believed to be caused by angle of arrival or low elevation angle multipath. These scintillations have a periodicity in the range of 15 seconds to greater than 1 minute that showed a large dependence on the local weather. A typical record of simultaneous 20 GHz and 30 GHz scintillations is given in Figure 5-10(a) and 5-10(b).

Model Adjusted Rain Rate

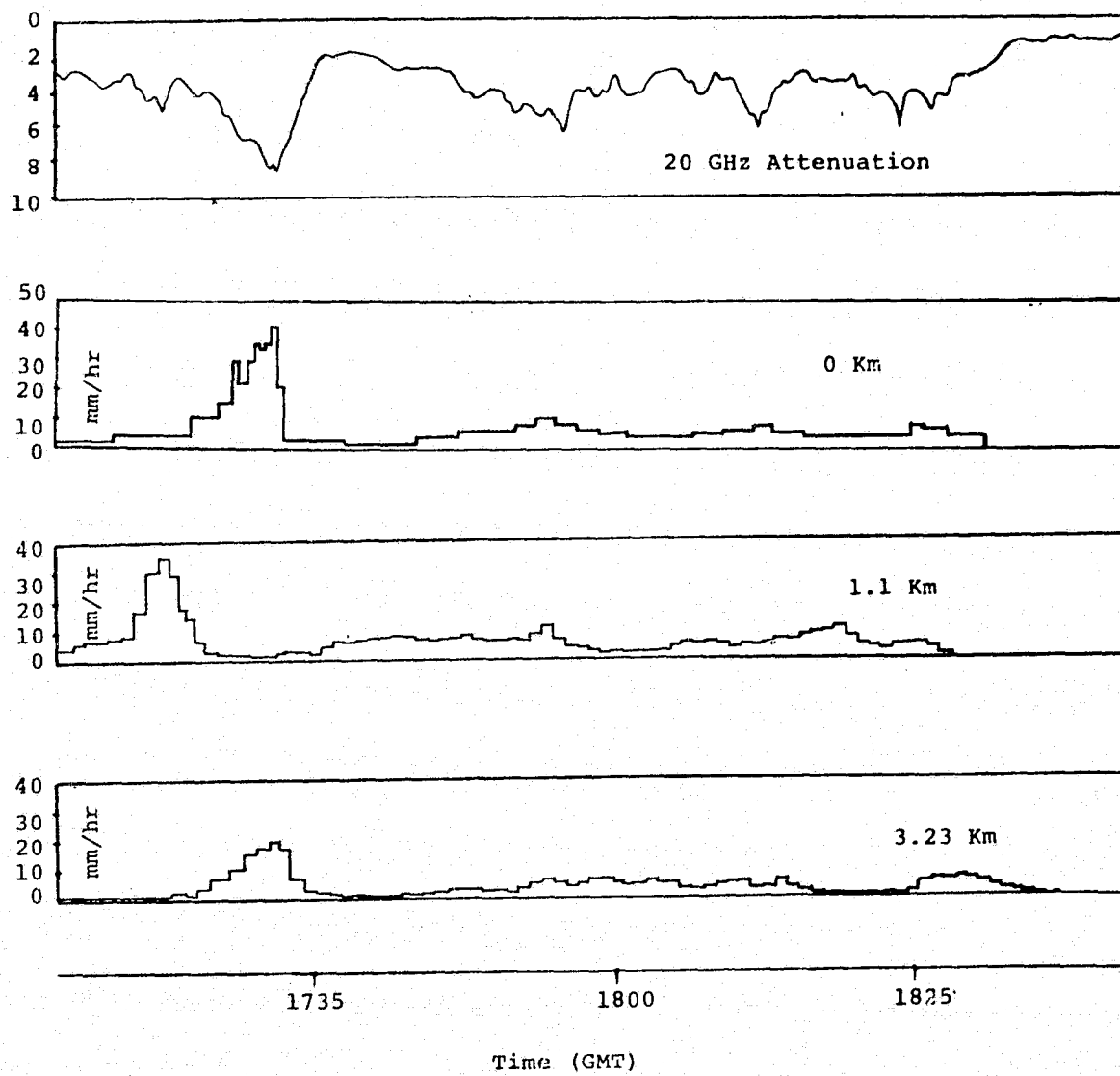


Figure 5-8. Model adjusted rainrate from original data given in Figure 4.

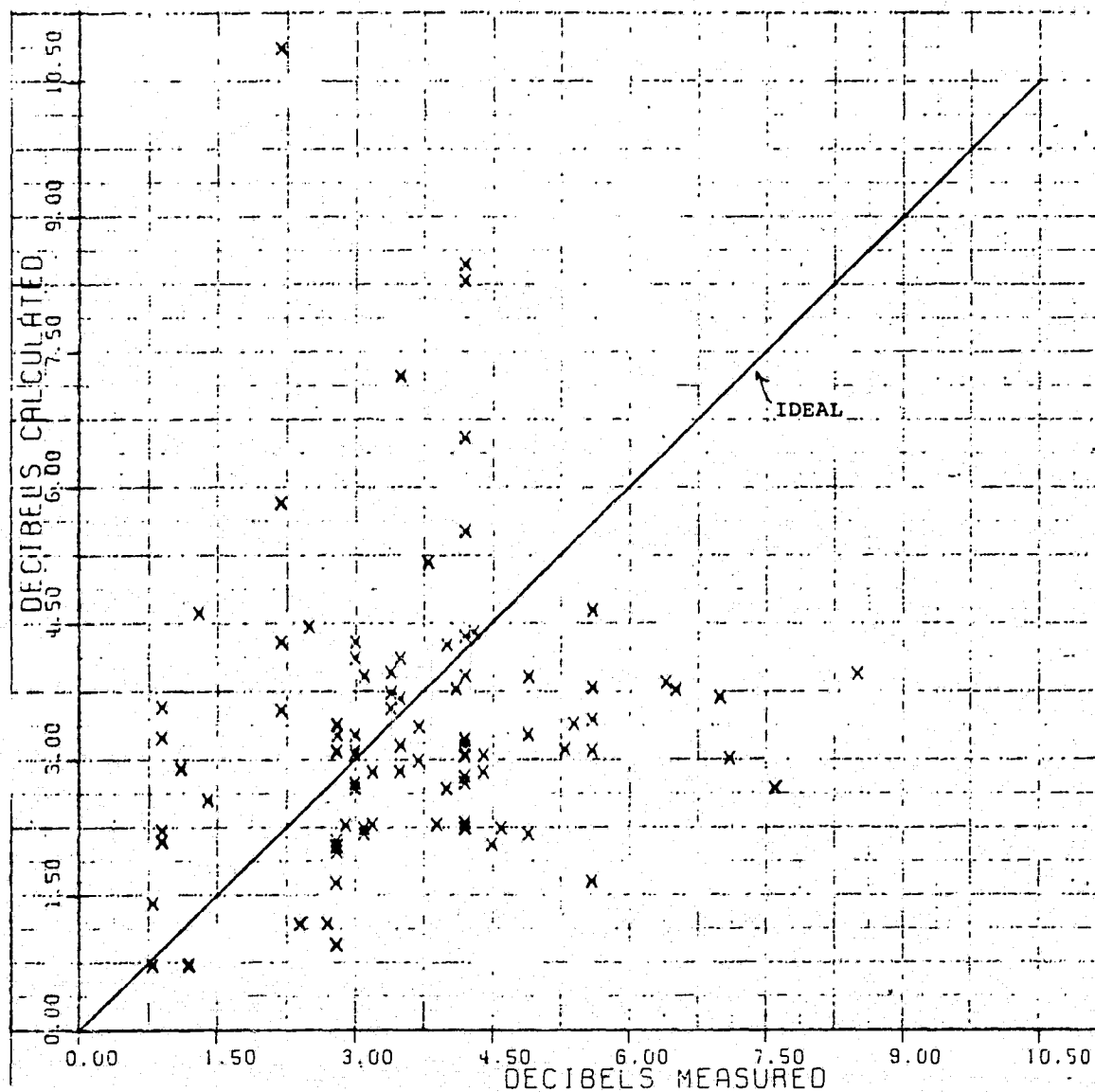


Figure 5-9(a). Scattergram of 20 GHz attenuation calculated vs. measured for 2 hour period on March 19, 1975 using original rain data from Figure 4.

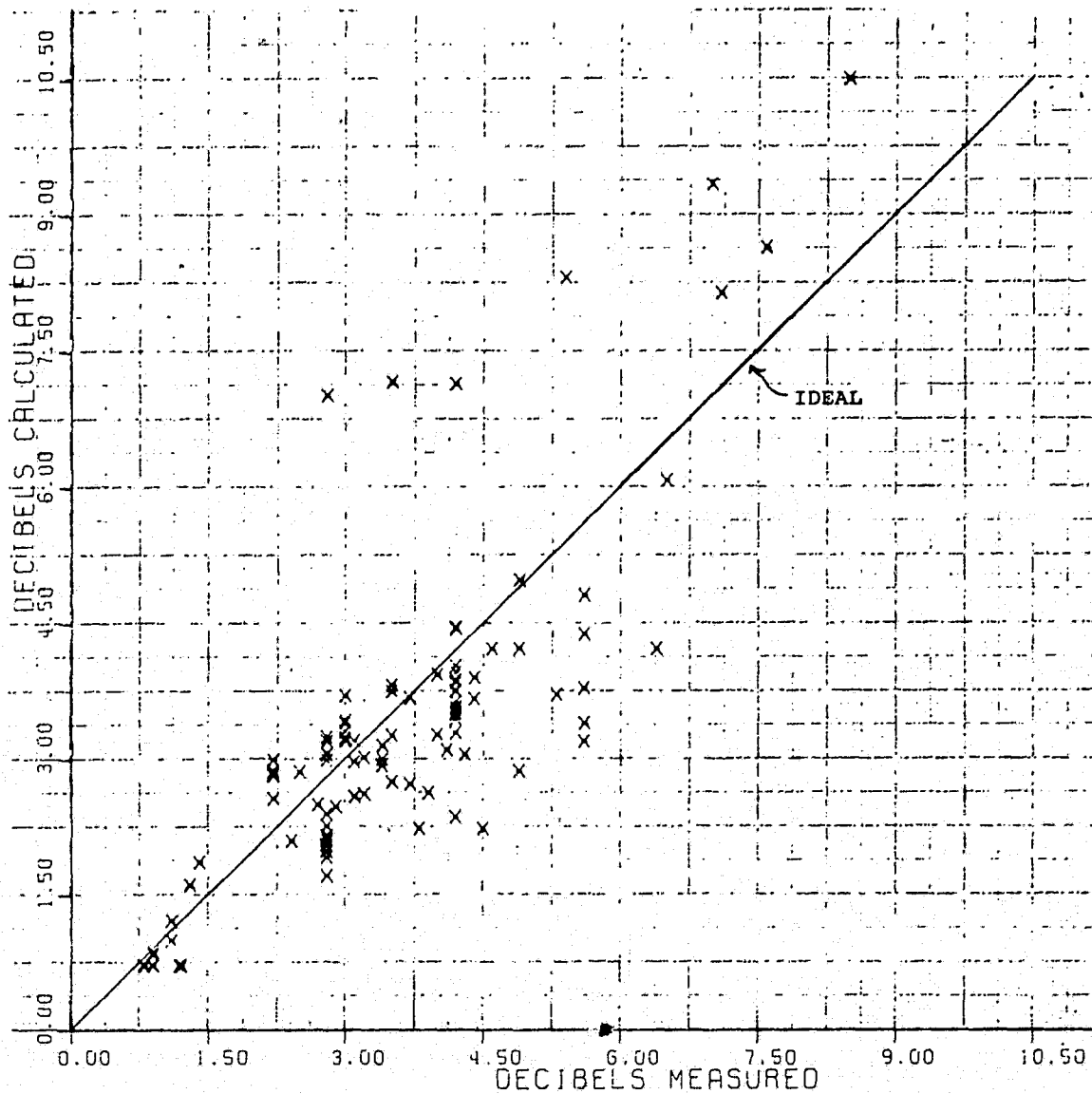


Figure 5-9(b). Scattergram of 20 GHz attenuation calculated vs. measured for 2 hour period on March 19, 1975 using model adjusted rain data from Figure 8.

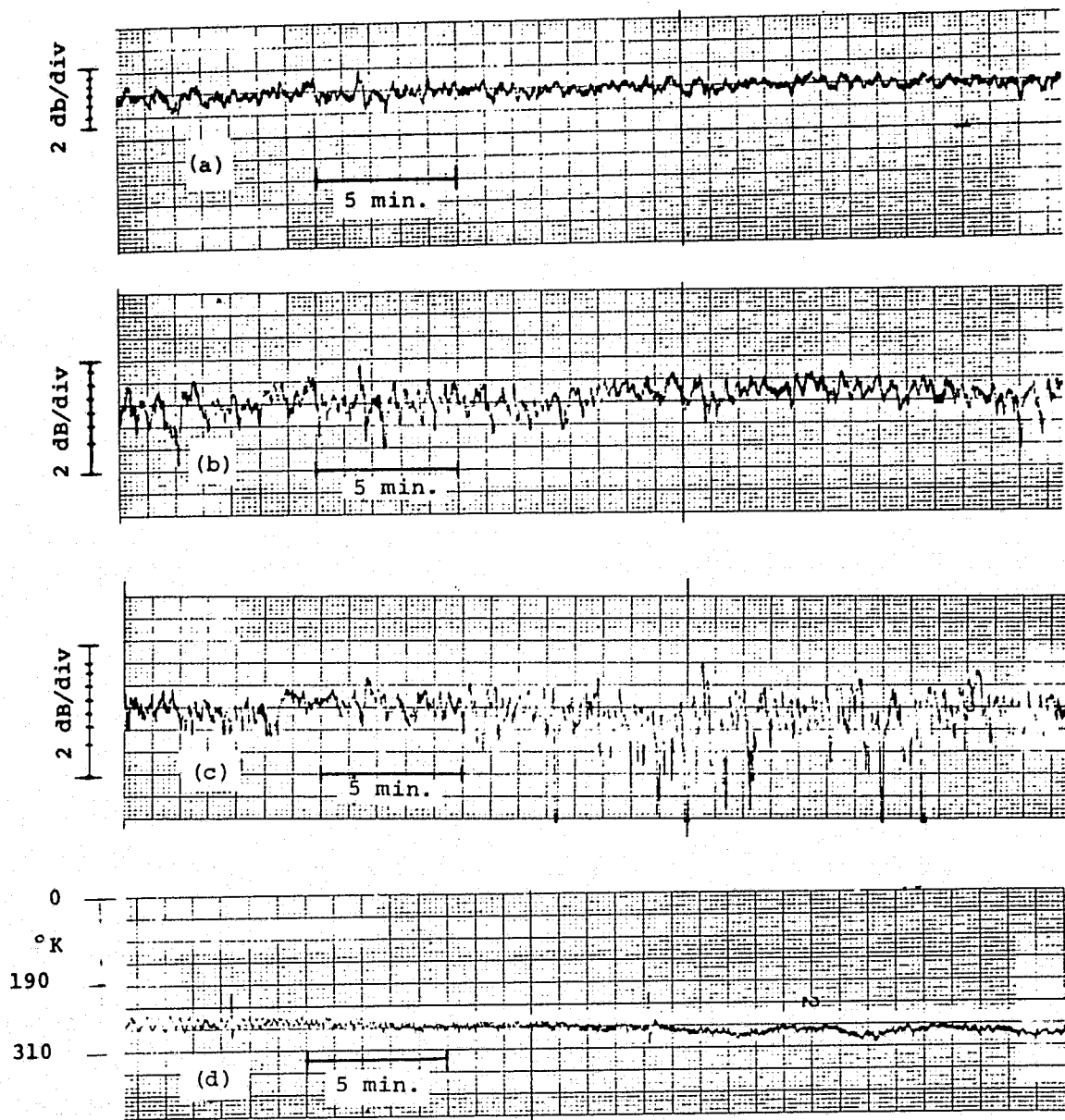


Figure 5-10. Recordings of 20/30 GHz low elevation angle signals. (a) and (b) show steady variations at 20 GHz and 30 GHz respectively. (c) and (d) show simultaneous recordings of 30 GHz ATS-6 signal and 30 GHz radiometer as light rain began. Antenna elevation angle 6.5° .

While several different physical mechanisms are probably responsible for the scintillations recorded, the occurrence of low elevation angle scintillation was expected. As noted earlier, the observed effect was no doubt a result of the combined influence of scattering by tropospheric irregularities, angle of arrival variations, rain, etc. However, most notable and identifiable was the effect of water-laden rain clouds and rain. The weather radar operated at the receiving site proved particularly useful in identifying the presence and movement of cloud systems. An interesting example is the 30 GHz recordings shown in Figures 5-10(c) and 5-10(d). Steady variations in the signal level of 5 dB peak-to-peak had been continuously recorded for well over an hour when the scintillation magnitude increased, significant absorption was also occurring as indicated by the average decrease in the signal strength and the radiometers. Figure 5-11 shows the extreme contrast in nature of scintillation recorded during rain and during early morning clear skies.

Since the scintillation magnitude is expected to be proportional to the path length through the lower atmosphere, the magnitude would be expected proportional to the cosecant of the antenna elevation angle. Because of the extreme variability of the local weather throughout the time when scintillations were recorded, the relationship between elevation angle and scintillation magnitude cannot be easily obtained. In spite of the strong effect of the weather however, some elevation angle dependence is evident from the data. The peak-to-peak magnitude of the 30 GHz scintillations were generally greater than that simultaneously recorded at 20 GHz. This fact was particularly evident during cloud and rain scintillations.

V. CONCLUSION

As we have mentioned, due to the rigid assignment of priorities, there was a considerable amount of difficulty in securing the 20/30 GHz beacon transmission from the satellite when heavy precipitation was in progress at the Clarksburg experiment site. This severely curtailed the data base on the whole experiment.

On the other hand, the program did yield many important results. For example, a new and more efficient method of estimating the slant-path microwave attenuation using a network of rain gauges was established. From event-by-event analysis, one can determine the accuracy of using a radiometric measurement of sky temperature as a substitute of direct satellite-signal attenuation measurement. The validity of using a radiometer to derive the yearly attenuation statistics, will be shown in the final report of this program when a one-year radiometric

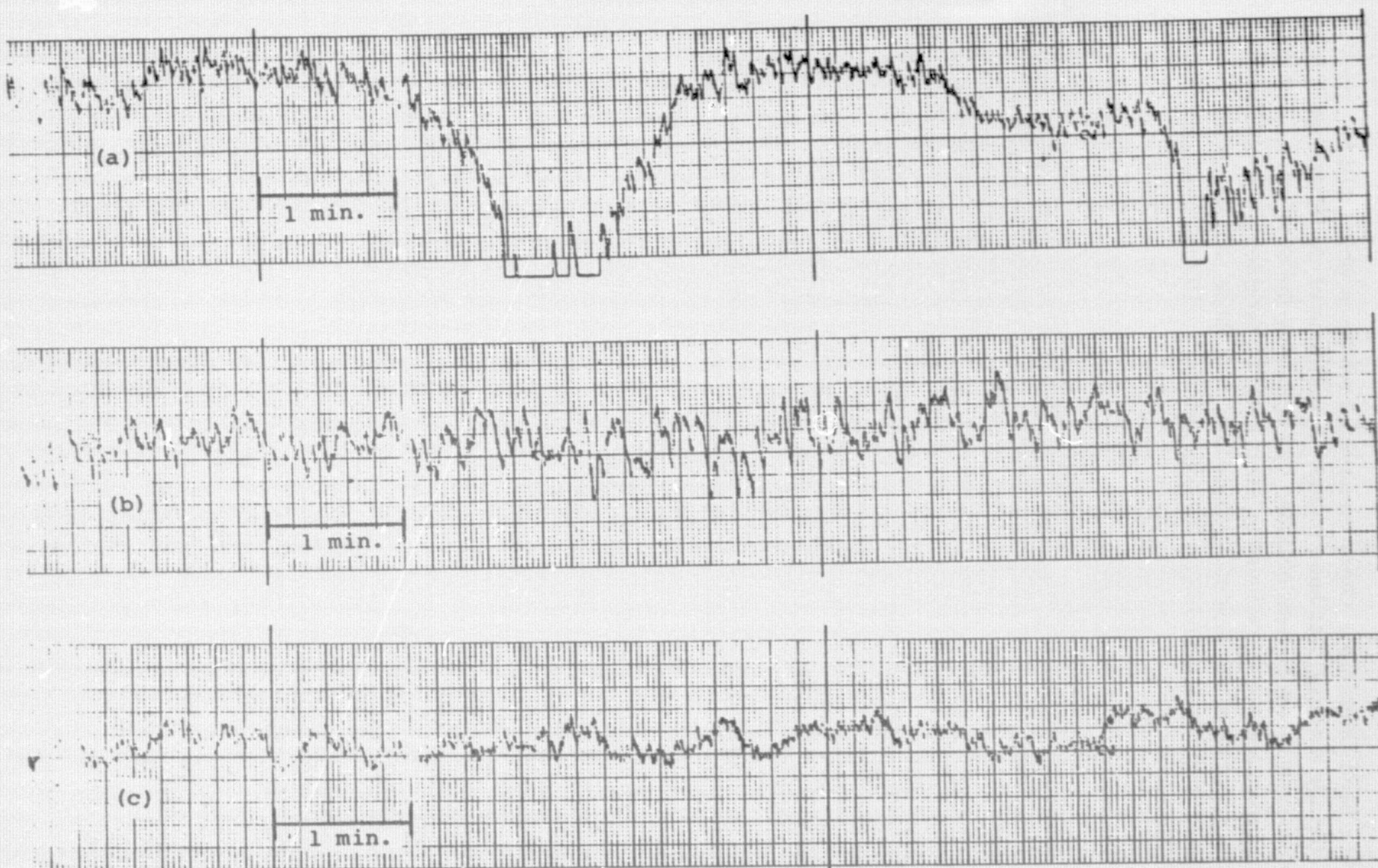


Figure 5-11. 20 GHz Recordings:

- (a) Rapid scintillations during moderate rainfall at $\sim 6^\circ$ elevation angle.
- (b) Strong scintillations during heavy local cloud cover at $\sim 6^\circ$ elevation angle.
- (c) Slow scintillations during overcast skies at $\sim 3.5^\circ$ elevation angle.

observation has been completed. Other meaningful analyses which will be generated later from the existing data base include an estimate of the scattering effect in radiometric measurement obtained by comparing the data at 11.6, 20 and 30 GHz frequencies, and the low-elevation propagation characteristics obtained by studying the records of the descending satellite. All these will be useful in identifying the precipitation phenomena that degrade microwaves communications at 20 and 30 GHz.

APPENDIX B. A NEW METHOD OF ESTIMATING MICROWAVE
ATTENUATION OVER A SLANT PROPAGATION PATH
BASED ON RAIN GAUGE DATA

Adjustments in time and drop size spectrum are needed for data collected from field rain gauges to realize the actual rainfall along the slant path for correlating rain gauge data with measured satellite signals.

INTRODUCTION

As a participant in the ATS-6 20/30-GHz Millimeter Wave Experiment Program [1], COMSAT Labs has conducted, among other experiments, measurements of the 20-GHz satellite beacon signals in conjunction with an 11.6-GHz radiometer and a network of six rain gauges aligned beneath the satellite boresight path at distances of 0, 0.92, 1.1, 3.23, 5.53, and 7.4 km from the beacon receiver. A typical record of a precipitation attenuation event is shown in Fig. 1. It can be seen that, while the radiometer curve correlates well with the satellite signal level, the data from the rain gauges do not have a consistent correlation with the 20-GHz curve. A particularly puzzling point is the peak registered on the rain gauge 3.23 km away from the receiver.

The lack of consistency in correlation is not uncommon. For example, in an earlier ATS-5 15.3/31.65-GHz NASA experiment at Rosman, North Carolina [2], it was found that neither the ground-averaged nor the height-averaged rainfall data of 10 rain gauges beneath the boresight path could exhibit a sufficiently detailed correlation with the satellite signals. Hence, the correlation could only be made meaningful by literally shifting the time scale of the rain gauge data so that the peaks of rainfall matched the peaks of the signal attenuations. This shifting scheme has been widely employed for determining the fading depth versus precipitation in satellite beam signal experiments as well as in radiometric experiments. The theoretical basis for such a scheme has yet to be established.

Data containing the apparent discrepancies in time and magnitude, such as those shown in Fig. 1, have been collected and analyzed. The following section provides a model for

A New Method of Estimating Microwave Attenuation over a Slant Propagation Path Based on Rain Gauge Data

D. J. FANG AND J. M. HARRIS

Abstract—A basic problem in estimating the microwave attenuation over a satellite-earth propagation path on the basis of rain gauge data is that, for a given precipitation event, the attenuation and the rainfall records very often do not have consistent detailed correlation. Such inconsistencies can be greatly reduced if the falling speed of the rain drops, i.e., 2 to 9 m/s for drop sizes of 0.05 to 0.7 cm, is taken into account.

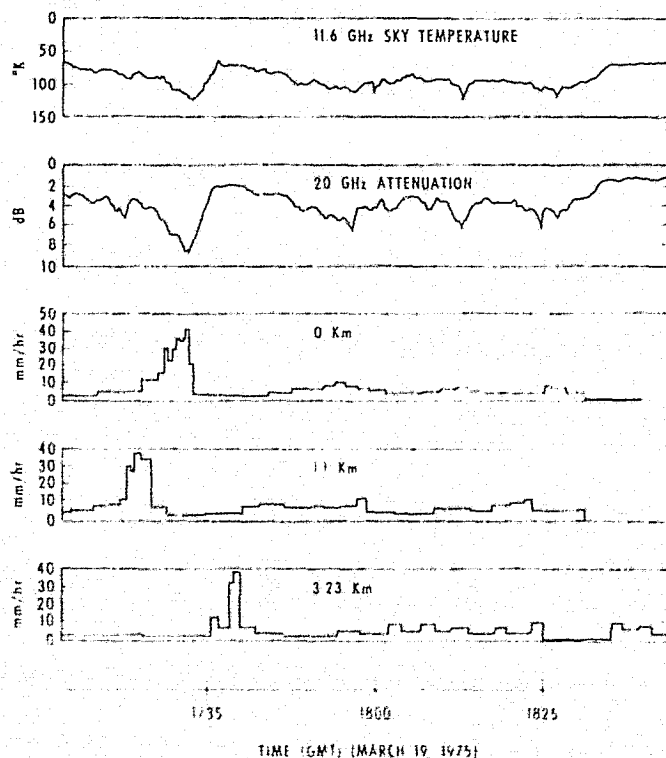


Fig. 1. Typical precipitation-attenuation record measured at Clarksburg, Md. Ground rain gauges were 0, 1.1, and 3.23 km from 20-GHz receiver and 11.6-GHz radiometer.

Manuscript received August 3, 1975; revised November 21, 1975. This paper is based on work performed in COMSAT Laboratories under the sponsorship of the Communications Satellite Corporation.

The authors are with COMSAT Laboratories, Clarksburg, MD 20734.

TABLE I
ACTUAL RAIN RATE AT 1000-M HEIGHT ESTIMATED FROM GROUND RAIN GAUGE RAINFALL READING (ESTIMATE IS BASED ON LAWS AND PARSONS DROP SIZE DISTRIBUTION AND DAVIES' TERMINAL VELOCITY PROFILE [5])

| Advanced Time (minutes) | | | | | | | | | | Ground Measured Rain Rate (mm/hr) |
|-------------------------|------|------|-------|-------|-------|-------|-------|-------|-------|--------------------------------------|
| 8.09 | 4.14 | 3.09 | 2.57 | 2.25 | 2.07 | 1.95 | 1.89 | 1.85 | 1.83 | |
| 0.07 | 0.13 | 0.05 | 0 | 0 | 0 | 1 | 0 | 0 | 0 | 0.25 |
| 0.14 | 0.46 | 0.39 | 0.17 | 0.06 | 0.02 | 0.01 | 0 | 0 | 0 | 1.25 |
| 0.18 | 0.70 | 0.82 | 0.48 | 0.20 | 0.08 | 0.04 | 0 | 0 | 0 | 2.5 |
| 0.24 | 1.02 | 1.55 | 1.11 | 0.59 | 0.29 | 0.13 | 0.05 | 0.02 | 0 | 5 |
| 0.33 | 1.44 | 3.06 | 3.18 | 2.16 | 1.26 | 0.54 | 0.29 | 0.15 | 0.09 | 12.5 |
| 0.43 | 1.9 | 4.6 | 5.98 | 4.98 | 3.20 | 2.05 | 0.88 | 0.53 | 0.48 | 25 |
| 0.6 | 2.7 | 6.25 | 9.95 | 10.45 | 7.8 | 5.45 | 3.35 | 1.65 | 1.8 | 50 |
| 1.0 | 4.6 | 8.8 | 13.9 | 17.1 | 18.4 | 15.0 | 9.0 | 5.8 | 6.4 | 100 |
| 1.5 | 6.15 | 11.4 | 17.55 | 20.85 | 26.55 | 24.15 | 17.85 | 11.55 | 12.45 | 150 |

adjusting the rain gauge data by taking the falling time of the raindrops into consideration. As shown in the third section, the adjusted rain data will provide a remarkably improved correlation with the signal level. Some of the defects and possible future refinements of the method will be discussed in the last section.

RAIN DROP SIZES AND TERMINAL VELOCITIES

The basic concept that rain drops take time to fall to the ground is intuitive [3], [4]. The rain rate registered at one instant on a ground rain gauge away from the receiver is actually responsible for wave attenuation at an earlier instant when the rain fall intercepts the slant propagation path. The detailed physics is not so intuitive because the drop size distribution is a function of rain rate and drops of different sizes fall at different terminal velocities.

Discussions of various drop size distributions with reference to different types of precipitation and of terminal velocities versus drop size are lengthy and beyond the scope of this paper. To illustrate the formulation of the above basic concept for actual application, it is sufficient to adopt the widely used Laws and Parsons drop size distribution and Davis' terminal velocity profile [5].

Let the rain rate measured by a ground gauge at instant t be $R_G(t)$ for 0.05- to 0.7-cm raindrops with falling velocity v ranging from 2 to 9 m/s. It follows that

$$R_G(t) = \sum_v R_V(t) \quad (1)$$

where $R_V(t)$ is the portion of rain rate falling at terminal velocity v . If that rain gauge is located h meters vertically below the slant propagation path, then $R_V(t)$ penetrates across the path at an advanced time h/v when there is no wind. Therefore, the actual rainfall $R_h(t)$ at height h and instant t' is

$$R_h(t') = \sum_{t,v} R_V(t) \Big|_{t-h/v=t'} \quad (2)$$

The summation for R_h at instant t' is over all the components of $R_V(t)$ in $R_G(t)$ for all t and v satisfying the relation $(t - h/v) = t'$. The decomposition of R_G into R_V for a different advanced time with $h = 1000$ m is shown in Table I.

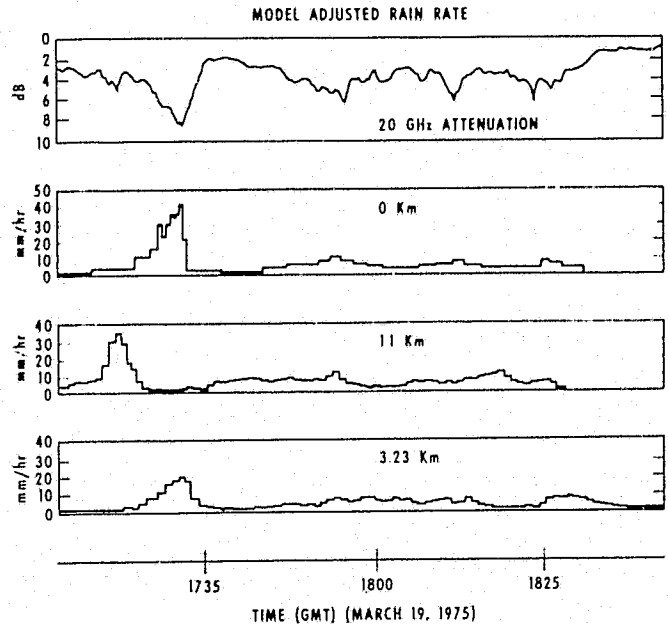


Fig. 2. Model adjusted rain rate intercepting slant path of 42° elevation angle based on original data given in Fig. 1.

The procedure of adjusting the surface rain rate R_G to obtain the actual rain rate R_h responsible for microwave attenuation can be illustrated as follows. Assume that the elevation angle of the slant path is 30° and a field rain gauge 1.2 km away from the receiver ($h = 693$ m) registers 100 mm/h at instant t . From Table I it can be determined a 13.9-mm/h rate crossed the slant path at an advanced time of $2.57 \times (693/1000)$ min. The 13.9-mm/h rate is responsible for microwave attenuation at the receiver at time $t - 1.78$ min, etc. In actual data processing, the sampling rate of the rain rate should be about 1 sample per second. The net effect of the adjustment is not only an advancement of the time of R_G , but also a dispersement of the rain rate peak into a less steep profile. Such an effect has been frequently observed when comparing the attenuation data to the data from a far-field rain gauge.

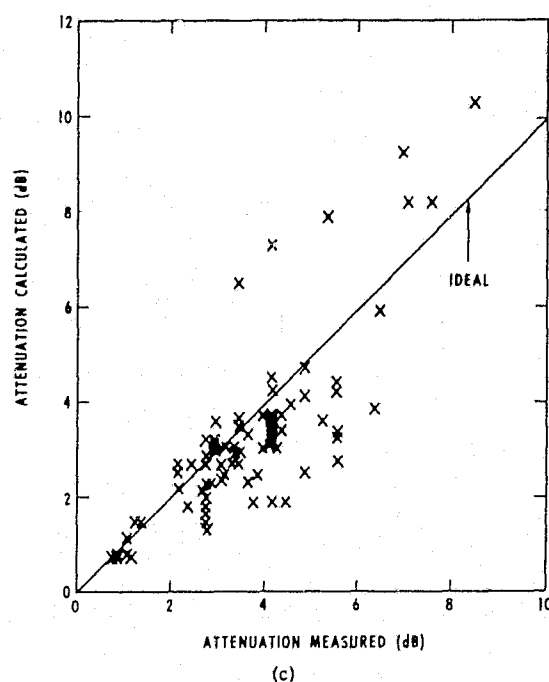
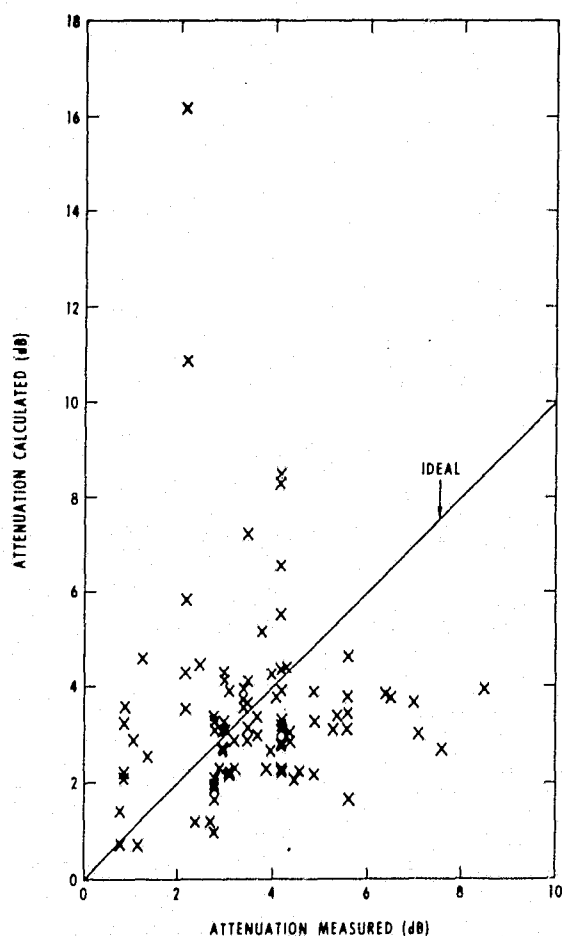
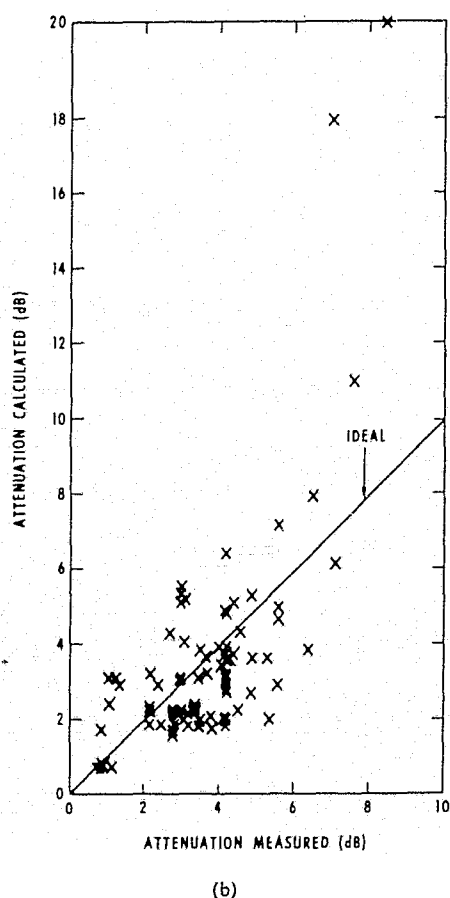


Fig. 3. Scattergram of 20-GHz attenuation calculated versus measured for 2-hour period on March 19, 1975. (a) Using original data from Fig. 1. (b) Using original rain data shifted so that peak rain rates occur at time of peak measured attenuation. (c) Using model adjusted rain data from Fig. 2.



DISCUSSION

The method postulated here has been applied at COMSAT Labs to the rain rate records collected from its network of six rain gauges for correlation with the ATS-6 20-GHz beacon signals. In most cases, the method does have the merit of relocating and dispersing the peaks of precipitation curves of field rain gauges for better alignment with the pattern of attenuation curves. Fig. 2 is the outcome of the adjusted rain rate distribution of the same event shown in Fig. 1. If it is assumed that the rain rate measured at a rain gauge applies over the distance between the middle points of the two adjacent rain gauges, attenuation can then be estimated from theoretical considerations [6]. The estimated value and the actual 20-GHz attenuation value are compared in the scattergrams presented as Figs. 3(a)–3(c). Fig. 3(a) is derived directly from the data shown in Fig. 1, while to derive Fig. 3(b), the measured data have been literally shifted, forward or backward in time, so that the peak rain rates occur at the time of peak attenuation. Fig. 3(c), which is obtained by using the model adjusted rain rates of Fig. 2, does exhibit a significant improvement in correlation relative to Figs. 3(a) and 3(b).

To correlate the slant microwave attenuation with rainfall from a field rain gauge, researchers often postulate a vertically decreasing rainfall profile. For the NASA-Rosman ATS-5 experiment [2], the profile was assumed to be linear with a height of zero precipitation assigned at 3.22 km. It is worthwhile to note that the present method reveals the physics of decreasing rainfall magnitude due to the readjustment of raindrops of different sizes, with increasing height. As can be seen from Fig. 2, the profile is not linear, and it depends not only on the magnitude, but also on the time distribution of the surface rain rate.

In a comparison of rain rate data derived from radars (3 and 8 GHz) and field rain gauges [7], it was found that there were distinctive time delays between them. A typical delay was about

4 min for a rain rate less than 10 mm/h registered by a gauge located about 900 m beneath the radar path and 3 min or less for rain rates higher than 10 mm/h. Such time differences can be easily predicted by using the present method if the overall advanced time averaged over the percentages of rainfall distribution is evaluated from Table I.

CONCLUSION

The method presented here is intended to improve the correlation between the data from rain gauges and the microwave attenuation caused by rain. Only with good correlation is it possible to assess the validity of using rain data as a prediction of satellite signal attenuation level. Needless to say, further improvement of the method is needed. Most important of all, the wind motion, which certainly affects the raindrops' falling processes, has been completely omitted. Evaporation, condensation, sublimation, accretion, and coalescence are all involved to different degrees.

In addition, it is necessary to consider the positions of the rain gauges with reference to the height of the rain cloud and the characteristic size of the rain cells; both are dependent upon the rain type and other meteorological conditions. As a general rule, in order to avoid the discrepancy between the precipitation rate determined by attenuation and the precipitation rate derived from the rain gauge fields, the rain gauges should be placed so

that the evaluation of R_h is at a height lower than the boundary of the rain cloud and so that the distance between rain gauges is smaller than the characteristic size of the rain cells.

All of these factors are extremely complicated, and efforts to incorporate them into precipitation attenuation studies have yet to be made. The method may also be significantly refined by using other distributions such as the Joss distribution [8], which is more appropriate for thunderstorms in certain climatological regions, instead of the Laws and Parsons distribution.

REFERENCES

- [1] L. H. Westerlund, J. Levatich, and A. Buige, "ATS-F COMSAT millimeter wave propagation experiment," *COMSAT Tech. Rev.*, vol. 3, pp. 323-340, Fall 1973.
- [2] L. J. Ippolito, "Effects of precipitation on 15.3- and 31.65-GHz earth-space transmissions with the ATS-V satellite," *Proc. IEEE*, vol. 59, pp. 189-205, Feb. 1971.
- [3] D. E. Kerr, *Propagation of Short Radio Waves*. New York: McGraw-Hill, 1951, pp. 616-617.
- [4] T. Oguchi, "Attenuation and phase rotation of radio waves due to rain: calculations at 19.3 and 34.8 GHz," *Radio Sci.*, vol. 8, no. 1, p. 34, 1973.
- [5] R. G. Medhurst, "Rainfall attenuation of centimeter waves: comparison of theory and measurement," *IEEE Trans. Antennas Propagat.*, vol. AP-13, pp. 550-564, July 1965.
- [6] D. J. Fang, "Attenuation and phase shift of microwaves due to canted raindrops," *COMSAT Tech. Rev.*, vol. 5, pp. 135-156, Spring 1975.
- [7] L. J. Ippolito, G. Hyde, and J. L. King, "Millimeter wave propagation experiments," in *Int. Conf. on Communications*, San Francisco, June 16-18, 1975, Paper no. 18F.
- [8] J. Joss and A. Waldvogel, "Raindrop size distribution and Doppler velocities," in *14th Radar Meteorology Conf.*, American Meteorological Society, Boston, 1970, pp. 153-156.

END